

Modelling and Performance Evaluation of an HV Impulse Test Arrangement with HVDC Bias

S.K. Shifidi

Thesis presented in partial fulfilment of the requirements for the degree of

Master of Science in Engineering

at the University of Stellenbosch



Supervisor: Prof H.J. Vermeulen

December 2009

DECLARATION

By submitting this dissertation electronically, I declare that the entirety of the work contained therein is my own, original work, that I am the owner of the copyright thereof (unless to the extent explicitly otherwise stated) and that I have not previously in its entirety or in part submitted it for obtaining any qualification.

Signature

December 2009

Copyright © 2009 Stellenbosch University

All rights reserved

Abstract

From a systems operation and design perspective, it is important to understand the behaviour of HVDC system insulation when presented with high voltage transients, such as induced by lightning and switching operations. Therefore, this thesis investigates the design, operation and performance of a circuit arrangement that can be used in high voltage laboratories to generate impulse voltage waveforms superimposed on a dc bias voltage. The circuit arrangement consists of an impulse generator and a dc source that supplies continuous dc voltage to stress the test object, which can be any type of insulator, i.e. composite, porcelain, glass, gap arrangements, etc. The composite waveform obtained from the test arrangement is used experimentally to investigate the impulse flashover of insulators.

For modelling and analysis purposes, the test circuit was transformed to a Laplace equivalent in order to derive the applicable nodal voltage equations. After substitution of circuit parameter values, the voltage equations are then transformed to time domain equations that predict the time-domain behaviour of the circuit. To validate this mathematical approach, the voltage waveforms obtained with this mathematical model is compared with the waveforms measured under laboratory conditions and also with waveforms simulated with HSPICE software. These comparisons are performed using graphical representations. Good correlation was obtained and the results are presented in this thesis.

The final stage of this thesis discusses the application of the designed test arrangement for flashover and withstands tests on a silicon rubber insulator. The determination of the flashover values is done by using the existing statistical methods. The insulator was tested under dry conditions and also under polluted wet conditions for both positive and negative impulses compared to the DC bias voltage polarity. The results show that the dc bias voltage does not affect the total voltage flashover of the insulator significantly. It was also observed that wetting affects the flashover for negative impulse more severely, while the influence of wetting is minimal with positive impulse voltages.

Opsomming

Vanuit 'n stelselbedryf en ontwerp perspektief, is dit is belangrik om die gedrag van HSGS stelsels te verstaan wanneer dit onderwerp word aan hoogspanning oorgangsverskynsels soos veroorsaak deur weerlig en skakeloperasies. Daarom ondersoek hierdie tesis die ontwerp, werking en werkverrigting van 'n stroombaanopstelling wat gebruik kan word in hoogspanningslaboratoriums om impulsspannings gesuperponeer op gelykspanning voorspannings op te wek. Die stroombaan bestaan uit 'n impulsgenerator en 'n gs-bron wat die langdurige gs-spanning voorsien aan die toetsvoorwerp, wat enige tipe isolator kan wees. bv. porselein, glas, gapings, ens. Die saamgestelde golfvorm wat met die toetsopstelling verkry word, is eksperimenteel gebruik om die impuloorvonking van isolators te ondersoek.

Vir die doel van modellering and analise, is die stroombaan na 'n Laplace ekwivalent getransformeer om die toepaslike knooppunt spanningsvergelykings af te lei. Na substitusie van die stroombaan parameter waardes, word die spanningsvergelykings getransformeer na die tydgebied vergelykings wat die tydgebied gedrag van die stroombaan voorspel. Om die wiskundige benadering te toets, word die spanningsgolfvorms wat met die wiskundige model voorspel word, vergelyk met golfvorms wat onder laboratorium toestande gemeet is en ook met golfvorms wat met HSPICE programmatuur gesimuleer is. Hierdie vergelykings word gedoen met behulp van grafiese voorstellings. Goeie korrelasie is verkry en die resultate word in die tesis gegee.

Die finale stadium van hierdie tesis bespreek die toepassing van die ontwerpte toetsopstelling vir oorvonk- en weerstaantoetse op 'n silikonrubber isolator. Die bepaling van die oorvonkwaardes word gedoen deur bestaande statistiese metodes te gebruik. Die isolator is onder droë en nat besoedelde toestande gedoen, vir beide positiewe sowel as negatiewe impulse met verwysing na die GS voorspan spanning. Die resultate toon dat die gs-voorspanning nie die oorvonkspanning van die isolator beïnvloed nie. Dit is ook waargeneem dat die benatting die oorvonking neer beïnvloed met 'n negatiewe impuls terwyl die invloed minimaal is met positiewe impulsspannings.

Table of Contents

1. INTRODUCTION

1.1	OVERVIEW	1
1.2	INTRODUCTION	1
1.3	PROJECT MOTIVATION	2
1.4	PROJECT DESCRIPTION	3
1.5	THESIS STRUCTURE	5

2. LITERATURE REVIEW

2.1	OVERVIEW	7
2.2	INTRODUCTION	7
2.3	HVDC TECHNOLOGY	8
2.3.1	<i>Brief history of HVDC</i>	8
2.3.2	<i>Advantages of HVDC Systems</i>	9
2.3.3	<i>HVDC configurations</i>	10
2.3.3.1	Towers configurations	12
2.3.3.2	Insulators	13
2.4	HIGH VOLTAGE SYSTEMS IN SOUTHERN AFRICA	14
2.5	HIGH VOLTAGE INSULATION	15
2.5.1	<i>Insulation level</i>	15
2.5.1.1	Insulator impedance	16
2.6	INSULATION MATERIALS UNDER HIGH VOLTAGE	17
2.6.1	<i>Corona discharge</i>	18
2.6.2	<i>Breakdown</i>	19
2.6.3	<i>Breakdown in non-uniform dc fields</i>	19
2.6.4	<i>Breakdown in non-uniform ac fields</i>	20
2.6.5	<i>Breakdown for impulse voltages</i>	20
2.6.5.1	Determining flashover and withstand of insulators	21
2.6.5.2	Comparisons of flashover levels	23
2.6.6	<i>Impulses superimposed on system voltages</i>	25
2.6.6.1	Test circuit arrangements	28
2.7	INSULATOR POLLUTION	29
2.7.1	<i>Mechanism of contamination flashover</i>	30
2.7.2	<i>Severity of contamination</i>	31
2.7.3	<i>Artificial contamination</i>	32
2.8	POWER SYSTEM IMPULSE OVERVOLTAGES	33

2.8.1	<i>Lightning overvoltages</i>	35
2.8.2	<i>Switching overvoltages</i>	35
2.9	GENERATION OF IMPULSES FOR LABORATORY EXPERIMENTS	36
2.9.1	<i>Single-stage generator circuits</i>	37
2.9.2	<i>Multiple stage impulse generators</i>	38
2.9.2.1	Marx impulse generator circuit	39
2.9.2.2	Goodlet impulse generator circuit	40
2.9.3	<i>High voltage construction kits</i>	40
2.10	MEASUREMENT TECHNOLOGIES USED IN HIGH VOLTAGE IN LABORATORIES	41
2.10.1	<i>Resistive voltage dividers</i>	41
2.10.2	<i>Compensated resistive dividers</i>	43
2.10.3	<i>Capacitive voltage dividers</i>	44
2.10.4	<i>Damped capacitive voltage dividers</i>	44
2.10.5	<i>Low voltage arm of the divider</i>	45
2.10.6	<i>High voltage probes</i>	46
2.11	CONCLUSIONS	47

3. DESIGN AND MATHEMATICAL MODELLING OF THE TEST TOPOLOGY

3.1	OVERVIEW	48
3.2	TEST ARRANGEMENT TOPOLOGY	48
3.3	THE IMPULSE GENERATORS	50
3.3.1	<i>Determining impulse waveshapes</i>	50
3.3.1.1	Calculating time to peak	53
3.3.1.2	Calculating time to half peak	53
3.3.2	<i>Marx-type multistage generator circuit</i>	55
3.3.3	<i>Messwandler Bau kit</i>	61
3.4	THE DC VOLTAGE SOURCE	62
3.5	THE TEST OBJECT	62
3.6	DESIGN AND ANALYSIS OF THE COMPLETE TEST TOPOLOGY	63
3.6.1	<i>Circuit topology</i>	63
3.6.2	<i>Mathematical analysis of the circuit</i>	64
3.6.2.1	Nodal voltage equations in the Laplace domain	64
3.6.2.2	Time domain voltage waveforms	69
3.6.3	<i>Effects of circuit variables on the voltage waveforms</i>	72
3.6.3.1	Introduction	72
3.6.3.2	Effects of coupling capacitor values of the voltage waveform	73
3.6.3.3	Effects of the coupling resistor value	78
3.6.3.4	Effects of resistance value of the test object	81
3.6.3.5	Effects of the capacitance of the test object on the voltage waveforms	85

3.7	CONCLUSIONS	88
-----	-------------------	----

4. THEORETICAL AND PRACTICAL VALIDATION OF THE COMPOSITE WAVEFORM GENERATOR CIRCUIT

4.1	INTRODUCTION	89
4.2	PRACTICAL TEST ARRANGEMENT	90
4.2.1	<i>Captured waveforms</i>	93
4.2.2	<i>Measuring equipment used</i>	93
4.2.3	<i>Processing of data</i>	94
4.2.3.1	Overview	94
4.2.3.2	Measurement of the impulse component of the composite voltage waveform	95
4.2.3.3	Measurement of the dc component of the composite voltage waveform.....	96
4.2.3.4	Addition of the measured dc and impulse waveforms.....	98
4.3	SIMULATION OF THE COMPOSITE WAVEFORM GENERATOR CIRCUIT WITH THE MATHEMATICAL MODEL	99
4.3.1	<i>Results obtained and comparisons with the practical measured results</i>	101
4.4	MODELLING THE COMPOSITE WAVEFORM GENERATOR CIRCUIT WITH HSPICE	103
4.4.1	<i>Results obtained and comparisons with results of the mathematical model</i>	104
4.5	THE EFFECTS OF LOADING, COUPLING COMPONENTS AND OPERATING VOLTAGE LEVELS OF THE PERFORMANCE OF THE COMPOSITE WAVEFORM GENERATOR	106
4.5.1	<i>The effects of different load impedances</i>	106
4.5.1.1	Results obtained	107
4.5.2	<i>The effects of different coupling component values</i>	108
4.5.2.1	Results obtained	109
4.5.3	<i>The effects of different operating voltages</i>	110
4.5.3.1	Results obtained	111
4.6	CONCLUSIONS	111

5. APPLICATION OF THE COMPOSITE WAVEFORM GENERATOR CIRCUIT TO OBTAIN FLASHOVER LEVELS OF AN INSULATOR

5.1	INTRODUCTION	113
5.2	INSULATOR UNDER TEST.....	114
5.3	ARTIFICIAL CONTAMINATION OF THE INSULATOR.....	115
5.4	TEST ARRANGEMENT.....	115
5.4.1	<i>Test circuit</i>	116
5.4.2	<i>Description of circuit parameters and operation</i>	117
5.4.3	<i>Theoretical simulation</i>	119
5.5	TEST PROCEDURE	121
5.6	DATA CAPTURING AND PROCESSING	121
5.7	TESTS PERFORMED	126

5.7.1	Overview.....	126
5.7.2	Tests under dry conditions.....	126
5.7.3	Tests under wet conditions.....	126
5.8	RESULTS ON THE DETERMINATION OF FLASHOVER LEVELS OF THE INSULATOR.....	131
5.8.1	Impulse flashover tests at different dc bias voltages.....	131
5.8.1.1	Dry insulator, Positive impulses.....	132
5.8.1.2	Wet insulator, positive impulses.....	134
5.8.1.3	Dry insulator, negative impulses.....	136
5.8.1.4	Wet conductor, negative impulse.....	138
5.8.2	Summary of flashover results.....	140
5.8.3	Dry conditions.....	140
5.8.4	Wet conditions.....	141
5.8.5	Discussions of results.....	145
5.8.5.1	The effect of impulse polarity.....	145
5.8.5.2	The effect of dc bias voltage.....	145
5.8.5.3	The effect of insulator wetting.....	145
5.9	CONCLUSIONS.....	146

6. CONCLUSIONS AND RECOMMENDATIONS

6.1	OVERVIEW.....	147
6.2	CONCLUSIONS.....	147
6.3	RECOMMENDATIONS.....	149

APPENDICES

APPENDIX.A	MATHEMATICAL ANALYSIS OF A SINGLE-STAGE IMPULSE GENERATOR CIRCUIT.....	155
APPENDIX.B	DERIVING THE PEAK VALUE OF AN IMPULSE WAVEFORM.....	160
APPENDIX.C	DERIVING THE FRONT AND TAIL TIMES OF AN IMPULSE WAVEFORM.....	162
C.1	OVERVIEW.....	162
C.2	DERIVING THE FRONT TIME.....	163
C.3	DERIVING THE TAIL TIME.....	166
APPENDIX.D	NODAL VOLTAGE ANALYSIS OF THE COMPOSITE WAVEFORM GENERATOR CIRCUIT.....	168
APPENDIX.E	THE PERFORMANCE OF MATHEMATICAL CALCULATIONS WITH MATHEMATICA SOFTWARE.....	181
APPENDIX.F	HSPICE CODE FOR THE SIMULATION OF THE COMPOSITE WAVEFORM GENERATOR.....	185
APPENDIX.G	MATLAB CODE.....	186
G.1	COMPARISON OF METHODS: MATHEMATICAL MODEL, HSPICE AND THE PRACTICAL MEASURED.....	186
G.2	ILLUSTRATION OF THE DRYING PROCESS.....	189
G.3	PLOTS OF FLASHOVER IMPULSES.....	190

Table of Figures

Figure 2.1: Monopole configurations with an earth or metallic return [9].	11
Figure 2.2: Bipole configurations with an earth or metallic return [9].	11
Figure 2. 3: Bipole configurations without an earth or metallic return [9].	11
Figure 2.4: Tower configurations: (a) Monopole configuration with an earth return and (b) Bipole configuration with an earth return.	13
Figure 2.5: Definition of creepage distance and clearance length of an insulator.	17
Figure 2.6: Illustration of the polarity effects with dc voltage: (a) When the sharp point is positive, and (b) when sharp point is negative [15].	20
Figure 2.7: Illustration of flashover and withstand waveforms [15].	21
Figure 2.8: Illustration of an impulse flashover probability curve.	22
Figure 2.9: Rod-plane gap 50-percent flashovers as obtained in CTH laboratories [20].	24
Figure 2.10: Rod-rod gap 50-percent flashovers as obtained in CTH laboratories [20].	25
Figure 2.11: Rod-plane gap 50-percent flashover voltages, switching surges applied, positive polarity, dry and wet conditions. Air conditions: Humidity 8-10 g/m ³ ; Temperature 21-23° C; Pressure 760mmHg [20].	27
Figure 2.12: Rod-rod gap 50-percent flashover voltages, switching surges applied, positive polarity, dry and wet conditions. Air conditions: humidity 11 g/m ³ ; temperature 21-23° C; Pressure 770 mmHg [20].	28
Figure 2.13: A block diagram of the circuit configuration.	29
Figure 2.14: Impedance model of an insulator string [15]	31
Figure 2.15: Illustration of the impulse waveform and its definitions [17].	34
Figure 2.16: Definition of a switching impulse waveform [16]	36
Figure 2.17: Two basic types of single stage impulse generator circuits [17].	37
Figure 2.18: An eight stage Marx type impulse generator circuit diagram [33].	40
Figure 2.19: An equivalent circuit of the resistive voltage divider [16].	42
Figure 2.20: An equivalent circuit of a compensated resistive divider [16].	43
Figure 2.21: A basic diagram of a damped capacitive divider [16].	45
Figure 2.22: Low voltage arm of the voltage divider [17].	46
Figure 3.1: A positive impulse voltage superimposed on a positive bias voltage.	49
Figure 3.2: Block diagram of the proposed test arrangement.	49
Figure 3.3: A standard single-stage impulse generator circuit.	51
Figure 3.4: Demonstration of front time values calculation for an impulse waveform.	54
Figure 3.5: Photograph of the Marx-type multistage impulse in the University of Stellenbosch's HV laboratory.	56

Figure 3.6: shows the circuit diagram of the eight-stage Marx-type impulse generator shown in Figure 3.1 [33].	56
Figure 3.7: Multistage impulse generator simplification process with R_L is ignored.	58
Figure 3.8: Multistage impulse generator simplification process with links between branches removed.	58
Figure 3.9: A simplified single-stage impulse generator circuit.	59
Figure 3.10: DC rectifier circuits: (a) Positive dc voltage and (b) Negative dc voltage.	62
Figure 3.11: Complete test circuit topology.	63
Figure 3.12: Low pass filter circuit for impulse blocking.	64
Figure 3.13: Laplace equivalent representation of the test circuit.	65
Figure 3.14: Voltage waveform $v_3(t)$ across the test object.	71
Figure 3.15: Voltage waveform $v_4(t)$ across the dc source.	72
Figure 3.16: Voltage impulse waveforms with different C_c values.	74
Figure 3.17: Plots of the effect of C_c on the peak values of voltages $v_3(t)$ and $v_4(t)$.	75
Figure 3.18: Efficiency plot of an impulse generator as a function of C_c .	76
Figure 3.19: Effects of R_c on peak values of voltages $v_3(t)$ and $v_4(t)$.	78
Figure 3.20: Leakage factor as a function of R_c .	79
Figure 3.21: Peak $v_4(t)$ voltages with different R_c values.	80
Figure 3.22: Effects of R_t on peak voltages $v_3(t)$ and $v_4(t)$.	82
Figure 3.23: DC voltage across the test object as a function of different R_t values.	83
Figure 3.24: Effects of C_t on peak voltage values $v_3(t)$ and $v_4(t)$ voltages.	85
Figure 3.25: Efficiency of impulse circuit as a function of C_t .	86
Figure 4.1: Schematic diagram of a test arrangement.	91
Figure 4.2: Messwandler Bau construction kit arrangement in the high voltage lab.	92
Figure 4.3: A sphere-to-sphere gap arrangement used as test object.	92
Figure 4.4: The captured waveform from the capacitor voltage divider.	95
Figure 4.5: A measured impulse signal with dc offset filtered out.	96
Figure 4.6: A voltage signal measured with high voltage probe.	97
Figure 4.7: The obtained pure dc voltage waveform.	97
Figure 4.8: The final voltage signal across test object.	98
Figure 4.9: The final voltage signal across test object, full waveform.	99
Figure 4.10: Capacitance geometry factor for spaced spheres [40].	101
Figure 4.11: Comparison of predicted and measured waveforms, front part.	102
Figure 4.12: Comparison of predicted and measured waveforms, full waveform.	103
Figure 4.13: Comparison of mathematical model with HSPICE simulation.	105
Figure 4.14: Comparison of mathematical model with HSPICE simulation, full waveform.	105
Figure 4.15: Highlights the test object impedance parameters in the circuit.	106
Figure 4.16: Location of coupling components in the test circuit.	108

Figure 5.1: Silicon rubber composite insulator which was tested.	114
Figure 5.2: A two-stage Messwandler Bau kit arrangement in the HV laboratory.....	116
Figure 5.3: The used dc supply set in the HV laboratory.	117
Figure 5.4 Circuit diagram of the test arrangement.	118
Figure 5.5: Laplace domain equivalent circuit representation of the test arrangement.	119
Figure 5.6: Plotted waveform (a) front part, (b) full waveform.....	120
Figure 5.7: Magnitudes of impulses (a) $V_{dc}+V_i$ for positive and (b) V_i for negative impulses.	122
Figure 5.8: Magnitudes of impulses (a) V_i for positive and (b) V_i for negative impulses.....	122
Figure 5.9: An illustration of a flashover positive waveform with dc bias voltage.....	123
Figure 5.10: Drying process of a composite insulator surface.....	128
Figure 5.11: Three drying stages of a composite.....	129
Figure 5.12: Distribution of impulses during positive impulse flashover tests on a dry composite insulator	133
Figure 5.13: Distribution of impulses during positive impulse flashover tests on a wet composite insulator.....	135
Figure 5.14: Distribution of impulses during negative impulse flashover tests on a dry composite insulator	137
Figure 5.15: Distribution of impulses during negative impulse flashover tests on a wet composite insulator.....	139
Figure 5.16: Compared series of results, for series of tests are all shown.	142
Figure 5.17: Voltage components of the composite waveforms, positive flashovers under dry condition.	143
Figure 5.18: Voltage components of the composite waveforms, positive flashovers under wet condition.	143
Figure 5.19: Voltage components of the composite waveforms, negative flashovers under dry condition.....	144
Figure 5.20: Voltage components of the composite waveforms, negative flashovers under wet condition.	144
Figure A.1: Laplace equivalent circuit of a standard impulse generator.	155
Figure B.1: The graph used to define and calculate the front time of the waveshape.	160
Figure C.1: Definition of front and tail times.	162
Figure C.2: The two exponential terms of an impulse waveform.....	163
Figure C.3: Illustration of the method used to calculate front time, t_f	164
Figure D.1: Laplace equivalent representation of the composite waveform generator circuit.	168

List of Tables

Table 3.1: Component values of the Marx-type impulse generator in the HV laboratory.....	57
Table 3.2: Basic elements of the Messwandler Bau construction kit.	61
Table 3.3: Summary of circuit parameters used in deriving $V_3(t)$	69
Table 3.4: Numerical values for the effects of the value of C_c on peak values of $v_3(t)$, $v_4(t)$ and the efficiency. ...	77
Table 3.5: Numerical values for the effects of the value of R_c on values of $v_3(t)$, $v_4(t)$ and the efficiency.....	81
Table 3.6: Numerical values for the effects of the value of R_t on the peak values of $v_3(t)$, $v_4(t)$ and V_{i3}	84
Table 3.7: Numerical values for the effects of the value of C_t on the peak values of $v_3(t)$, $v_4(t)$ and the efficiency.	87
Table 4.1: Parameter values for the practical test arrangement.	90
Table 4.2: List of circuit parameters and variables used in the simulation.....	107
Table 4.3: Effects of the resistance and capacitances of the test object on the output voltage, V_3	108
Table 4.4: List of parameters used in the prediction.....	109
Table 4.5: Results of coupling capacitor effects on voltage V_3 across the test object.	109
Table 4.6: of coupling resistor effects on the voltage across test object, V_3	110
Table 4.7 List of circuit variables used in the prediction.....	111
Table 4.8: Results obtained with different voltages levels of V_g and V_{dc}	111
Table 5.1: Summary of parameter values for the test circuit shown in Figure 5.4.....	119
Table 5.2: Determination of CFO, the 20 recorded impulses.	124
Table 5.3: Summary of the recorded impulses.	124
Table 5.4: Kaolin composition used as an insulator contaminant.	127
Table 5.5: Flashover tests at different stages of insulator drying.	130
Table 5.6: Positive impulse tests on a dry composite insulator at different dc bias voltages.	132
Table 5.7: Positive impulse tests on a wet composite insulator at different dc bias voltages.....	134
Table 5.8: Negative impulse tests on a dry composite insulator at different dc bias voltages.....	136
Table 5.9: Negative impulse tests on a wet composite insulator at different dc bias voltages.	138
Table 5.10: Recorded voltage CFO values at dry condition.....	140
Table 5.11: Recorded CFO voltage values at wet condition.	141

Nomenclature

ABB	Asea Brown Boveri
AC	Alternating Current
CFO	Critical Flashover Voltage
DC	Direct Current
DRC	Democratic Republic of the Congo
ESDD	Equivalent Salt Deposit Density
HV	High Voltage
HVAC	High Voltage Alternating Current
HVDC	High Voltage Direct Current
IEC	International Electrotechnical Commission
NaCl	Sodium Chloride
ROW	Right Of Ways
SADC	Southern African Development Community
U_{50}	Fifty percent voltage flashover level
V_{50}	Fifty percent voltage flashover level
VARIAC	Variable Autotransformer
V_{dc}	DC voltage
V_i	Impulse voltage
WESTCOR	Western Power Corridor
α	alpha, time constant
β	beta, time constant
η	efficiency

1. INTRODUCTION

1.1 Overview

This chapter discusses the background to this study. The research problem is identified and the motivation to undertake the study and design is highlighted. It then continues with a description of the project and summarises the research steps to be undertaken. The chapter closes with a summary of how this thesis is formulated, referring to the various chapters and contents thereof.

1.2 Introduction

Electrical insulation is a crucial and challenging aspect of High Voltage (HV) transmission systems. As with material properties, mechanical performance and performance under normal operating conditions, the performance of insulation systems under transient overvoltage conditions, mainly caused by lightning and switching operations, requires particular attention. Also, due to the expansion of High Voltage Direct Current (HVDC) transmission systems, the need to look into the impulse behaviour of insulators pre-stressed with dc voltage has arisen.

The behaviour of different insulators materials and geometries at dc voltage has been explored in the past in several high voltage laboratories. The performance of air gaps for ac and dc voltages superimposed with an impulse has also received considerable attention [[1], [2], [3], [4]]. However, the effects were never really extended to composite insulators when pre-stressed with dc voltage. The effects of different polarity impulses on high voltage insulators that are pre-stressed with dc voltages of different polarities need to be studied and understood. However, an accurate test configuration for this test scenario needs to be designed first. Once

the test configuration has been designed and analysed, tests on different types of insulators can be performed and the results analysed.

1.3 Project motivation

In the past few years, HVDC systems have been gaining popularity over High Voltage Alternating Current (HVAC) systems. The advancement of power electronics and reduced costs thereof are the main driving factors. Although already existing in the southern African region, the prospects of HVDC transmission systems are even greater as the need for cross-country power lines and inter-country connections intensifies.

Overvoltages on transmission lines pose a great danger for the equipment, continuity of supply and, more importantly, the safety of personnel. Hence, further research in this field, particularly on the effects of overvoltage transients on insulation is desired. Lightning is a common phenomenon in the region, and the long energized power lines are quite exposed, while switching surges are induced at re-energization of a line or during reclosing of a circuit breaker. The dc charge that has usually been trapped on the line, together with these high superimposed surges can trouble system insulation performance.

Although there are various measures protecting the systems against lightning strikes, there is still a reasonable probability of direct strikes. Lightning induced backflashes pose a large threat for power systems, especially if the system insulation is poorly designed. Generally, the lightning impulse flashover voltage of an insulator is higher than that of a switching impulse, however, the effects are almost identical. Results obtained in this study will aid the understanding of dc insulation design in order to accommodate typical field conditions.

There has been a substantial amount of research in the field of HVAC insulation. However, more research is required on the insulation of HVDC systems. The existence of a space charge between electrodes makes the breakdown process of insulation under dc field gradients different from that of ac. It follows that the presence of a dc bias voltage can have an effect on the impulse breakdown performance of insulation. This motivates the need for practical HV impulse tests in the presence of a dc bias voltage [[2], [3], [4], [5]]. These tests are usually

designed to simulate conditions which may arise on HVDC transmission lines and the associated substation apparatus under transient overvoltage conditions [1].

With most high voltage laboratories already equipped with impulse generators and dc supply sets, it should not be technically difficult to integrate these into a test configuration that will be able to apply dc and impulse voltages simultaneously to an insulator. Appropriate design work is however needed to integrate these different systems.

Using a mathematical approach, the proposed circuit is simplified and analysed in the time and frequency domains. The ultimate objective of developing the mathematical model is to assist in the design, protection and performance assessment of such test topologies and to improve understanding of the circuit operation. This would help researchers and design engineers engaged in similar studies and applications.

1.4 Project description

This investigation considers impulses on insulators with dc bias voltages under laboratory conditions. It starts with a review of impulse generators and dc supply circuits in high voltage engineering. A test arrangement, consisting of an impulse generator combined with a dc test set is designed, modelled and tested in the HV laboratory [[2], [3], [4]]. Careful consideration is taken when integrating these components, including the use of appropriate coupling components.

The project consisted of the following main research tasks:

- A complete test arrangement, including a multi-stage impulse generator, dc test source and the necessary coupling components was designed and represented as an equivalent circuit.
- A detailed mathematical model of the test topology was then derived for the circuit. In modelling the design, all circuit components that can influence the output of the test circuit were taken into consideration.

- The individual effects of all important circuit elements and parameter values were investigated.
- Since test objects such as insulators vary widely in terms of circuit representation and parameter values, to be explained.

Using software, such as MATLAB and MATHEMATICA, the mathematical model was simulated in order to obtain the predicted output. The model was validated for representative practical parameter values and loads using simulations conducted with HSPICE and measurements obtained under laboratory conditions. The validation is based on the comparison of these simulated and measured waveforms. This exercise was performed for different circuit values in order to verify the robustness of the model.

This test scheme was eventually used to perform tests on spark gaps and polluted insulators under different operating conditions. Depending on the insulator to be tested, some variables such as the input voltage, coupling capacitor value, coupling resistor value, etc. were changed to yield the desired operational result.

1.5 Thesis Structure

This thesis document is structured into six chapters and a number of appendices. The following details apply:

- Chapter 1 presents the project overview. The project motivation presents the background information and the driving force behind this research, while the project description describes the research objectives.
- Chapter 2 presents a literature review on the main components of this study. HVDC technology is reviewed and its background and main advantages over the ac counterpart are highlighted. Past research in this field was mainly done on air gaps, and these studies are revisited. Insulators represent crucial components of these systems and a general review on insulators and insulator performance for different voltage types are given. Pollution and the performance of polluted insulators under field conditions are also reviewed. Since the impulse generator is a fundamental part of the experimental arrangement, and there are different types used in practice, impulse generator circuit configurations are reviewed. High voltage and high frequency measurement options and challenges are also highlighted in this section.
- Chapter 3 summarises the design of a topology for the test circuit arrangement. It starts with simplification of the impulse generator model, followed by simplification of the whole circuit configuration. A Laplace equivalent of the circuit is derived, followed by the nodal voltage equations in the frequency domain. Actual circuit variables are then substituted into the nodal equations. With the aid of the inverse Laplace transform, time domain expressions of the node voltages are obtained. The final time domain voltage to appear across the test object (at no flashover) is derived and simulated. The effects of different circuit variables are also reviewed.
- Chapter 4 presents the performance assessment of the test circuit topology. The circuit of a practical test arrangement is presented and simplified. The mathematical equations obtained as in chapter 3 are populated with practical component values and output waveforms are plotted using MATLAB software. Practical experiments are

performed and results obtained for comparison. The same circuit arrangement is also modelled using HSPICE simulation software. Graphical plots of these simulations are then used as a means to compare these different methodologies. This verifies the accuracy of the proposed mathematical model. The circuit was subsequently tested for its ability and consistency to perform under different conditions i.e. different loading and coupling values.

- Chapter 5 presents the application of the test arrangement for an actual insulator. The test circuit is used for determining the flashover levels of a composite insulator under different operating conditions. The results are corrected against atmospheric factors, recorded and graphs summarising the results are presented in this chapter. These results are used to study the effects of different operating conditions, i. .e dry and wet, with and without dc bias voltage, on the flashover level of an insulator. These experiments also validate the practical application and validity of the mathematical model for actual experimental conditions.
- Chapter 6 summarises the results of the study and presents conclusions and proposes recommendations for further work.

2. LITERATURE REVIEW

2.1 Overview

The subject of HVDC technology, including the background, advantages and the general structures, i.e. towers and insulators, are reviewed in this chapter. The importance of proper insulator rating and design is also highlighted. As it is important to understand the nature of typical power system transients, e.g. lightning and switching induced overvoltages, these are also defined and reviewed in this chapter. Experimental results in previous studies for impulse voltages superimposed on HVDC bias voltage are also revisited in this chapter. Since the project focuses on laboratory tests, the impulses that represent the lightning and switching waveforms will be obtained using impulse generators. Therefore, various types of impulse generators are investigated. The review also considers different types of HV measurement methods.

2.2 Introduction

Insulators are crucial components of a high voltage transmission line. Before the insulators are deployed in the field, it is important to evaluate their performance under typical field conditions. In HVDC systems, for example, the behaviour of system insulation and how it is affected by transient voltages is a subject of interest that cannot necessarily be determined from the behaviour of its ac counterpart.

Overvoltage transients induced by lightning and switching on high voltage power systems pose a threat to the system insulation. A considerable amount of research has been done on the simulation of impulses on energised power lines. However, it has been mostly concentrated on air gap arrangements. It is important to revisit past studies and research in this field and then

build on that foundation in search of a system and methodology of impulse testing of dc insulators with dc bias voltage.

2.3 HVDC Technology

High and growing electricity demands needs the transmission of electrical power over long distances. Right-of way (ROW) and better efficiency are some of the challenges that have faced the power transmission industry over the years. High Voltage Direct Current (HVDC) technology is mainly used in long distances and it is gaining popularity over ac technology in this contest. The modern form of HVDC employs the technology that was developed and commercialized some 50 years ago by ABB (Asea Brown Boveri) company. The recent rapid development in the power electronics field is aiding this advancement of HVDC technology [[1], [6]].

2.3.1 Brief history of HVDC

The first commercial electricity generated (by Thomas Edison) was Direct Current (DC) electrical power. The first electricity transmission systems were also direct current systems. One of the earliest examples is a 2 kV dc line built between Miesbach and Munich, Germany in 1882. At that time, dc conversion by means of rotating dc machines was the only possible method to get consumer voltage levels from transmission voltages [[1], [6]].

DC power transmission at low voltages has high losses over long distances, thus giving rise to High Voltage Alternating Current (HVAC) electrical systems. It was realized that for an ac system voltage conversion is simple with the development of a high power transformer. Further, a three phase synchronous generator is superior to a dc generator in every aspect. For these reasons ac technology was introduced at a very early stage in the development of electrical power systems and it was soon accepted as the only feasible method of generation, transmission and distribution of electrical energy [[6], [7]].

However, some shortcomings in the HVAC transmission technology led to research into the application of HVDC transmission systems. With the development of high voltage valves, it

became possible to transmit dc power at high voltages and over long distances, giving rise to HVDC transmission systems. This has grown tremendously in the recent years due to the fast development of modern solid state power electronic [[6], [7]].

2.3.2 Advantages of HVDC Systems

Although an ac system seems to be simpler, there are various disadvantages associated with this transmission system. Therefore, engineers continued to engage in the development of technologies for dc transmission as a supplement to ac transmission. Innovations in almost every area of HVDC transmission have been constantly improving the reliability of this technology with economic benefits for users throughout the world. The result is a very competitive, flexible and efficient way of transmitting electrical energy with a very low environmental impact e.g. reduced ROWs [6].

The main advantage of HVDC is the ability to transmit large amounts of power over very long distances at much lower capital costs and with much lower losses than the ac counterpart. Moreover, there are also some other positive aspects associated with HVDC transmission systems. Some of these aspects are the following [[7], [8]]:

- A dc link allows power transmission between ac networks with different frequencies or networks that cannot be synchronized for other reasons.
- Inductive and capacitive parameters do not limit the transmission capacity or the maximum length of a dc overhead line or cable. The conductor full cross section is fully utilized as there is no skin effect. This is valid for both overhead lines and sea or underground cables.
- HVDC transmission provides very fast control of power flow, which implies stability improvements, not only for the HVDC link but also for the surrounding ac system.
- The direction of power flow can be changed very quickly (bi-directionality).

- An HVDC link does not increase the short-circuit power at the connecting point. This means that it will not be necessary to change the circuit breakers in the existing network.
- For the same transmitted power, the need for ROW (Right Of Way) is much smaller for HVDC than for HVAC, and thus the environmental impact is smaller.
- An HVDC line can carry more power per conductor, because for a given power rating the constant voltage in a dc line is lower than the peak voltage in an ac line. This voltage determines the insulation requirements and conductor spacing. This allows existing transmission line corridors to be used to carry more power into an area of high power consumption, which can lower costs.

2.3.3 HVDC configurations

The three main elements of an HVDC system are as follows [6]:

- The converter stations at the transmission and receiving ends.
- The transmission medium.
- The electrodes which facilitate the earth current return path.

For bulk power transmission over land, the most frequent HVDC transmission line is used. This overhead line is normally bipolar, i.e. two conductors with opposite polarities. HVDC cables are normally used for submarine transmission. The most common types of cables are the solid and the oil-filled ones. The solid type, where the insulation consists of paper tapes impregnated with high viscosity oil, is in many cases the most economic one. No length limitation exists for this type and designs are now available for depths up to 1000 m. The self-contained oil-filled cable is completely filled with low viscosity oil and always works under pressure. The maximum length for this cable type seems to be around 60 km [[7], [9]].

The following are typical HVDC configurations (a dc line with associated converters is referred to as a pole) [9]:

- Monopole with an earth return or metallic return. With monopole designs, the earth electrode or metallic earth return conducts full current during normal operation as shown in Figure 2.1[9].

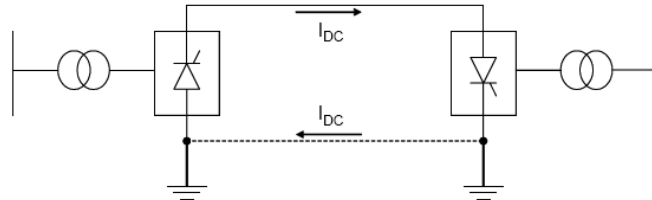


Figure 2.1: Monopole configurations with an earth or metallic return [9].

- Bipole with earth return or metallic return as shown in Figure 2.2.

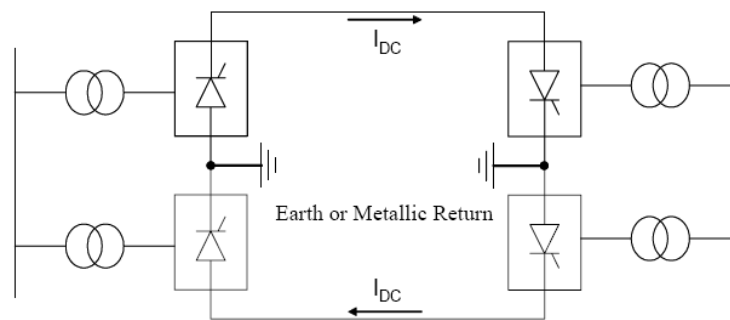


Figure 2.2: Bipole configurations with an earth or metallic return [9].

- Bipole without an earth return or metallic return as shown in Figure 2.3.

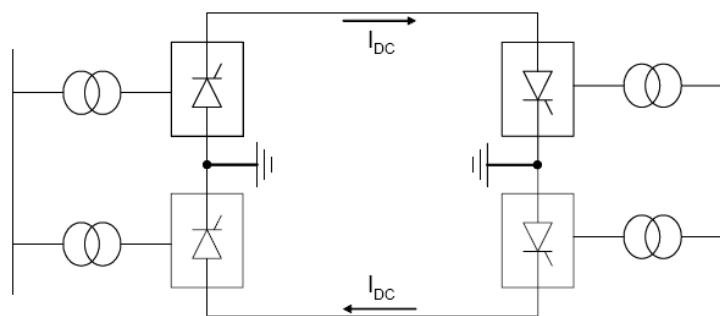


Figure 2.3: Bipole configurations without an earth or metallic return [9].

In a bipole configuration, the converter stations are arranged to operate at equal but opposite line voltages, so that the current in the earth return path is very small under normal operation. One of the advantages of the dc bipole configuration if there is a working earth return path or a metallic return is its 50% redundancy. With one pole out of service, the remaining pole operates in monopole mode and can still transmit 50% of the link power. Bipoles can be designed to transmit up to 75% of link power for short periods under contingencies, if the converter equipment is designed for short-time overload. Although the bipole configuration has a 50% redundancy, it is more expensive than the monopole arrangement. In some cases there is restriction on the operation of an earth return using earth electrodes, for environmental reasons [9].

2.3.3.1 Towers configurations

DC transmission lines are mechanically designed according to the same principles applying for normal ac transmission lines. The main differences are as follows [9]:

- The conductor configuration.
- The electric field requirements.
- The insulation design

Figure 2.4 shows two tower configurations, namely a monopole configuration with earth return and a bipole configuration with the same earth arrangement.

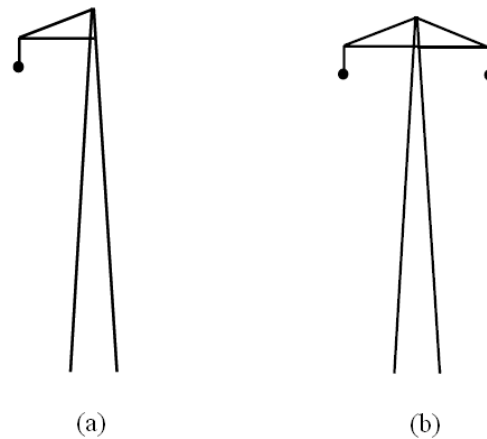


Figure 2.4: Tower configurations: (a) Monopole configuration with an earth return and (b) Bipole configuration with an earth return.

2.3.3.2 Insulators

The importance of insulators is sometimes underestimated. The development of insulators for extra-high ac voltages has taken place over many years. Due to the extremely variable and unpredictable nature of the surrounding atmosphere, this development has been based mainly on experimental data. It has led to an assessment of insulator performance by comparing it with corresponding performance for ac under the same range of operating conditions [[6], [7]].

There are various types of insulators used on HVDC lines. The three common types are as follows [6]:

- Cap and pin type.
- Long-rod porcelain type.
- Composite long-rod type.

The composite long-rod is widely used in HVDC systems. It has numerous advantages over its counterparts. The main reasons are hydrophobicity, light-weight, good mechanical strength, robustness, self cleaning properties, good corona behaviour, etc. [6].

2.3.3.2.1 *Insulation design criteria*

The adopted design criteria for HVDC insulation is based on the recommendations of IEC 60815. This standard was initially designed for ac lines and it has to be observed that the creepage distances recommended are based on the phase-to-phase voltage. When transferring these creepage distances recommended by IEC 60815 to a dc line, it has to be observed that the dc voltage is a peak-to-ground. Therefore, the creepage distance has to be multiplied with factor $\sqrt{3}$. Insulators operated under dc voltage are also subjected to more unfavourable conditions compared to ac voltages due to higher collection of surface contamination caused by the unidirectional electric field [10].

2.4 High voltage systems in Southern Africa

A large part of Southern Africa experiences heavy lightning activity. Apart from the physically devastating effect of direct strokes, the main effect as far as the power system is concerned has to do with induced overvoltages on the power system and hence, the power system insulation. These induced overvoltages are a main concern especially in medium voltages systems.

Africa is characterized by dispersed loads and generation sources spanning hundreds and in some cases thousands of kilometres. Connecting these generating sources and load centres is a challenge and one solution to address this challenge is via HVDC transmission. This section briefly discusses some existing and future HVDC projects in the Southern African region. At the moment, there are two schemes in Africa, namely the Cahora Bassa scheme interconnecting Mozambique and South Africa, and the Inga-Shaba scheme in the Democratic Republic of Congo (DRC) [[9], [11]].

Many of the South African Development Community (SADC) countries have major generation and transmission projects under construction or at various stages of planning. Loads in the region are growing at a rate of between 3% and 6%. The region's maximum demand is fast catching up with the installed generating capacity. Hence, there is a need for high capacity interconnections. With the potential and envisaged hydropower projects in the

Democratic Republic of Congo (DRC), the use of HVDC is becoming inevitable. The power utilities in the SADC countries will be seeking to maximize their reserve margins and trade any surpluses of power using transmission systems connecting the large new power sources with the large load systems in compliance with the South African Power Pool (SAPP). It is envisaged to have HVDC links between the DRC and Angola, South Africa, Botswana and Namibia as part of the Western Power Corridor (WESTCOR) [9].

As part of the current developments, a 1000 km HVDC line between Katima Mulilo and Gerus (outside Otjiwarongo) is already close to completion in Namibia. This will strengthen the Namibian transmission networks and ultimately the SADC interconnections.

These long lines are exposed to overvoltages induced by internal and external phenomena. These overvoltages pose a great danger to system insulation especially when the insulation is not adequately designed. Therefore, there is a need for research into the performance of insulation for transient overvoltages superimposed on a dc bias voltage.

2.5 High voltage insulation

In a dc system, overvoltages will occur at inverters, rectifiers and transmission lines during converter starting and shutting down operations, etc. The overvoltages caused by those activities are referred to as internal overvoltages. There are also external overvoltages caused by lightning and switching. Lightning strikes pose a great danger to insulation. Although there are shielding systems that protect power systems against lightning strikes, direct strikes are still possible. Most lightning problems however, come through indirect strikes.

2.5.1 Insulation level

For the HVDC lines, the correct insulation design is the most essential pre-requisite for undisturbed operation during the lifetime of the system. Generally, insulation design of a transmission line involves the following basic considerations [12]:

- The ability to withstand the operating voltage under abnormal weather conditions.

- The ability to withstand transient over-voltages arising from faults and switching operations.
- The insulation should be such as to reduce the likelihood of outages due to lightning strokes to an acceptable figure.

2.5.1.1 Insulator impedance

The impedance of a chain of discs or an insulator rod consist of a very high internal leakage resistance, surface leakage resistances, capacitances to each disc and the capacitances between discs. Contamination and atmospheric conditions play a big role in the impedance parameters. Similarly, the impedance of a gap consists mainly of the capacitance between the two electrodes.

With dc operation of an insulator string, the surface insulation resistance is responsible for the voltage distribution over the insulator as no capacitive current flow under steady state. Under dry, clean conditions the insulator leakage resistances are very high, and the voltage distribution might be determined by the electric field distribution [12].

Generally, the insulator strength depends on the clearance length between electrodes. If the surface of the insulator is fairly conductive, the creepage distance comes into play. Creepage distance and clearance length are two of the common terms used to describe an insulator's physical characteristics. These are illustrated in Figure 2.5. Creepage distance is the shortest path between two conductive parts, or between a conductive part and the bounding surface of the equipment, measured along the surface of the insulation. Clearance length is the shortest distance in air between the two electrodes of an insulator [13].

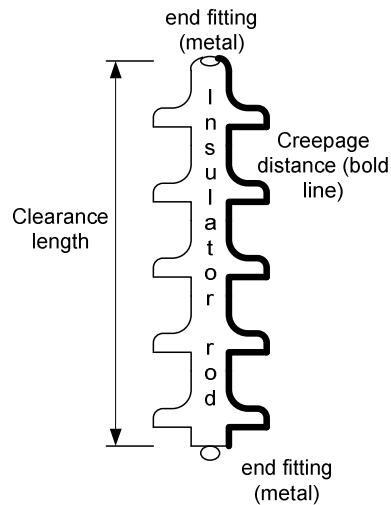


Figure 2.5: Definition of creepage distance and clearance length of an insulator.

2.6 Insulation materials under high voltage

The most important feature of any insulation material is that it can fulfil its function within the device with the required level of reliability for the whole of the design life. In order to determine whether the material fulfils this criteria, it is essential that the following three questions be answered [12]:

- What is the electrical stress distribution that the material will experience within the device.
- What is the breakdown strength of the material under these conditions and hence the device reliability.
- How does reliability change through the life of the device as a result of the reduction in the material breakdown strength (ageing) and changes in the electrical stress distribution.

Breakdown happens when the dielectric strength of the insulation material is exceeded. For air, it starts with corona, and is eventually followed by total flashover when the dielectric strength of the entire insulation path is exceeded [[14], [15], [16], [17]].

2.6.1 Corona discharge

Corona is a self-sustaining discharge occurring in air when the critical field strength is exceeded. It is the result of voltage stresses produced in the air surrounding a charged conductor. For conductors in air, the voltage gradient is maximum at the surface of the conductor and decreases by the relationship of $1/r$, where r is the radius of the conductor. As the conductor voltage is increased, the gradient also increases until a point is reached when the air immediately surrounding the conductor breaks down and becomes an ionized conducting medium [[12], [14]].

Corona is known to be initiated at the positive electrode by incoming natural electrons driven at ionizing velocity caused by the corresponding electric field strength, and at the negative electrode by outgoing electrons liberated by the impact of incoming positive ions. Corona is an extremely variable phenomenon. Apart from dependence on factors such as conductor type and diameter, distance between conductors (which is constant for a specific line), it also depends on atmospheric conditions and pollution on the surface and the roughness of the conductor [12].

Both ac and dc transmission lines can generate corona. For ac, corona is generated in the form of oscillating particles. For dc, it is in the form of a constant wind. Due to the space charge formed around the conductors, a dc system may have about half the loss per unit length compared to a high voltage ac system carrying the same amount of power. With monopolar transmission the choice of polarity of the energized conductor leads to a degree of control over the corona discharge. In particular, the polarity of the ions emitted can be controlled, which may have an environmental impact on particulate condensation (particles of different polarities have a different mean-free path) [12]. Negative corona generate considerably more ozone than positive corona, and generate it further below the power line, creating the potential for health effects. The use of a positive voltage will reduce the ozone impacts of monopole HVDC power lines [12].

2.6.2 Breakdown

If the voltage applied between two electrodes is raised, partial breakdown of insulation starts and when the voltage is increased further, the insulation breaks down entirely as the withstand level is exceeded. This constitutes flashover of the insulation material.

2.6.3 Breakdown in non-uniform dc fields

Tests with dc excitation show that in a uniform gap, the lowest flashover voltage is obtained when the sharpest electrode has a positive polarity with respect to the other electrode. This is due to different characteristics of positive and negative corona.

Once corona starts, the electric field becomes distorted by space charge. Here the dependence of the breakdown voltage on the electrode configuration is much more complex than the dependence of the corona onset voltage. In sphere-to-plane and point-to-point gaps, if the stressed electrode is positive, it acts differently to when the stressed electrode is negative [16].

The physics of the polarity effects in dc is explained in Figure 2.6 (a) and (b), where a positive and a negative sharp electrode is shown opposite a plane. In both cases, the electrons with a low mass are swept away by the field and are absorbed by the positive electrode. In Figure 2.6 (a) the heavier positive ions move away more slowly and positive space charge builds up near the sharp electrode. In the case of the positive sharp electrode, the positive charge may be seen as an extension of the positive electrode, thus reducing the gap and increasing the field in the remainder of the gap. The ionization processes are therefore accelerated and flashover occurs [15].

Exactly the opposite applies in the case of sharper negative point, as the space charge has a positive polarity that is different from that of the electrode. This is shown in Figure 2.6 (b). Basically, the space charge acts as a screen that decreases the field in its vicinity and thus tends to raise the breakdown voltage [16].

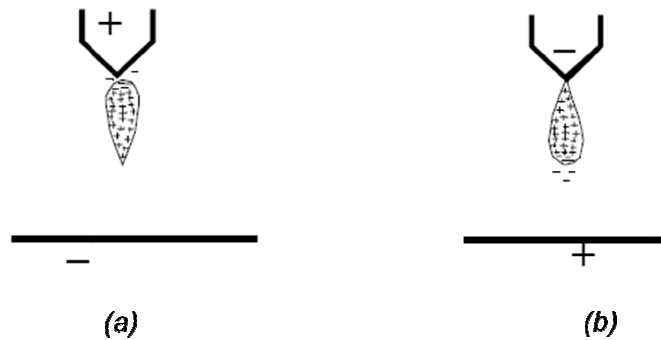


Figure 2.6: Illustration of the polarity effects with dc voltage: (a) When the sharp point is positive, and (b) when sharp point is negative [15].

2.6.4 Breakdown in non-uniform ac fields

For an ac system, the breakdown process is completed in an interval in an order of nanoseconds. This represents an extremely small fraction of a half cycle of the power frequency. Therefore, the mechanism of breakdown is essentially the same as for dc. The difference is that the ions in the gaps will be subjected to a slow alternating field. If the applied ac voltage magnitude is such that the voltage peak of the discharge onset condition is reached, electron avalanches will be produced in the same way as for dc. The space charge produced will have ample time to leave the gap before the field reverses polarity [[12], [15], [16]].

2.6.5 Breakdown for impulse voltages

It is important to appreciate that insulation breakdown under impulse voltages is different from cases of steady dc or low frequency ac. For an impulse, a time lag is observed between the instant the applied voltage is sufficient to cause a breakdown and the actual event of breakdown. The two basic relevant phenomena are the appearance of electrons for initiating the avalanches and their ensuing temporal growth [16].

In the case of slowly varying fields, there is usually no difficulty in finding an initiatory electron from natural sources, e.g. cosmic rays or detachment from negative ions. However,

under an impulse voltage of short duration in the order of microseconds, depending on the gap volume, natural sources may not be sufficient to provide the initiating electron at the appropriate site in time for the breakdown to occur. The probability of breakdown increases from zero to 100% over a suitable voltage range [17].

With impulse flashovers, the time that elapses between the application of the voltage and a voltage greater than the gap's static breakdown voltage and the appearance of a suitably placed initiatory electron is called the statistical time lag of the gap because of its statistical nature. After such an initial electron appears, the subsequent time required for the breakdown of the gap to materialize is known as the formative time lag. The sum of statistical time lag and formative time lag is the total time to breakdown. This is explained well by Salam et al [16].

2.6.5.1 Determining flashover and withstand of insulators

With the impulse voltages, it is more difficult to interpret the flashover level of an insulator as at certain voltage levels, as some of the impulses may result in flashovers while others result in withstands. Flashover is therefore a statistical phenomenon as it depends on the availability of initializing electrons and some environmental and atmospheric influences. Even in dc or ac tests, some variations may be expected. Figure 2.7 illustrates the principle of flashover and withstand for impulses [15]

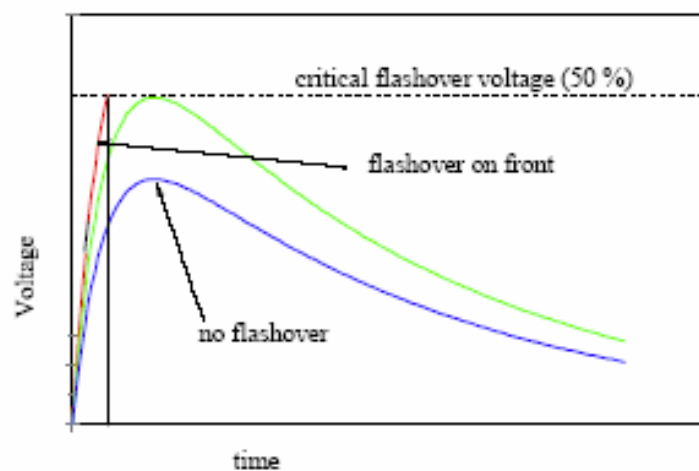


Figure 2.7: Illustration of flashover and withstand waveforms [15].

With impulse testing, the critical flashover value is not well defined. Out of a considerable number of tests, a number of them result in withstand and the others in flashover. Therefore, these test results are always treated in statistical terms. For an insulator, a probability curve as shown in Figure 2.8 can be constructed. The Critical Flashover Voltage (CFO) () of an insulator is a point on the probability curve where 50% of the applied tests results in flashover and 50% in a withstand. The CFO is also referred as U_{50} or V_{50} .

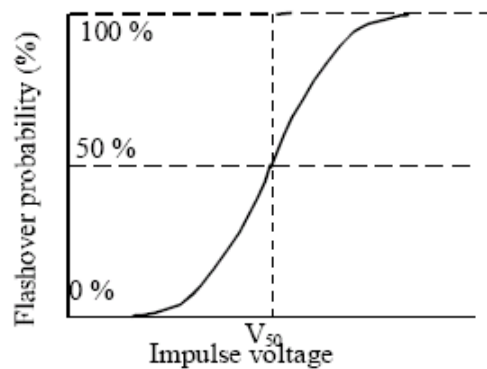


Figure 2.8: Illustration of an impulse flashover probability curve [15].

There are various ways of determining this value as explained in the relevant IEC publication [10]. One of the notable methods is called an up and down method, which often determines the 50-percent flashover probability of a test object with a sufficient degree of accuracy for practical engineering applications.

For a rough estimation of a percentage flashover zone, a start is made at low voltage and is increased in steps of about 10 percent after each voltage application until the first flashover is recorded. The real test procedure then starts. The voltage is reduced with an amount in the range of 1 to 10 percent of the initial flashover value and up again when necessary. The average of 50-percent flashover voltage value is then determined after a considerable number of impulses have been applied, i.e. 10 flashovers, 10 withstands, etc. This method of determining the flashover voltage value is explained in [18].

2.6.5.2 Comparisons of flashover levels

For air-gap arrangements, dc flashover voltages are almost the same as 50 Hz ac flashover voltages. Under wet conditions, all flashover voltage levels are affected, the effect is worse with negative dc voltage especially in the rod-rod arrangement. For composite insulators, positive and negative dc flashover voltages are lower than the 50 Hz ac flashover voltages, for both dry and wet conditions. Wet conditions cause the flashover voltages of composite insulators to fall to up to 50 percent of the dry and clean flashover voltage level. It is under wet conditions that negative dc flashover voltages are extremely affected [19].

As for impulses, under dry conditions, the highest flashover is obtained with a negative impulse voltage. Typically, for a given gap spacing, the positive lightning impulse breakdown will be at least 30 percent higher than the positive switching-impulse breakdown. Therefore, positive switching impulses are ideal in the determination of air gap requirements [[2], [19]].

Figure 2.9 and Figure 2.10 give a general view of the behaviour of the rod-plane and rod-rod gaps at dc, ac, switching and lightning impulses. With the scope of available data, the dc voltage characteristics approach the ones of standard impulses more than any other.[20]. These tests were performed at Chalmers Institute of Technology (CTH) laboratories. These are withstand voltage levels of these configurations. Because of polarity effects, characteristics obtained with a pointed positive electrode are usually more important for practical applications [20].

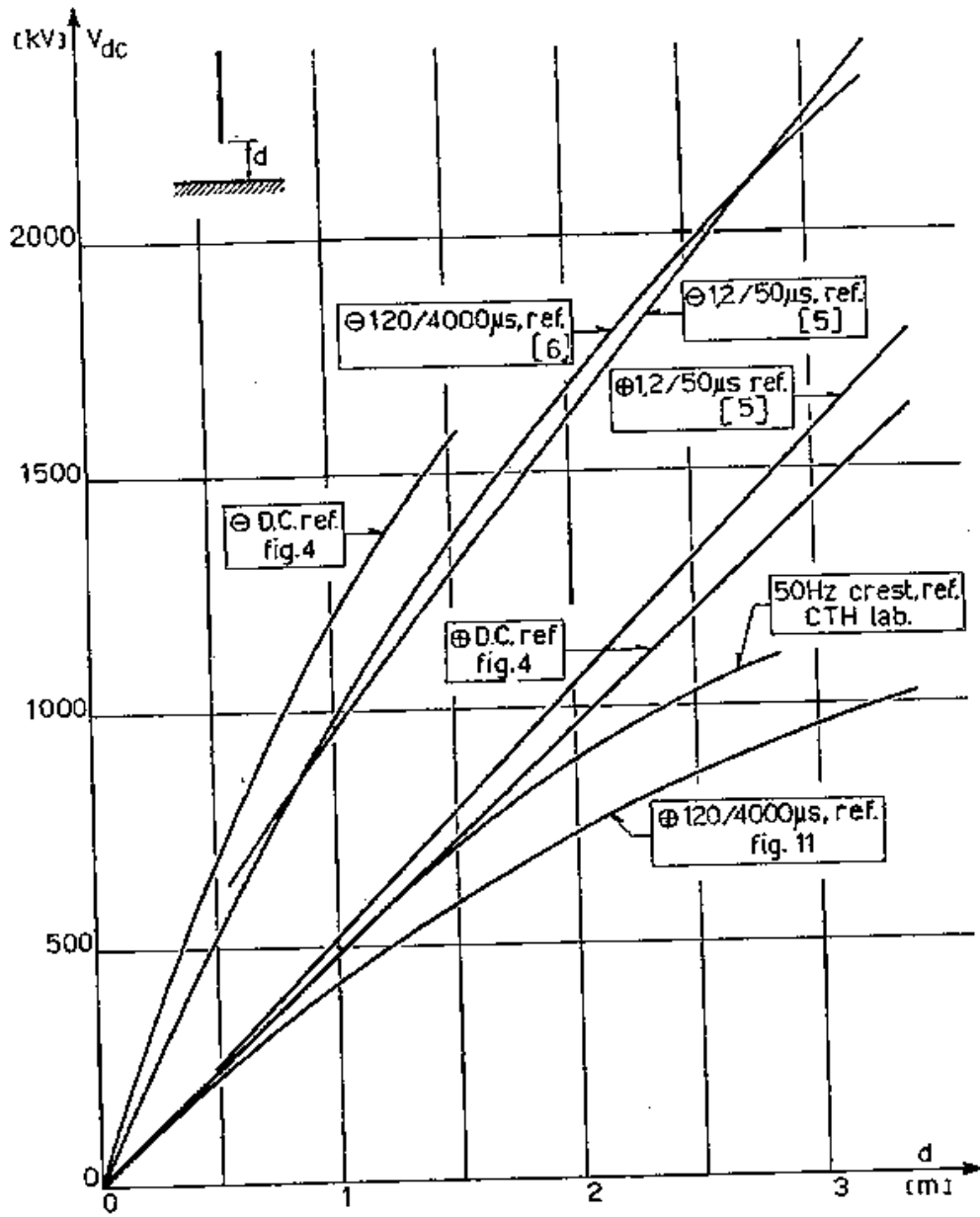


Figure 2.9: Rod-plane gap 50-percent flashovers as obtained in CTH laboratories [20].

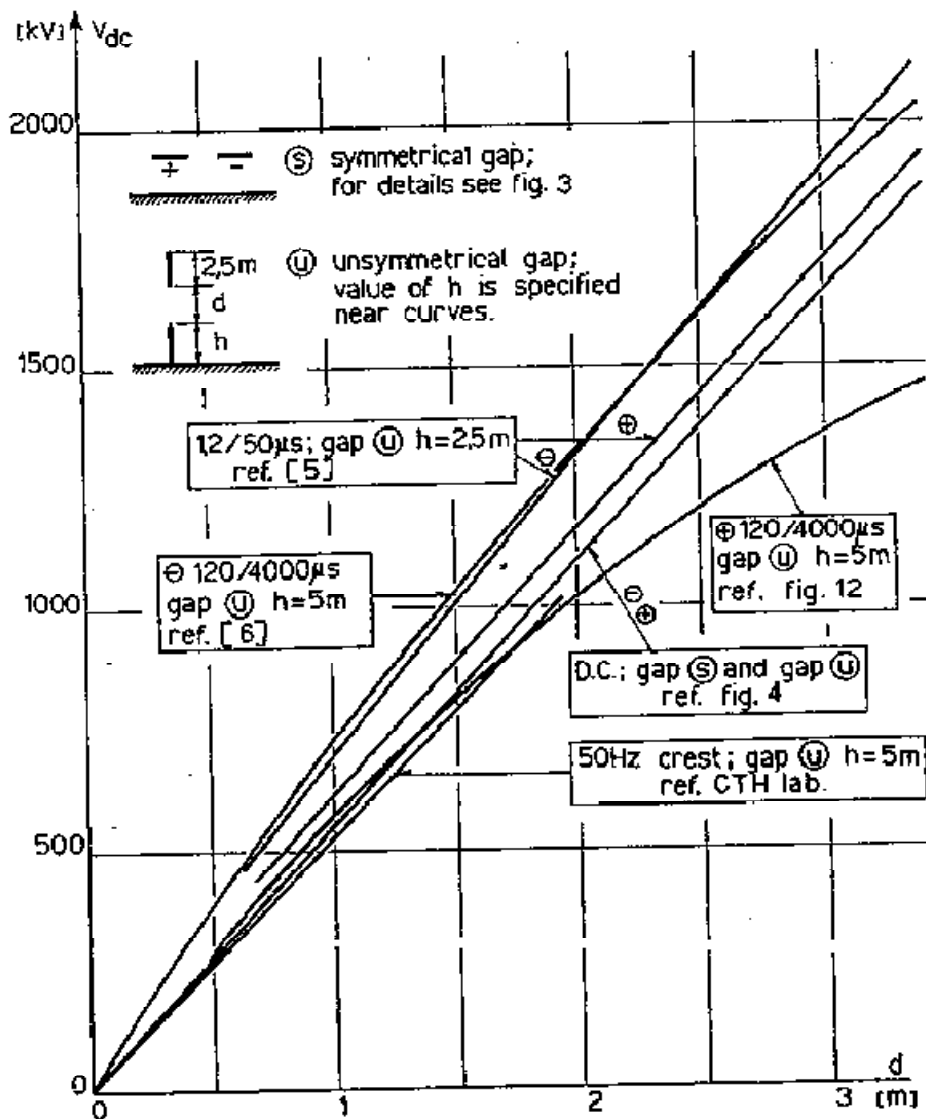


Figure 2.10: Rod-rod gap 50-percent flashovers as obtained in CTH laboratories [20].

2.6.6 Impulses superimposed on system voltages

The most practical scenario of impulses superimposed on dc voltage experiments is the effect of overvoltage impulses on power systems. These impulses are caused by lightning or re-energization (switching) of power systems. In the case of lightning, the impulse hits the fully energized line so the impulse gets superimposed on the ac or dc system voltage. In the case of switching, it can be auto-reclosing of a system or manual switching after a long absence of

power. Auto reclosing happens so fast that the line, especially in the dc case, is still holding a high amount of dc space charge, so in a sense it will be the superposition of an inrush impulse on a dc system.

Many researchers and authors have gone into the question of fundamental air-gap arrangements, but the behaviour of how insulators behave for complex waveforms also needs understanding. Different circuits to perform impulse tests on insulators under dc bias have so far been proposed and developed and some results have been gathered from past experiments.

Most often, it is the positive polarity that is considered because negative polarity gives larger flashover voltages for the same insulator arrangement. Tests on air gap arrangements have been explained by Feser, Knudsen and Watanabe [[4], [20], [21]]. Different circuit arrangements to perform impulse flashover tests of insulators under dc bias voltage have been proposed and used, and the circuits all contain similar basic components like impulse generator circuits, dc supply circuits, coupling (shielding) components and of course the test object [[2], [4], [20], [21]].

The work of Knudsen and Iliceto expanded the knowledge in this area up to a gap spacing of 3m. Figure 2.11 and Figure 2.12 show the results of work done with rod-to-rod and rod-plane gaps with a positive switching surge (120/4000 μ S). Figure 2.11 shows the comparison of impulse and dc CFO across a rod-to-rod gap. Figure 2.12 shows dc and impulse characteristics of the rod-plane gap with different voltage configurations V_{dc} and V_i . The effect of wetting is also shown [21].

A large amount of data is available in the technical literature on the switching impulse characteristics of insulator strings, but no test experiments were done with the dc pre-stressed arrangement. The influence of rain on impulse withstand depends mainly on the electrode arrangement, and it has been observed that the negative impulse flashover level is more affected by wetting than by positive impulse withstand [[19], [20], [21], [22], [23]].

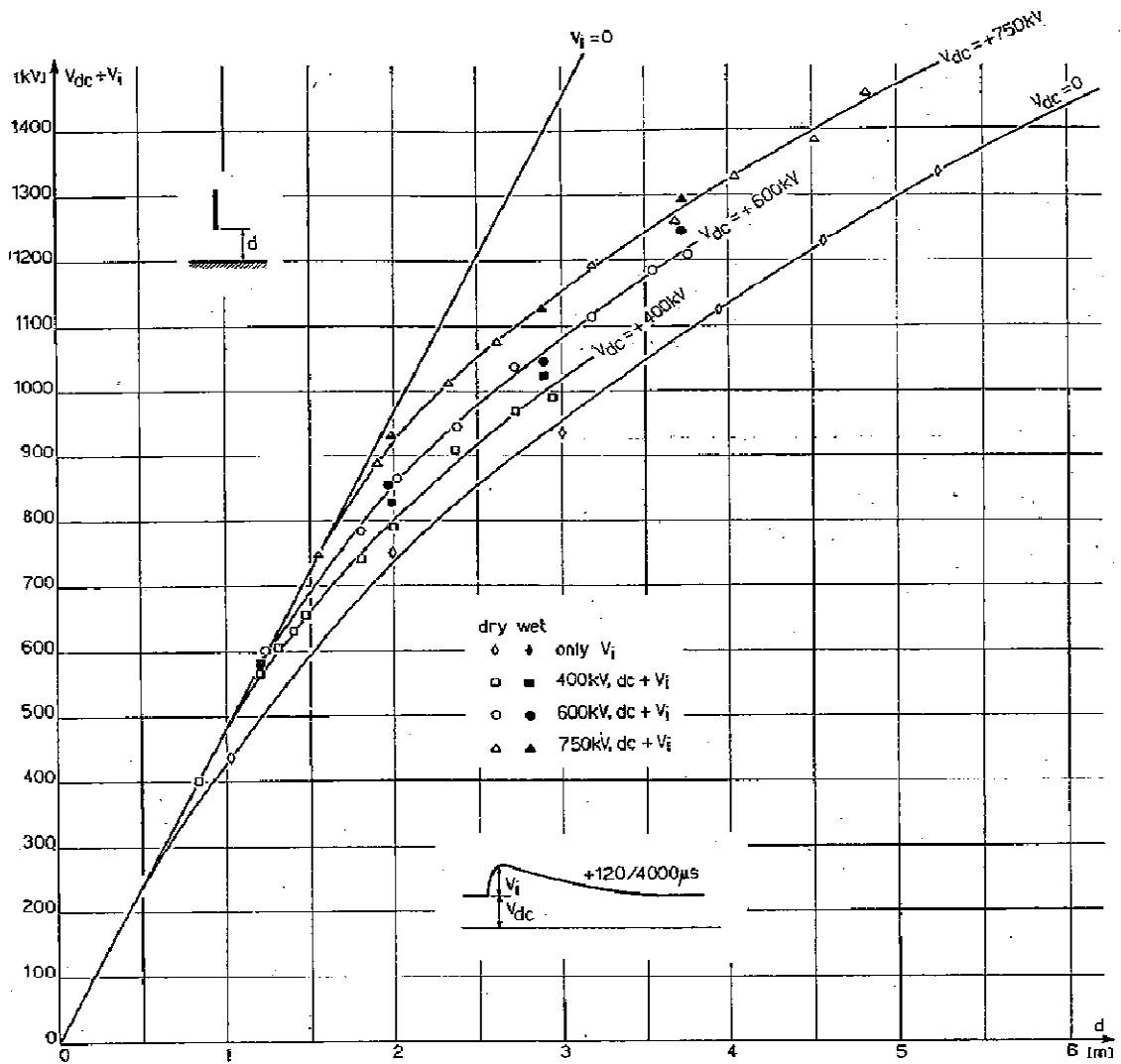


Figure 2.11: Rod-plane gap 50-percent flashover voltages, switching surges applied, positive polarity, dry and wet conditions. Air conditions: Humidity 8-10 g/m³; Temperature 21-23° C; Pressure 760mmHg [20].

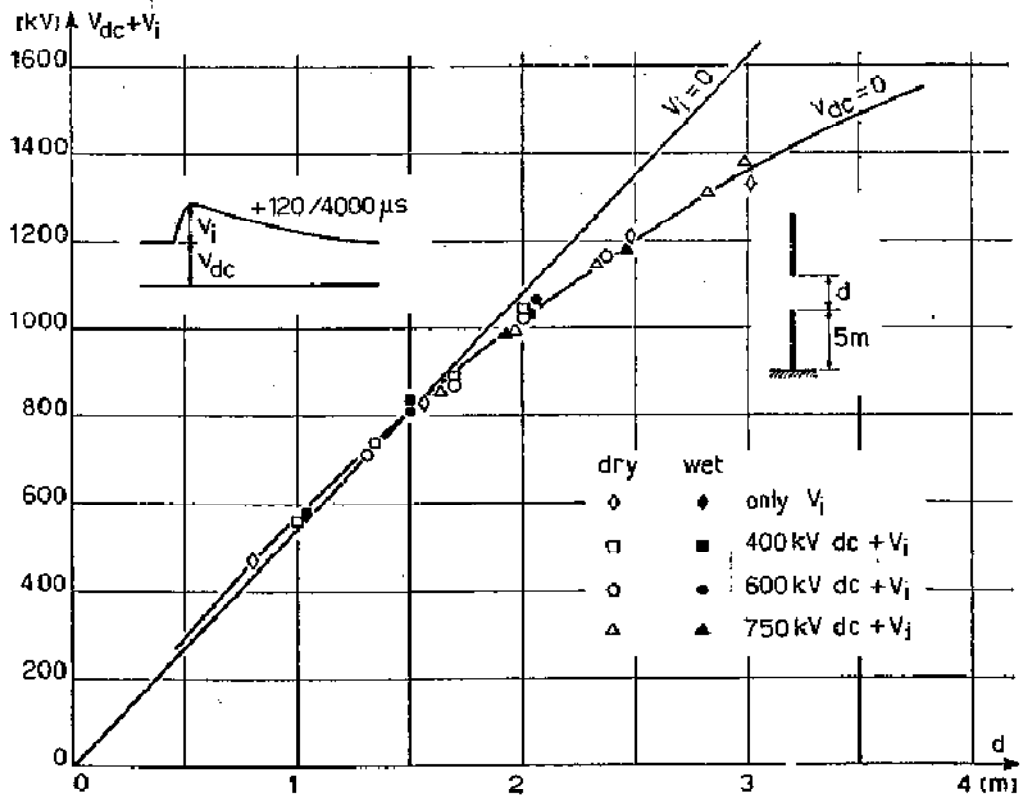


Figure 2.12: Rod-rod gap 50-percent flashover voltages, switching surges applied, positive polarity, dry and wet conditions. Air conditions: humidity 11 g/m³; temperature 21-23° C; Pressure 770 mmHg [20].

2.6.6.1 Test circuit arrangements

The test circuits employed by authors differ in some respects from each other. However, they all consist basically of impulse circuit, dc source, a test object (object under test) and some coupling components [[2], [4], [21]]. Figure 2.13 shows a block diagram of the arrangement.

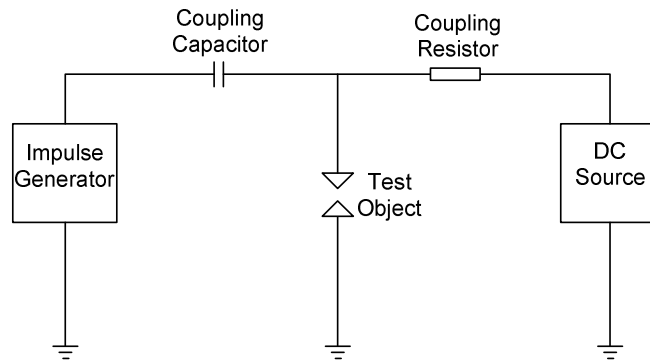


Figure 2.13: A block diagram of the circuit configuration.

The coupling components come in the form of a resistor shielding the dc circuit and a capacitor shielding the impulse generator. Sometimes an air gap is used in the absence of a coupling capacitor, as discussed by Watanabe [21]. A proper design of these coupling components is essential in order to protect the respective sections of the circuit effectively.

2.7 Insulator pollution

Contamination of insulators is naturally of most significance in the polluted atmosphere of heavy industrial areas and salty atmospheres near the coast. Most forms of industrial pollution, such as soot and cement, are not very conductive so long as it is dry. When moistened by rain, mist or fog, these contaminants produce a conducting film. Continuous rain has the advantage of washing off the contaminants from insulators, but mist, fog and light drizzling rain produce no washing effect. The worst kinds of contamination are those that contain a high proportion of soluble matter. This mixture creates a conducting film on the insulator surface, such that a current flows through the contamination layer [24].

At locations such as the narrow portion of a post insulator or in the rib area underneath a line insulator, the current is concentrated to such a degree that the layer dries, i.e., a dry band is created. The total line-to-ground voltage now appears across these small dry bands, and flashover of dry bands occurs. These arcs gradually grow outwards, and total flashover occurs when the arcs extend and meet [12].

2.7.1 Mechanism of contamination flashover

Contamination flashover occurs when insulators become coated with a wet conducting film containing dissolved salts. As current flows through the conducting surface film, the heat is dissipated evaporating some of the moisture, causing dry bands to form. On suspension insulators, the dry bands usually form near the cap or pin where the current flow is most concentrated. Because these dry bands have much greater resistance than the wet surface, the voltage stress concentrates across them, occasionally leading to small, intermittent scintillating electric discharges bridging the dry band. These scintillating discharges are visible and range in current from a few milliamperes to about one ampere peak [[25], [26]].

As the surface is wetted further, the discharge current increases until at some point the discharges elongate to bridge the entire insulator and trigger an arc. Because the flashover discharges grow along the insulator surface, the hot power arc which follows their path may damage the insulator [26].

Once the arc bridges the insulator, there is no longer any series resistance to limit the current, and a power arc develops. In reality, there may be many dry bands and discharges on the insulator depending on insulator shape and contamination distribution.

The equivalent circuit of a wet insulator can be represented by a network of capacitances only as depicted by C_{glass} in Figure 2.14. The distribution is usually non-uniform, mainly as a result of capacitance between insulator sections and ground denoted by C_{air} in Figure 2.14. As wetting progresses, a conductive pollution layer represented by R_{pol} is formed. The surface impedance becomes a combination of capacitance and resistance. The resistance value associated with a section is influenced by the drying effect created by leakage current, which is a function of the voltage across the section. Therefore, the resistances of different sections are not equal to each other [[12], [16]].

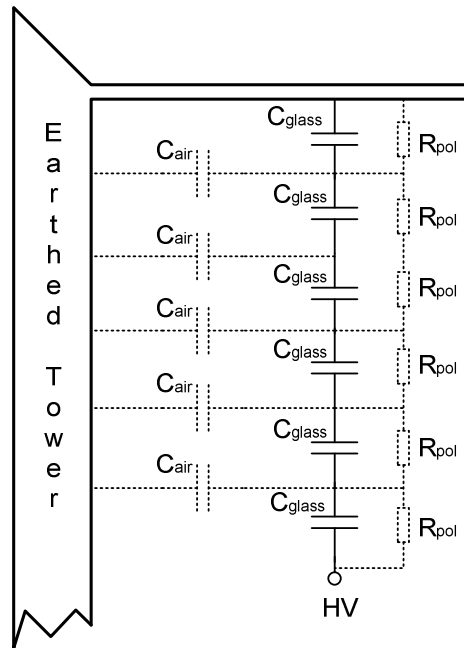


Figure 2.14: Impedance model of an insulator string [15]

2.7.2 Severity of contamination

Dry contamination usually has little effect on the flashover voltage of insulators. A decrease in flashover voltage, if any, occurs only when the layer becomes conductive due to high humidity, fog or rain [19]. A critical amount of wetting is needed to affect the flashover of any insulator to any extent.

The contamination material can be viewed as consisting of two components, namely conductive and inert components. The most common conductive component consists of ionic salts such as sodium chloride, magnesium chloride, sodium sulphate, etc. These salts, when in solution, influence the flashover voltage by providing a conductive coating on the surface of the insulator. The severity of contamination due to these salts is generally quantified in terms of the Equivalent Salt Deposit Density (ESDD) stated in units of mg per cm^2 NaCl. ESDD is the equivalent amount of NaCl that would yield the same conductivity at complete dilution. ESDD considers only the steady state solubility of the contaminant [27].

Another important consideration, although difficult to quantify, is the rate at which the salt dissolves into the solution [24]. Thus, the influence of a slowly dissolving salt such as magnesium chloride on the flashover voltage is much less than that of a rapidly dissolving salt such as sodium chloride.

The inert component of the contaminant is the portion of the solid material which does not go into solution as ions. This inert component may, however, decrease the electrical withstand strength. Materials such as silicon dioxide, clays (kaolin, bentonite, etc.) and industrial cement may form a mechanical matrix in which particles of a conductive component are embedded. The presence of this matrix generally decreases the effect of natural or mechanical washing of the insulator. The increased resistance to natural washing is particularly noticeable in the pin region of suspension insulators and is probably a factor in the significant difference in contamination usually observed between top and bottom surfaces [27].

Inert materials may be hydrophilic (clay, silicon dioxide, inorganic cement, etc.) and increase the wetting rate of the insulator, or hydrophobic (oil, grease, etc.) and decrease its effective wetting [26].

2.7.3 Artificial contamination

Laboratory tests are frequently employed to assess the contamination flashover characteristics of different insulator types. Since these tests are performed under laboratory conditions, a standardized method of artificially contaminating these insulators is necessary to simulate the field condition as closely as possible. There are various methods to achieve this process. The most widely used methods to evaluate the pollution flashover performance of high voltage insulators is described in the standard IEC 507 [28].

The salt fog method is the oldest method recognized in international standards. This is the salt spray test as developed in United Kingdom [27]. The test consists of the simultaneous application of voltage and a salt fog having a specific salinity, defined in terms of kg of NaCl per cubic meter of water. If no flashover occurs within about one hour, withstand is recorded.

The salinity for which three or four such tests are withstood is termed the withstand salinity for the applied voltage.

Two solid layer procedures have been developed. The *A* method solid layer procedure, developed by the Germans, consists of (a) applying the uniform layer of NaCl and Kieselgur (diatomaceous earth) to an insulator, (b) drying the insulator until ambient conditions are reached, (c) moistening the insulator with steam until the layer reaches maximum conductance, and then (d) applying the voltage and continuing the steam fog [27]. The mixture consists of 100g of Kieselgur, 10g of silicon dioxide, 1000g of water and a suitable amount of NaCl. Another alternative to the solid layer method is the kaolin composition. This mixture consists of 40g of kaolin, 1000g of water and suitable amount of NaCl [[13], [28]].

The *B* method solid layer procedure, developed by *IEEE*, entails spraying or dipping the insulator in the contamination mixtures such as, Kaolin or Kieselgur [27]. Drying and cooling of the contaminated insulator might be necessary. Voltage is then applied across the insulator for flashover determination. This test simulates the slow build up of the contamination of an energized line and is the best representative test of the three, since the test conditions represent the usual contamination event [[13], [29], [30]].

2.8 Power system impulse overvoltages

The study of overvoltages on power systems takes cognizance of their magnitudes, shapes, durations and frequency of occurrence. Disturbances of electrical power transmission and distribution systems are frequently caused by two kinds of transient voltages whose amplitudes may greatly exceed the peak amplitudes of the nominal operating voltage. These are lightning and switching impulse overvoltages [17].

The waveshapes associated with the overvoltage impulses are represented by equation 2.1, where α and β are circuit constants of the order of microseconds and V_g is the charging voltage (voltage across the charging capacitor) [17].

$$V_o = \frac{V_g}{k} [e^{-(\alpha-\beta)t} - e^{-(\alpha+\beta)t}] \quad (2.1)$$

The equation represents a unidirectional curve which usually has a rapid rise time to the peak value and slowly falls to zero value. Impulse waveforms are specified by defining their rise or front time, fall to 50% peak value (referred to as tail time), and the peak voltage value. Thus, 1.2/50, 1000kV wave represents an impulse voltage waveform with a front time of 1.2 μ s, tail time of 50 μ s and a peak of 1000 kV [[29], [32]].

Figure 2.15 illustrates the definition of an impulse waveform. The peak value is when the voltage is at 1.0 per unit. Although the definitions are clearly indicated, it should be emphasized that the virtual origin O_1 is defined where the line AB cuts the time axis. Time t is the time between the instants when the pulse is 30 per cent and 90 percent of the peak value. The front time (t_1) is a virtual parameter defined as 1.67 multiplied by t . The tail time (t_2) is defined as the time from the projected line that meets at O_1 to the time it takes for the wave to fall to 50% value [17].

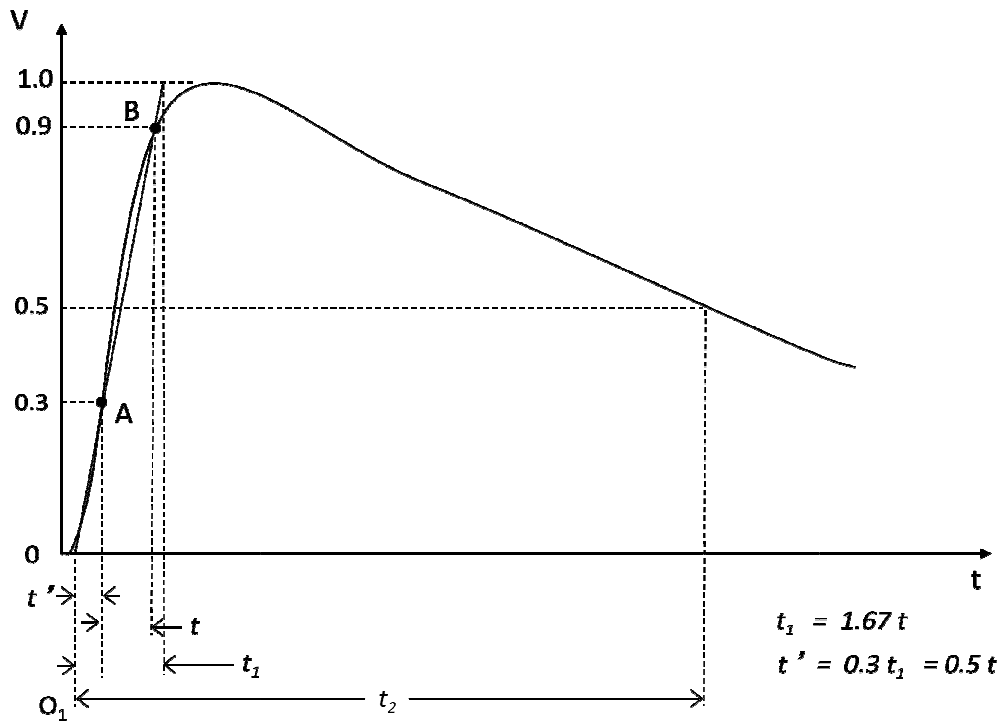


Figure 2.15: Illustration of the impulse waveform and its definitions [17].

2.8.1 Lightning overvoltages

The most severe lightning incident occurs when lightning strikes a phase conductor of the transmission line directly, as it produces the highest overvoltage for a given stroke current. The probability of direct strikes is however small, due to the fact that electrical lines are shielded from lightning. In most cases it is the induced voltages from indirect lightning strikes that affect the power systems.

The lightning current injected into the ground causes a potential rise near the electrode. Since the lightning induced current near power lines contains a high frequency component, it induces high frequency voltage into power systems. The magnitudes of lightning induced overvoltages can be in the region of mega-volts (MV) and the duration is in the order of tens to hundreds of microseconds. A typical lightning impulse waveform is expressed as 1.2/50 μ s [17].

2.8.2 Switching overvoltages

When the power flow of a transmission line is interrupted, overvoltage transients result. These are as a result of oscillatory effects of the system's capacitances and inductances. Depending on the damping, these oscillations could last a few cycles. Typical sources of these overvoltages are:

- Energization of lines and cables
- Reenergization of a line
- Load rejection
- Fault initiation and clearing.

Where the lightning impulse dies out in approximately one hundred microseconds, the switching impulse lasts for some milliseconds. The standard values for the time parameters of switching impulses are 250 μ s for time to peak and 2500 μ s for time to half value. The tolerances for these times are 20% and 60%, respectively. The tolerance for the peak value is 3% [17]. The time parameter definitions as illustrated in Figure 2.16 are different from those

for lightning impulse. There is no front time definition for a switching impulse. Instead, the time to peak T_p is defined as the time interval between the actual origin and the instant when the voltage has reached its maximum value. The time to half value T_2 , is the time interval between the actual origin and the instant when the voltage has first decreased to half the peak value. Because of their longer durations, switching surges are accompanied by energies much larger than for lightning impulses [16].

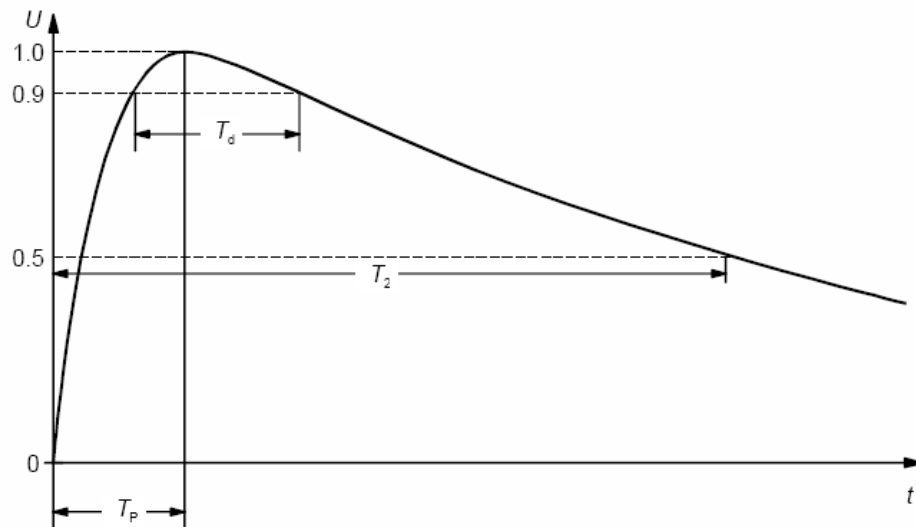


Figure 2.16: Definition of a switching impulse waveform [16]

2.9 Generation of impulses for laboratory experiments

In high voltage laboratories, the generation of high voltages (dc, ac and impulse voltages) are required for several applications. Testing the insulation of power apparatus requires high voltages of up to millions of volts. Simulation of overvoltages that occur in power systems requires high impulse voltages of very short to longer durations.

There are various types of these generators available, but they all work on the same principle. The rapid increase and slow decay can obviously be generated by discharging circuits with two energy storage components as the waveshape is basically a superposition of two exponential functions. These circuits are shown Figure 2.17.

2.9.1 Single-stage generator circuits

There are two common basic single stage impulse generator circuits. They are as shown in Figure 2.17 (a) and (b) respectively. Capacitor C_g is slowly charged from a dc source until the spark gap G breaks down. This spark gap acts as a voltage limiting and voltage sensitive switch, whose time to breakdown is very short in comparison to the waveform front time. Sphere gaps are ideal for this purpose. In bigger impulse generators, the charge voltages can be of the order of megavolts (MV).

Resistors R_d , R_e and capacitance C_g form the wave shaping network. R_e will primarily damp the circuit and control the front time t_f while R_d will discharge the capacitors and therefore essentially control the wavetail. Capacitance C_L represents the full load, i.e. the capacitance of the load itself and the other capacitive elements in parallel with the load component. When the spark gap breaks down, capacitor C_g discharges into the circuit consisting of R_d , R_e and C_L . Multiple stage impulse generators are discussed in the next section.

The basic simplified circuits of the double exponential impulse generator are shown in Figure 2.17 (a) and (b).

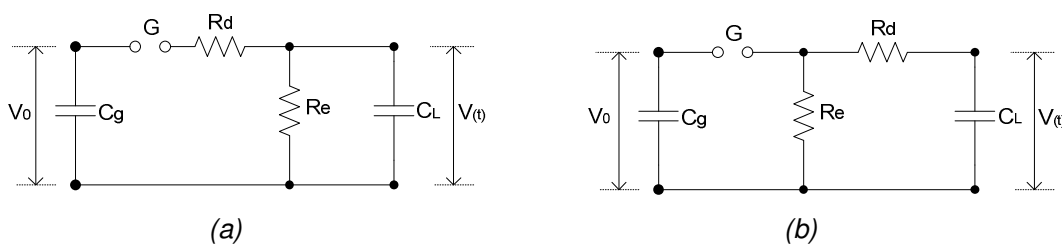


Figure 2.17: Two basic types of single stage impulse generator circuits [17].

These are used to generate fast impulses, and for slightly slower impulses i.e. switching, various modifications are applied. The addition of a series inductance with R_d is one of the possible methods applied to obtain a longer time impulse wave [17]. The difference in circuit arrangements also causes a difference in the efficiency of the impulse generators.

The d.c. voltage (V_g) is obtained from a high voltage transformer combined with a high voltage rectifier. The d.c. need not be very smooth as it only has to charge the first capacitor to peak value.

A sphere gap is used as the switch, and as the charge on the capacitor builds up, so does the voltage across the sphere gap. The sphere can be allowed to fire naturally or for more accurate operation it can be controlled through various methods. A trigatron spark gap is one of the common methods [17].

2.9.2 Multiple stage impulse generators

For reasons below, the single stage circuit can become inconvenient in the generation of especially very high voltages [16].

- The difficulties encountered with spark gaps for the switching of very high voltages.
- The increase in size of the circuit elements.
- The efforts necessary to obtain high d.c. voltages to charge C_g .
- And last but not least, the difficulties of suppressing corona discharges from the structure and leads during the charging period.

Smaller single-stage circuits can be cascaded into a multi-stage circuit with a higher magnitude of output voltage. The basic idea is to charge a number of capacitors in parallel through a rectifier from a high voltage transformer. The charged capacitors then discharge in series, giving the nominal output voltage equal to the charging voltage multiplied by the number of stages in the impulse generator.

In the practical circuit, the capacitors are not all charged to the same voltage, due to the series resistances associated with the charging circuit, these not being negligible compared to the leakage resistances of the capacitors. In theory, the number of stages of the generator may be increased to give almost any desired multiple of the charging voltage and it has been found feasible in practice to operate a 50-stage impulse generator. The number which can be used

successfully is limited by the fact that the high resistance between the supply and the distant capacitors reduces the impulse voltage obtainable [16].

Two of the commonly used multiple stage impulse generator circuits are Marx Impulse and Goodlet circuits. Since the principles involved are similar, only one is fully explained.

2.9.2.1 Marx impulse generator circuit

In multiple stage circuits, various circuit stages are charged in parallel and discharged in series. This principle was invented by Marx in 1923. There are many different types of multistage impulse generators and some modifications have been made to the initial Marx circuit [29].

In Figure 2.18, resistors R_{L1} to R_{L8} are the charging resistors, which are very high in value. They are selected in such a way that charging of all capacitors occurs in about one minute. The waveshaping circuit is external to the capacitor stages shown. The waveform of the impulse generated also depends on the resistance, inductance and capacitance of the testing circuit connected [17].

For correct operation, all the gaps in the impulse generator should be approximately of the same spacing. The spheres of the gaps are typically fixed along an insulating rod which can be rotated so that the gaps simultaneously increase or decrease as required.

In the case of a controlled impulse generator, the magnitude of the impulse voltage is not directly dependent on the gap spacing as in the case of uncontrolled generators. In this case, a certain range of impulse voltages are available for the same gap spacing. This range is determined by the various considerations, so that (a) uncontrolled operation should not occur, (i.e. the spark over voltage of the gaps must be greater than the applied direct voltage) and (b) the spark overvoltage must not be very much larger than the applied voltage (in which case breakdown cannot be initiated even with the pulse) [[17] [33]]. An eight-stage Marx type impulse generator circuit is shown in Figure 2.18 [33]. This circuit is similar to the one used at the University of Stellenbosch's high voltage laboratory.

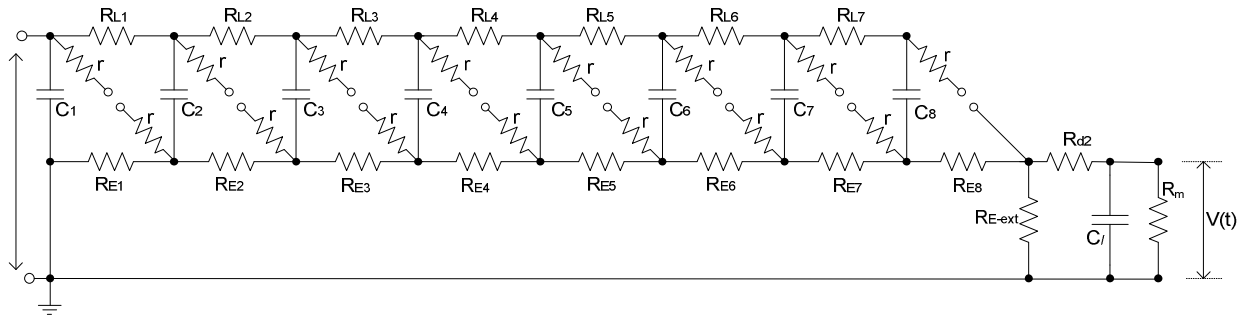


Figure 2.18: An eight stage Marx type impulse generator circuit diagram [33].

2.9.2.2 Goodlet impulse generator circuit

The Goodlet impulse generator circuit is very similar to the Marx impulse generator circuit. The difference is that the Goodlet circuit yields a negative polarity output for a positive polarity input while the Marx circuit yields the same polarity output [17].

2.9.3 High voltage construction kits

The high voltage construction kit is a system of components for high voltage test applications. All components have the same length and mechanical interconnections. They can be combined to form a test configuration and yields an very versatile test system.

Test configurations are available which allow the generation of ac voltages up to 300 kV, dc voltages up to 400 kV and impulse voltages up to 400 kV with different output power ratings. These test configurations are compact and their flexibility allows the test system to be matched to the conditions prevailing in the test room (dimensions, height etc.). The application range of the high voltage kit covers not only use in high voltage laboratories of technical universities, but also use as an industrial test system for routine and type tests on electrical equipment [34]. Indeed there are various types of high voltage kits available, in the design of which different points have been emphasized. The high voltage laboratory at the University of Stellenbosch has a two-stage Messwandler Bau construction kit.

2.10 Measurement technologies used in high voltage in laboratories

In industrial testing and research laboratories, accurate measurement of high voltages, i.e. dc, ac, or impulse voltages, is one of the most essential aspects that determine the type of tests that can be performed. There are many challenges involved in these measurements. These challenges increase with the magnitude of the voltage and with frequency.

The classification of the measuring methods according to the type of voltages to be measured is challenging. Instrument transformers, sphere gaps, current and voltage dividers are some of the common tools and principles used in measurement.

Voltage dividers essentially consist of two impedances connected in series. The components that constitute the impedances are referred to as the high and low voltage arms of the divider. Connection between low voltage arm and the recording instrument (oscilloscope, etc.) must be with a shielded coaxial cable. This is done to avoid the adverse effects of stray capacitance between that connection and the high voltage arm. High Voltage dividers generally consist of either resistors or capacitors, but sometimes a combination is used, either in series or in parallel to obtain the optimum results [16].

2.10.1 Resistive voltage dividers

Resistive voltage dividers are most suited for the measurement of dc voltages. They usually have very high resistance values to limit the amount of current drawn from the dc supply.

When a time-dependent voltage (ac or impulse) is connected to a resistive divider, stray capacitance will influence the divider accuracy. The most general representation of these dividers has to assume inductive components in series with the resistive elements, capacitance elements in parallel with high-arm resistor and stray capacitances to ground. The high resistance values in conjunction with the inherent stray capacitances and series inductances will cause undamped oscillations (resonance) to occur across the device when subjected to an impulse voltage [16].

However, in practice, the parallel capacitance and series inductance have minimal effects on the operation of the divider. Therefore, these can be neglected, unlike the stray capacitance to earth. Figure 2.19 shows the common equivalent circuit representing the voltage divider circuit when a low to high frequency signal is applied. Resistor R_1 is the high-voltage arm of the divider, and R_2 the low-voltage arm. To achieve a low voltage at the LV terminal, R_1 will have a very large value compared to R_2 .

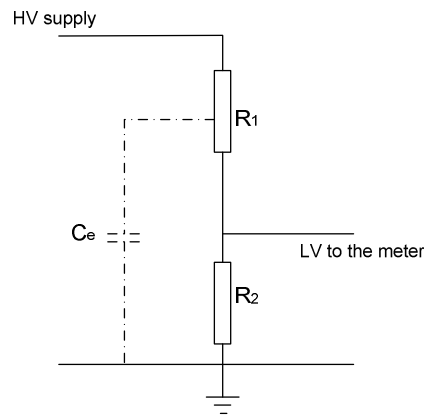


Figure 2.19: An equivalent circuit of the resistive voltage divider [16].

Stray capacitance C_e , causes the step response of a resistive voltage divider to exhibit a gradual approach to the final value, thereby increasing the response time. Equation 2.2 shows the dependency of the response time, T^0 on the stray capacitance C_e , and the resistance value, R of the divider. The capacitance value is a function of the resistor column dimensions which is bound to the rated voltage and is therefore fixed [17].

$$T^0 = \frac{RC_e}{6} \quad (2.2)$$

High value resistive voltage dividers can be damaged when subjected to sudden voltage changes due to an unequal voltage distribution across the individual elements of the resistor [40]. The unequal voltage distribution is brought about by the different stray capacitance values from the top to the bottom of the divider column. For these reasons high value resistive voltage dividers cannot be used to measure fast transients. There are however some ways to improve the unit step of such dividers as explained by Kuffel [17].

A further problem is created by heat dissipation within the resistors. For constant R values and increasing voltage, the energy dissipated in the resistive materials increases proportionally with V^2 , where V is the applied voltage. During the short time of voltage application not much heat can be transferred to the surrounding insulation material. The energy must be stored within the resistor. A calculation of the temperature increase within the wire-wound metal resistors will indicate the difficulties of achieving low inductive resistor units suitable for this high voltage stress. These are some of the main reasons why resistor voltage dividers for voltages higher than 1.5 - 2 MV and resistance values of 10-20 $k\Omega$ cannot be built [[2], [16], [17]].

2.10.2 Compensated resistive dividers

Compensated resistive voltage dividers are made up of distributed components. A resistor in parallel with a capacitor forms the distributed elements of the divider. This type of divider acts as a resistive voltage divider for dc voltages. The objective of this method is to reduce the effect of stray capacitances to earth. The equivalent circuit of this arrangement is illustrated in Figure 2.20.

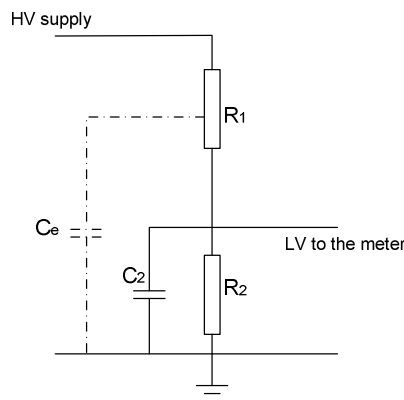


Figure 2.20: An equivalent circuit of a compensated resistive divider [16].

The parallel capacitor values, being much higher than the stray capacitance, ensure a uniform voltage distribution when an ac voltage is measured. The relatively high capacitance forms an RC circuit with a time constant adequate for measurements up to about 1 kHz [16]. This type of divider is not suited for the measurement of fast transients, e.g. lightning impulse voltage.

2.10.3 Capacitive voltage dividers

Capacitive voltage dividers cannot be used to measure dc voltages. Capacitive dividers are widely used to measure ac voltages and can be used to measure the peak value of impulse voltages.

Pure capacitor voltage dividers are sensitive to input voltages with short rise times and the output voltage may oscillate with non oscillating input voltages [16]. In addition, such a capacitance divider in combination with the rest of the measuring circuit, i.e. with leads connected to its input, will form a series resonant circuit. Thus, it is obvious that pure capacitor dividers are not suitable to measure impulse voltages with steep fronts (front-chopped lightning impulses) or any other fast transient phenomena (voltage chopping). However, the crest values of switching impulses or even full lightning impulse voltages can be properly recorded, if the transient phenomena during the front part of the impulse waveform have disappeared [[2], [16], [17]].

In some cases the low-voltage capacitor of the voltage divider is shunted by a high resistance. This high resistor is introduced deliberately to avoid the accumulation of random charge on the capacitor or on the measuring instrument. A high-voltage capacitor can either be screened or unshielded. A series resistor can then be connected in series to dampen the oscillation, as explained in Section 2.10.4.

2.10.4 Damped capacitive voltage dividers

The inherent lead inductance together with the capacitance of pure capacitive dividers forms a series resonant circuit. This resonance will cause excessive oscillations in response to a step potential. When chopped lightning impulses are to be measured, a damping resistance is added in series with the capacitance (usually distributed) to form a damped capacitive divider. The damped capacitive voltage divider circuit is shown in Figure 2.21 [[16], [17]].

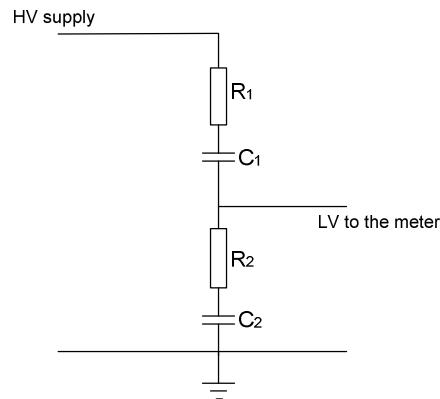


Figure 2.21: A basic diagram of a damped capacitive divider [16].

The input impedance of these dividers increases with decreasing frequencies, hence, the loading effect of the voltage generating system is limited. If the ratio is properly matched so that R_1C_1 is equal to R_2C_2 , the divider response becomes frequency-independent. Their application for ac, switching or lightning impulse voltages without any restrictions is therefore possible.

2.10.5 Low voltage arm of the divider

The low voltage arm of the voltage divider is an integral part of the divider and provides an impedance structure which is equivalent to the high voltage part of the divider. This consists of a low voltage part of the voltage divider itself, the measuring cable that connects to the oscilloscope and the relevant compensation components [17].

For the measurement of steady state voltages, the design of the dividers is not critical. However, if any fast transient voltage is to be measured, the measuring cable in the LV arm may introduce large disturbances to the response. The signal cable is mainly treated as lossless, so the surge impedance $Z_k = \sqrt{L_k / C_k}$ becomes independent of frequency and the travel time is expressed as $\tau_k = \sqrt{L_k \cdot C_k}$, where, Z_k , L_k and C_k are cable impedance, inductance and capacitance respectively [17]. This arrangement is shown in Figure 2.22 [17].

For resistive voltage dividers, the cable matching is done with a pure ohmic resistance $R = Z_k$ at a cable end. The compensation components are coaxially designed to meet the frequency requirements. For capacitor voltage dividers, the signal cable cannot be matched at its end. A low ohmic resistor in parallel with C_2 would load the low voltage arm of the divider too heavily and decrease the output voltage with time. To avoid travelling wave oscillations, the cable must be terminated at its input end [17].

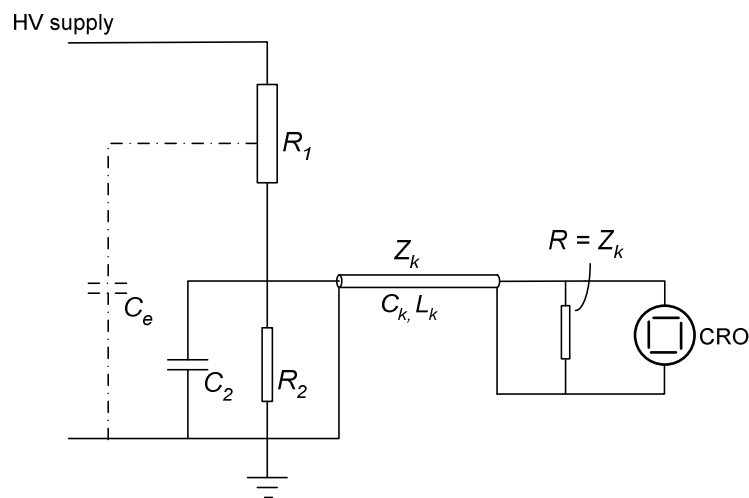


Figure 2.22: Matched impedance in series low voltage arm of the voltage divider [17].

2.10.6 High voltage probes

A high Voltage probe basically uses the voltage divider principle of the resistive and capacitive voltage dividers combined. By inserting a large resistor in series with the probe, and by providing a sufficient amount of electrical insulation, it is possible to create a probe that allows an ordinary voltmeter to measure very high voltages. The value of the resistor must be chosen to form an appropriate voltage divider with the input resistance of the voltmeter.

For correct frequency response, the implementation of capacitors to control the response is necessary. These capacitors are used to compensate for the stray capacitances in the probe system. Damped capacitance voltage dividers are connected in parallel for the measurement of

high frequency components. Most of these components are tuned to suit the contemplated measurement scenario.

There are a number of high voltage probes available in the market. Tektronix P6015A type is available at Stellenbosch University.

2.11 Conclusions

HVDC has proved to be the better system when it comes to high voltage transmission lines over long distances. However, there has not been sufficient research when it comes to the performance of HVDC insulators, especially for polluted conditions. The design of HVDC insulation systems have always been incorporated to those of ac systems. Also, their performance for transient overvoltages needs to be better understood.

Most of the past research and studies have covered air gaps configurations. These results could still be useful, because air also forms part of a composite insulator especially under dry and clean conditions. It is only under polluted and wet conditions that the effect of surface leakage comes into play. Wetting seems to have a more effect on negative flashover voltage levels. Generally, under dry conditions, lower flashover levels are recorded with positive voltages (dc and impulses) compared to negative voltages. These experimental flashover results are well illustrated in Figure 2.9 and Figure 2.10.

The basic circuits used in the past to perform experiments of the impulse flashovers of insulation under dc bias voltage prove to be similar. These include an impulse generator, a separate dc source to supply the bias voltage, coupling components, an insulator to be tested and of course measuring equipment. Measuring is one of the most crucial aspects in high voltage engineering and the high frequencies involved in these experiments makes it even more challenging. Therefore, it is necessary to select an appropriate measuring configuration from the available technologies.

3. DESIGN AND MATHEMATICAL MODELLING OF THE TEST TOPOLOGY

3.1 Overview

In this chapter, the design of a circuit used to represent the operation of an impulse applied on an insulator pre-stressed with dc voltage is explained. The design contains different components namely an impulse generator, a dc source and a test object and coupling components are used to connect these basic components. The function of each of these circuit elements and circuit variables is summarised in the sections that follow.

The circuit arrangement is simplified in order to obtain a mathematical model in the form of frequency- and time domain equations. The effects of the different circuit variables, i.e. coupling components, and test object, on the output waveshape are subsequently investigated, and the results are presented using suitable graphs and tables.

3.2 Test arrangement topology

The function of the desired test topology is to generate a test waveform consisting of an impulse of pre-determined shape superimposed on a specified dc bias voltage. The waveform is then applied to a test object such as an insulator. Figure 3.1 shows an example of the waveshape of the desired waveform, where a positive impulse is superimposed on a positive dc bias voltage.

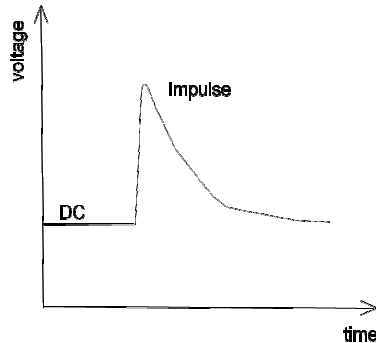


Figure 3.1: A positive impulse voltage superimposed on a positive bias voltage.

Figure 3.2 shows a basic block diagram of the proposed test arrangement. The arrangement consists of the following main components:

- A single or multi-stage impulse generator.
- A coupling capacitor.
- A dc source.
- A coupling resistor.
- A test object.

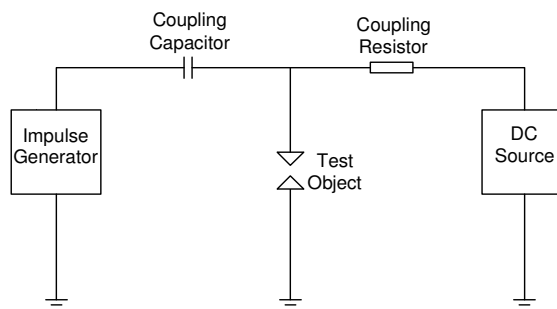


Figure 3.2: Block diagram of the proposed test arrangement.

The impulse generator generates the high voltage impulse that is applied across the test object, while the dc source supplies the continuous dc voltage used to pre-stress the test object. The test object can be any type of insulator, i.e. composite, porcelain glass, or an air-gap arrangement. This insulator can be under any condition e.g. wet or dry.

The coupling capacitor couples the impulse waveform from the impulse generator to the test object. The coupling capacitor also shields the impulse generator from the dc source. The coupling resistor couples the dc voltage from the dc source to the test object, while blocking the impulse voltage from the dc source. The coupling circuitry requires careful design in order to select optimum components for protection purposes without compromising too much on the circuit efficiency. In the absence of the coupling capacitor, an air gap can be used as a means of separating the dc source circuit and the impulse signal [[4], [19], [21]].

3.3 The impulse generators

An impulse generator is required to generate an impulse waveshape such as the standard lightning impulse waveshape of $1.2/50 \mu\text{s}$. There are two types of impulse generators at the University of Stellenbosch, namely:

- A two-stage Messwandler Bau construction kit.
- An eight-stage Marx type generator circuit.

These are general purpose impulse generators, and depending on the output required, some circuit variables can be varied. They are however limited to the generation of short impulses, i.e. lightning impulses, unless some alterations in the circuit arrangement are performed. Both positive and negative impulses can be obtained by reversing the impulse generator's rectifier diode. The two stage Messwandler Bau generates up to 200 kV standard lightning impulse voltage, while the Marx type is rated for a 1.4 MV lightning impulse voltage.

For design and test circuit analysis purposes, the multistage impulse generators are simplified into a standard single-stage equivalent circuit. The operation of the circuit and the steps in determining the waveshapes produced are explained in the following sections.

3.3.1 Determining impulse waveshapes

A standard single-stage impulse generator circuit is shown in Figure 3.3. The circuit parameters are defined as follows:

- C_g denotes the equivalent generator capacitance.
- C_l denotes the equivalent load capacitance.
- R_d denotes the equivalent wave shaping resistance.
- R_e denotes the equivalent wave tail resistance.

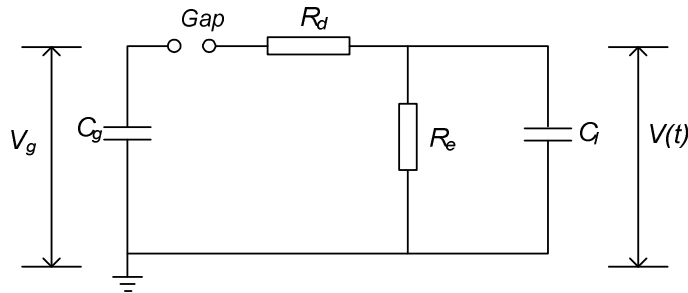


Figure 3.3: A standard single-stage impulse generator circuit.

Capacitance C_g is charged to a predetermined dc voltage V_g which causes a discharge through the spark gap onto the rest of the circuit. Capacitance C_g may consist of a single capacitance in case of a single stage impulse generator. Alternatively, C_g may consist of groups of capacitances charged in parallel and discharged in series by means of a switching arrangement. These operations are well covered in Chapter 2.

Once the gap fires, an impulse voltage appears across resistance R_e to which the test object is connected. The functions of R_e and R_d are mainly to control the front and tail time durations of the waveform. C_l includes the capacitance of the test object and any other load capacitance which may be required for producing the required waveshape [34].

Capacitance C_g is a function of the number of stages used and is thus fixed once the number of stages has been set. C_l will also be known since it is dependent on the test object capacitance plus any parallel loading capacitance, sometimes including that of a measuring device used. Once the circuit values are known, it is possible to calculate the efficiency of the generator, which is defined as the peak output voltage divided by the charging voltage per stage multiplied by the number of stages. The efficiency η is mainly determined by the ratio of C_g to the sum of the capacitances C_g and C_l [17], as shown below:

$$\eta = \frac{C_g}{C_g + C_l} \quad (3.1)$$

The next step is the determination of the approximate front and tail resistances R_d and R_e to give the desired impulse shape with a particular value of load capacitance. Since finding the exact values is complicated, an approximation method is used. These equations have been derived in Appendix.C.

The exact analysis of an impulse generator is rather a tedious process and it is generally necessary to perform a complete analysis for each different circuit configuration used. Different procedures like special charts and computer programs are currently used to analyse and design impulse waveshapes. The standard double exponential waveshape is expressed in equation 3.2, where α and β are tail and front time constants respectively. These are functions of the circuit capacitor and resistor values respectively.

$$v(t) = \frac{V_g}{k} [e^{-(\alpha-\beta)t} - e^{-(\alpha+\beta)t}] \quad (3.2)$$

Constant k is expressed as follows:

$$k = \frac{1}{2\beta R_d C_l} \quad (3.3)$$

The time constants α and β are given by the relationships

$$\alpha = \frac{1}{2} \left[\frac{1}{R_e C_g} + \frac{1}{R_d C_g} + \frac{1}{R_d C_l} \right] \quad (3.4)$$

and

$$\beta = \frac{1}{2} \left[\sqrt{\left(\frac{1}{R_e C_g} + \frac{1}{R_d C_g} + \frac{1}{R_d C_l} \right)^2 - 4 \left(\frac{1}{R_d R_e C_g C_l} \right)} \right] \quad (3.5)$$

With the circuit constants α and β known, the time values of the waveform are determined as explained below.

3.3.1.1 Calculating time to peak

If the waveform is specified in the usual manner, namely by the time to peak value t_p and the time to one-half peak t_2 , then both α and β must have unique values irrespective of the particular circuit used. The time to peak value t_p is determined from the solution given by Craggs and Meek [36], i.e. $\frac{dv}{dt} = 0$ when the impulse waveform curve is at maximum value.

The equation adopted for obtaining t_p is shown in equation 3.6. The mathematical derivation is given in Appendix.B.

$$t_p = \frac{1}{2\beta} \ln \left(\frac{\alpha + \beta}{\alpha - \beta} \right) \quad (3.6)$$

By substituting t in equation 3.2 with t_p , equation 3.7 is obtained. This equation expresses the peak voltage of the impulse.

$$v_p(t) = \frac{V_g}{k} [e^{-(\alpha-\beta)t_p} - e^{-(\alpha+\beta)t_p}] \quad (3.7)$$

The peak voltage is also very useful in determining the efficiency of the impulse generator circuit, which is another aspect of evaluating the circuit.

3.3.1.2 Calculating time to half peak

The time to half the peak t_2 is also referred to as the tail time of the waveform. It is the time it takes from the peak of the waveform to when the waveform decreases to half of the peak. This is explained below. The complete derivation is given in Appendix.C. The voltage waveform decreases to half peak when

$$v_h(t) = \frac{V_g}{k} [e^{-(\alpha-\beta)t^2} - e^{-(\alpha+\beta)t^2}] = \frac{V_g}{2k} [e^{-(\alpha-\beta)t^2} - e^{-(\alpha+\beta)t^2}] . \quad (3.8)$$

After simplifications are introduced, the tail time, for results to be within a 2% error [32], can be expressed by the relationship

$$t_2 = \frac{0.7}{\alpha - \beta} + t_p \quad (3.9)$$

Time t_2 is also referred to as t_h .

By definition, the front time t_1 is the rising time it takes to reach 90 percent of the peak (t_{90}) less the rising time it takes to reach 30 percent of the peak voltage (t_{30}) multiplied by 1.67 [17]. This yields

$$t_1 = (t_{90} - t_{30}) \times 1.67 . \quad (3.10)$$

After obtaining the t_p value, times t_{30} and t_{90} can be obtained with the help of Figure 3.4.

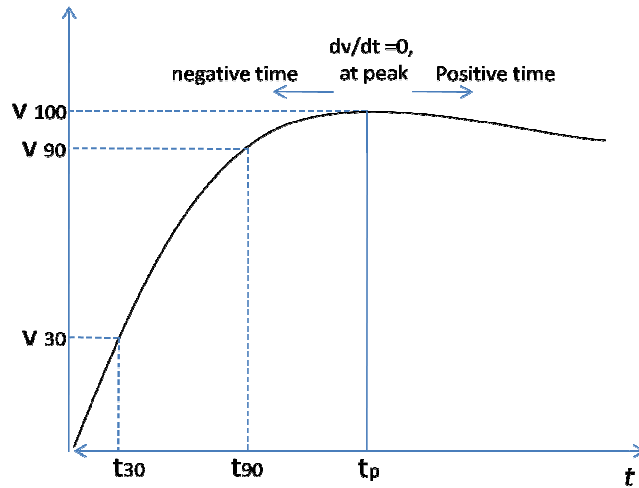


Figure 3.4: Demonstration of front time values calculation for an impulse waveform.

As shown in Appendix.C, the time between t_{30} and t_p is given as

$$t_p - t_{30} = \frac{1}{\alpha + \beta} \ln \left(\frac{10}{7} e^{-(\alpha + \beta)t_p} \right)$$

and time between t_{90} and t_p is given by

$$t_p - t_{90} = \frac{1}{\alpha + \beta} \ln \left(\frac{10}{1} e^{-(\alpha + \beta)t_p} \right).$$

Times t_{30} and t_{90} are defined as follows:

$$t_{30} = t_p - \left[\frac{1}{\alpha + \beta} \ln \left(\frac{10}{7} e^{-(\alpha + \beta)t_p} \right) \right] \quad (3.11)$$

$$t_{90} = t_p - \left[\frac{1}{\alpha + \beta} \ln \left(\frac{10}{1} e^{-(\alpha + \beta)t_p} \right) \right] \quad (3.12)$$

With all these formulas obtained, the next step will be applying them to an actual impulse generator circuit, e.g. the Marx type multistage simplified into a single stage equivalent.

3.3.2 Marx-type multistage generator circuit

Figure 3.5 shows a photograph of a Marx-type multi-stage generator at the HV laboratory at University of Stellenbosch. Figure 3.6 shows the circuit diagram of the 8-stage Marx type impulse generator shown in Figure 3.5.



Figure 3.5: Photograph of the Marx-type multistage impulse in the University of Stellenbosch's HV laboratory.

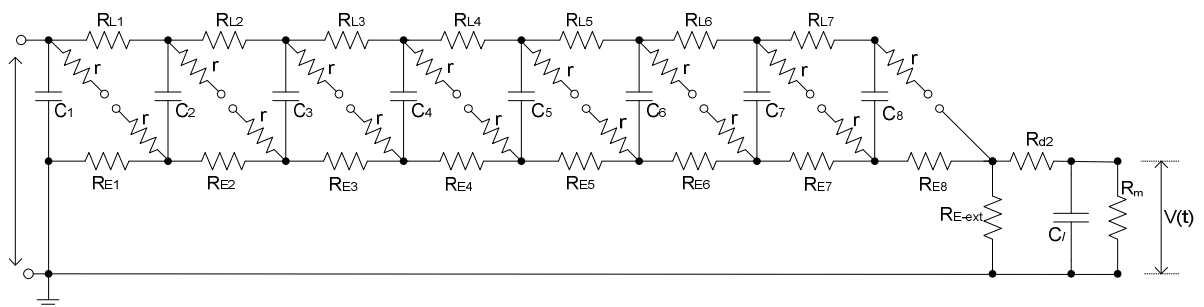


Figure 3.6: shows the circuit diagram of the eight-stage Marx-type impulse generator shown in Figure 3.1 [33].

A number of surge capacitors C_1 to C_8 are charged up in parallel through high ohmic charging resistors R_{L1} to R_{L7} as well as through the discharge resistors R_{E1} to R_{E8} , which are of course much smaller than R_L . At the end of the charging period, the voltage at the last stage of the

circuit with respect to earth will be n times the charging voltage V_g , where n is the number of stages [[17], [37]].

Eventually, after a certain threshold voltage, the surge capacitors start to discharge. The discharge or firing of the generator is initiated by the breakdown of the first gap which is followed by a nearly simultaneous breakdown of all remaining gaps. Capacitor C_l represents the load capacitance. It becomes charged by the accumulated circuit voltage and then discharges through R_e and also through the rest of the circuit. The output of the impulse circuit is measured across capacitor C_l .

Charging resistors R_{L1} to R_{L7} need to be properly sized for both charging and discharging. However, because of practical inefficiencies, the output voltage is somewhat less than n (number of stages) multiplied with V_g (impulse circuit's input voltage). Proper performance depends upon the selection of capacitors and resistors for the timing of the discharge.

As mentioned earlier, for analysis the complicated multistage impulse generator is simplified into a standard single stage equivalent. The values of the specific multistage generator are given in Table 3.1.

Table 3.1: Component values of the Marx-type impulse generator in the HV laboratory.

<i>Circuit component</i>	<i>Value</i>
R_{L1} to R_{L7}	10 k Ω
r	25 Ω
R_E	750 Ω
C_1 to C_8	0.125 μF
C_L	2500 pF

When simplifying a complicated circuit, including the multistage impulse generator, assumptions are sometimes needed. During the discharging of the capacitors, the following assumptions apply:

- Since R_L is relatively large, it can be ignored or virtually be considered as an open circuit. Therefore, the circuit can be expressed as shown in Figure 3.7.

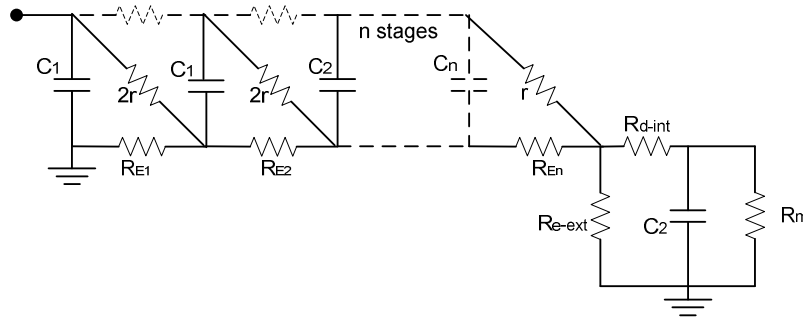


Figure 3.7: Multistage impulse generator simplification process with R_L is ignored.

- When C_1 to C_8 are equally charged, it can be assumed that no current will be exchanged between the branches of the stages. Therefore, the links can be removed as shown in Figure 3.8.

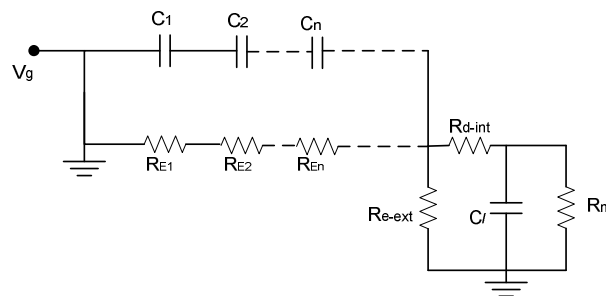


Figure 3.8: Multistage impulse generator simplification process with links between branches removed.

With few assumptions, the circuit can be reduced to get a single-stage equivalent circuit. The following the single-stage values of the simplified circuit.

- $R_d =$ the sum of r values = 375Ω
- $R_E =$ the sum of R_{E1} to R_{E8} values = 6000Ω
- $C_g = C_1/\text{number of capacitors } (C_1 \text{ to } C_8) = 15.625 \text{ pF}$
- $C_1 = C_2 = 2500 \text{ pF}$

The final wave tail resistance is then obtained. R_e equals R_E in parallel with the parallel combination of R_{e-ext} and R_{e2} . Without any external value (R_{e-ext} and R_m), R_e stands at 6000Ω . The single-stage equivalent circuit is shown in Figure 3.9.

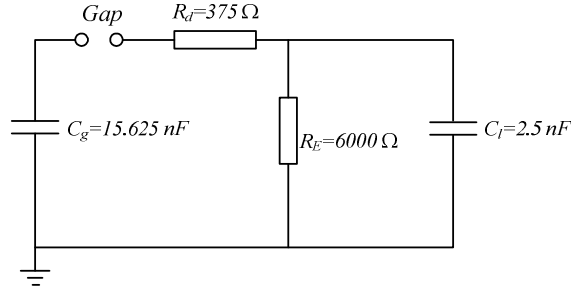


Figure 3.9: A simplified single-stage impulse generator circuit.

With all circuit variables known, the circuit time constants and time durations can be determined. Circuit time constants α and β can be obtained through using equations 3.3 and 3.4. These constants are given by

$$\alpha = 1\ 313\ 889$$

and

$$\beta = 1\ 299\ 718.$$

Using equations 3.6, 3.9 and 3.10, the respective time values can be obtained as shown below:

$$t_p = 2.014\ \mu s,$$

$$t_1 = 1.21\ \mu s,$$

and

$$t_2 = 50\ \mu s.$$

As shown in the circuit diagram in Figure 3.6, R_m is the measuring resistor and can be included in the circuit operation. That changes the value of R_e as shown below.

$$\frac{1}{R_e} = \frac{1}{R_E} + \frac{1}{R_m} \quad (3.13)$$

$$\frac{1}{R_e} = \frac{1}{6000} + \frac{1}{20000}$$

$$R_e = 4615 \Omega$$

The time to peak, front-time and time to half of the waveforms change to:

$$t_p = 1.84 \mu s,$$

$$t_1 = 1.21 \mu s,$$

and

$$t_2 = 38.34 \mu s.$$

If the external component of R_e , i.e. (R_{e-ext}), which is 2530Ω , is considered, the new equivalent R_e is obtained and the time values become

$$t_p = 1.43 \mu s,$$

$$t_1 = 1.21 \mu s,$$

and

$$t_2 = 15.75 \mu s.$$

The time to half values obtained in the calculations above show that in order to obtain a standard lightning waveform in this particular circuit, R_{e-ext} is not needed. The use of an external tail resistor R_{e-ext} in this circuit does not only reduce the tail times but also the circuit efficiency. The connection of external parameters i.e. R_{d-ext} and R_{e-ext} is optional, and they are basically used to change the waveshape.

3.3.3 Messwandler Bau kit

A smaller scheme can be constructed using a Messwandler Bau construction kit as it permits modular construction for limited voltages. A modular construction allows the user to choose the component values best suited for the specific application. Component values and ratings require careful circuit design when non-standard circuits are constructed. The construction set provides both capacitive and resistive voltage dividers for ac and dc voltage measurement. Although the kit's components are limited, they can be placed in any position as long as the voltage rating is appropriate. The modular design of this kit makes the whole procedure more versatile.

With a construction kit, components can easily be assembled to produce a standard lightning impulse. The impedance values of the external measuring equipment, however, need to be considered when doing the mathematical circuit analysis. The list of components available for the Messwandler Bau kit is given in Table 3.2 [38].

Table 3.2: Basic elements of the Messwandler Bau construction kit.

<i>Symbol</i>	<i>Construction element</i>	<i>Circuit components</i>	<i>Specifications</i>
CM	Measuring Capacitor	C_g	A.C. 100 kV, 100 pF
RM	Measuring Resistor		D.C. 140 kV 140 M Ω
GR	Rectifier		Peak inverse voltage 140kV, 5mA
RS	Protective Resistor		Impulse, d.c. 140kV, 10 M Ω , 60W
CS	Impulse Capacitor	C_c	Impulse, d.c. 140kV, 10 nF
CB	Load Capacitor	C_L	Impulse, d.c. 140kV, 1.2 nF
RD	Damping Resistor	R_d	Impulse 375 Ω (1.2/50 μ S),
RE	Discharge Resistor	R_E	Impulse 6100 Ω (1.2/50 μ S),

The construction elements *CM*, *RM*, *CB* and *RE* have a measuring terminal attached at the side of the insulating tubes (voltage dividers) for coaxial cables. The LV terminals of measuring capacitors should be shorted when not in use. In addition to the basic elements, other components are available in the high voltage kit which have the same terminal dimensions as the basic elements or at least conform in their external dimensions to the kit system. These include insulating supports *IS*, a sphere gap *KF*, conducting links *V*, measuring gaps, etc [38].

3.4 The dc voltage source

A dc source is one of the basic elements of the proposed test circuit arrangement. The rectification of ac is the most efficient means of obtaining dc supplies. The dc supply is obtained through the normal rectification method, namely a half wave rectifier. In the case of a reverse polarity dc voltage, the diode will have to be switched around. Figure 3.10 shows the half wave rectifier circuits for positive and negative output voltages respectively.

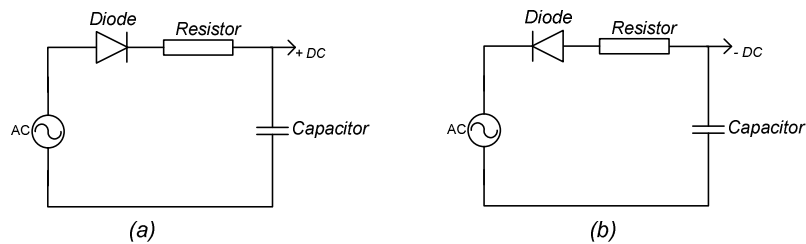


Figure 3.10: DC rectifier circuits: (a) Positive dc voltage and (b) Negative dc voltage.

When using a Marx-type multi-stage generator, the $300kV$ dc source set also available at the high voltage test facility of the University of Stellenbosch, can be utilized. This dc source set is designed for a maximum output current of $5mA$. This (current rating) needs to be taken into consideration when loading this part of the circuit as it tends to be the limiting factor for most practical applications, particularly for the insulator pollution tests contemplated in this study.

3.5 The test object

Insulators come in many forms including air-gaps and composite insulators. This test arrangement is designed to suit all of these. With similar research already done on air-gaps, it is the objective to focus this study on composite insulators. The test insulator, allowing for various dry and wet contaminated surfaces, will be subjected to a dc voltage superimposed with impulses while the performance is observed.

The equivalent circuit presented earlier shows that the characteristics of the test object also plays a role in determining the properties of the output waveform. It is typically represented by a parallel combination of a leakage resistor and a capacitor.

3.6 Design and analysis of the complete test topology

3.6.1 Circuit topology

With the basic components designed, the circuit layout is now completed. Figure 3.11 shows the complete equivalent circuit model of the test arrangement. The three basic components of the circuit are shown with the coupling components located between them. The voltage measuring transducers are denoted by M_1 , M_2 and M_3 . The rest of the circuit elements are defined as follows:

- V_g denotes the dc input voltage to the impulse generator.
- C_c and R_c denote the coupling capacitor and coupling resistor respectively.
- C_d denotes the charging capacitor of a dc source.
- T denotes the object under test.

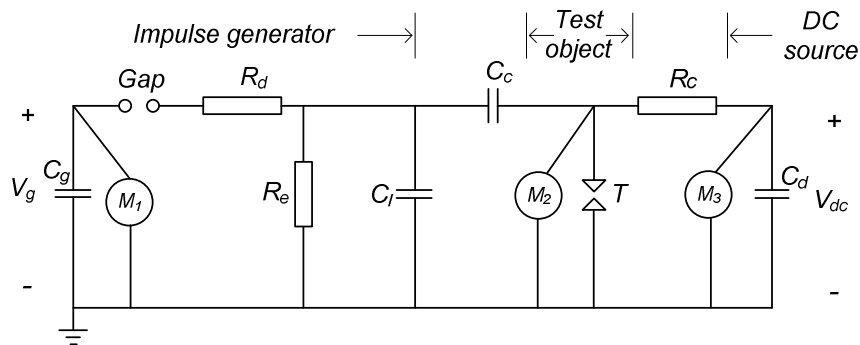


Figure 3.11: Complete test circuit topology.

Since the voltage waveform applied to the test object consists of a dc component as well as the impulse component (high frequency), it can be difficult to measure accurately in practice. A wideband measuring transducer is also required to measure the voltage across the dc source terminals in order to determine the magnitude of the unwanted impulse applied to the dc source.

The voltage across the generator capacitor C_g needs to be measured (M_1). This is the actual dc input voltage to the generator circuit. The measurement across the test object will comprise of

composite waveform (M_2). This is the dc component as well as the impulse component, ($V_{dc} + V_{impulse}$). To regulate the voltage across the dc source effectively, a measuring device (M_3) is needed. This also helps in monitoring the unwanted impulse component entering the dc source.

Coupling devices C_c and R_c are shown in the complete circuit layout, Figure 3.11. The impulse generator needs to be protected against high direct voltage from the dc supply. Therefore, capacitor C_c is needed, which acts as an open circuit for dc voltage. The resistor R_c on the other hand blocks impulse voltages from reaching the dc circuit.

R_c and C_d form a high frequency blocking circuit operated on low pass filter principle. This means that if the frequency is low, more voltage will appear across the resistor R_c . Therefore, virtually zero impulse voltage will appear across C_d . This is illustrated by Figure 3.12.

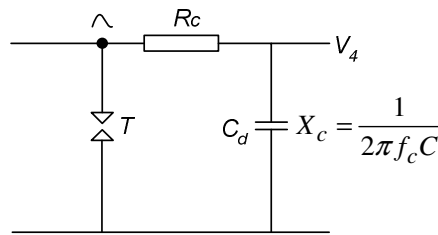


Figure 3.12: Low pass filter circuit for impulse blocking.

The advantage of using a capacitor as separating element between the dc and the impulse generators is that it is also possible to superimpose impulses having amplitude which is just a fraction of the dc voltage V_{dc} . In the absence of a capacitor, a sphere gap can be used to separate an impulse generator from the dc voltage, with the consequence that impulse voltage V_i has to be larger than V_{dc} [21].

3.6.2 Mathematical analysis of the circuit

3.6.2.1 Nodal voltage equations in the Laplace domain

The Laplace transform provides a useful method of solving certain types of differential equations. This is possible when certain initial conditions are given, especially when the initial

values are zero. The Laplace transform is very useful in the area of circuit analysis, as it is often easier to analyse the circuit in its Laplace domain, than to solve differential equations in the time domain.

The equivalent circuit shown in Figure 3.13 is transformed into the Laplace equivalent. This means that all components of the circuit are transformed into the frequency domain. Resistors are kept the same, capacitors are replaced by $1/sC$ while voltage sources are replaced V/s . This yields the Laplace equivalent shown in Figure 3.13. When the gap of an impulse generator fires, it is treated as a closed switch.

The high impedances of the measuring components are incorporated into existing parallel circuit elements, e.g. R_t and C_t . The initial voltages that exist across the various capacitors before the spark-gap is bridged, are represented by voltage sources V_g , V_{i1} , V_{i2} , V_{i3} and V_{dc} .

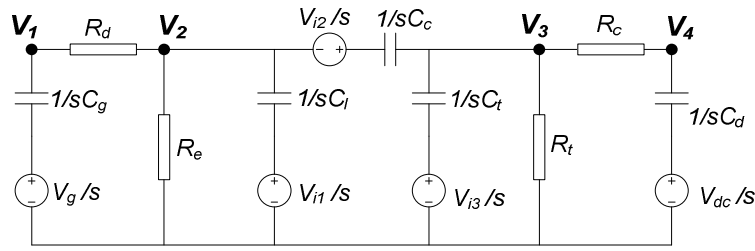


Figure 3.13: Laplace equivalent representation of the test circuit.

The circuit shown in Figure 3.13 gives rise to the following nodal equations for nodes V_1 , V_2 , V_3 and V_4 , i.e. the Laplace domain voltages at nodes 1 to 4 respectively:

Node V_1 :

$$\frac{V_1 - \frac{V_g}{s}}{(1/sC_g)} + \frac{(V_1 - V_2)}{R_d} = 0. \quad (3.14)$$

Node V_2 :

$$\frac{V_2 - V_1}{R_d} + \frac{V_2 + \frac{V_{i2}}{s} - V_3}{(1/sC_c)} + \frac{V_2 - \frac{V_{i1}}{s}}{(1/sC_t)} + \frac{V_2}{R_e} = 0 \quad (3.15)$$

Node V_3 :

$$\frac{V_3 - \frac{V_{i2}}{s} - V_2}{(1/sC_c)} + \frac{V_3 - \frac{V_{i3}}{s}}{(1/sC_t)} + \frac{V_3}{R_t} + \frac{V_3 - V_4}{R_c} = 0 \quad (3.16)$$

Node V_4 :

$$\frac{V_4 - V_3}{R_c} + \frac{V_4 - \frac{V_{dc}}{s}}{(1/sC_d)} = 0 \quad (3.17)$$

Equations (3.14) to (3.17) can be expressed in a matrix format as follows:

$$[A][V] = [I] \quad (3.18)$$

where, $[A]$ denotes the admittance matrix, $[V]$ denotes the nodal voltages vector and $[I]$ denotes the branch currents. These matrices are defined by the following relationships:

$$[A] = \begin{pmatrix} (sC_g + \frac{1}{R_d}) & -\frac{1}{R_d} & 0 & 0 \\ -\frac{1}{R_d} & (\frac{1}{R_d} + sC_c + sC_t + \frac{1}{R_e}) & -sC_c & 0 \\ 0 & -sC_c & (sC_c + sC_t + \frac{1}{R_t} + \frac{sC_d}{sR_cC_d + 1}) & -\frac{1}{R_c} \\ 0 & 0 & -\frac{1}{R_c} & \frac{1}{R_c} \end{pmatrix}$$

$$[V] = \begin{pmatrix} V_1 \\ V_2 \\ V_3 \\ V_4 \end{pmatrix}$$

$$[I] = \begin{pmatrix} V_g C_g \\ C_t V_{i1} - C_c V_{i2} \\ C_c V_{i2} + C_t V_{i3} - \frac{C_d V_{dc}}{sR_cC_d + 1} \\ C_d V_{dc} \end{pmatrix}$$

By solving the set of linear equations represented by equation 3.15, the nodal voltages can be expressed in terms of the circuit parameters. This yields the following result for $V_3(s)$, i.e. the voltage applied to the test object:

$$V_3(s) = \frac{a_3 s^3 + a_2 s^2 + a_1 s + a_0}{b_4 s^4 + b_3 s^3 + b_2 s^2 + b_1 s + b_0} \quad (3.19)$$

where, the coefficients in equation 3.18 are defined as follows:

$$a_3 = R_c R_d R_e R_t C_c C_d C_g C_l V_{i1} + R_c R_d R_e R_t C_c C_d C_g C_l V_{i2} + R_c R_d R_e R_t C_c C_d C_g C_l V_{i3} + R_c R_d R_e R_t C_d C_g C_l C_t V_{i3} \quad (3.20)$$

$$\begin{aligned} a_2 = & R_c R_e R_t C_c C_d C_l V_{i1} + R_d R_e R_t C_c C_g C_l V_{i1} + R_c R_d R_t C_c C_d C_g V_{i2} + R_c R_e R_t C_c C_d C_g V_{i2} + R_c R_e R_t C_c C_d C_l V_{i2} + \\ & R_d R_e R_t C_c C_g C_l V_{i2} + R_c R_d R_t C_d C_g C_l V_{i3} + R_c R_e R_t C_c C_d C_l V_{i3} + R_c R_e R_t C_d C_g C_l V_{i3} + R_c R_e R_t C_d C_l C_t V_{i3} + \\ & R_d R_e R_t C_c C_g C_l V_{i3} + R_d R_e R_t C_g C_l C_t V_{i3} + R_d R_e R_t C_c C_d C_g V_{dc} + R_d R_e R_t C_d C_g C_l V_{dc} + R_c R_e R_t C_c C_d C_g V_g \end{aligned} \quad (3.21)$$

$$\begin{aligned} a_1 = & R_e R_t C_c C_l V_{i1} + R_c R_t C_c C_d V_{i2} + R_d R_t C_c C_g V_{i2} + R_e R_t C_c C_g V_{i2} + R_e R_t C_c C_l V_{i2} + R_c R_t C_d C_l V_{i3} + R_d R_t C_g C_l V_{i3} + \\ & R_e R_t C_c C_t V_{i3} + R_e R_t C_g C_t V_{i3} + R_e R_t C_l C_t V_{i3} + R_d R_t C_d C_g V_{dc} + R_e R_t C_c C_d V_{dc} + R_e R_t C_d C_g V_{dc} + R_e R_t C_d C_l V_{dc} + \\ & R_e R_t C_c C_g V_g \end{aligned} \quad (3.22)$$

$$a_0 = R_t C_c V_{i2} + R_t C_l V_{i3} + R_t C_d V_{dc} \quad (3.23)$$

$$b_4 = R_c R_d R_e R_t C_c C_d C_g C_l + R_c R_d R_e R_t C_c C_d C_e C_t + R_c R_d R_e R_t C_d C_g C_l C_t \quad (3.24)$$

$$\begin{aligned} b_3 = & R_c R_d R_e C_c C_d C_g + R_c R_d R_e C_d C_g C_l + R_c R_d R_t C_c C_d C_g + R_c R_d R_t C_d C_g C_t + R_c R_e R_t C_c C_d C_g + R_c R_e R_t C_c C_d C_l + \\ & R_c R_e R_t C_c C_d C_t + R_c R_e R_t C_d C_g C_t + R_c R_e R_t C_d C_l C_t + R_d R_e R_t C_c C_d C_g + R_d R_e R_t C_c C_g C_l + R_d R_e R_t C_d C_g C_l + \\ & R_d R_e R_t C_c C_g C_t + R_d R_e R_t C_g C_l C_t \end{aligned} \quad (3.25)$$

$$\begin{aligned} b_2 = & R_c R_d C_d C_g + R_c R_e C_c C_d + R_c R_e C_d C_g + R_c R_e C_d C_l + R_d R_e C_c C_g + R_d R_e C_g C_l + R_c R_t C_c C_d + R_c R_t C_d C_t + \\ & R_d R_t C_c C_g + R_d R_t C_d C_g + R_d R_t C_g C_t + R_e R_t C_c C_d + R_e R_t C_c C_g + R_e R_t C_d C_g + R_e R_t C_c C_l + R_e R_t C_d C_t + \\ & R_e R_t C_c C_t + R_e R_t C_g C_t + R_e R_t C_l C_t \end{aligned} \quad (3.26)$$

$$b_l = R_c C_d + R_d C_g + R_e C_c + R_e C_g + R_e C_l + R_l C_c + R_l C_d + R_l C_t \quad (3.27)$$

$$b_0 = 1 \quad (3.28)$$

Similarly, the voltage $V_4(s)$ at node 4, is given by:

$$V_4(s) = \frac{c_3 s^3 + c_2 s^2 + c_1 s^1 + c_0}{d_4 s^4 + d_3 s^3 + d_1 s^2 + d_1 s^1 + d_0} \quad (3.29)$$

where, the coefficients are defined as follows:

$$c_3 = R_c R_d R_e R_l C_c C_d C_g C_l V_{dc} + R_c R_d R_e R_l C_c C_d C_g C_l V_{dc} + R_c R_d R_e R_l C_d C_g C_l C_l V_{dc} \quad (3.30)$$

$$\begin{aligned} c_1 = & R_c R_d C_d C_g V_{dc} + R_c R_e R_m C_c C_d V_{dc} + R_c R_e C_d C_g V_{dc} + R_c R_e C_d C_l V_{dc} + R_c R_l C_c C_d V_{dc} + R_c R_l C_d C_l V_{dc} + \\ & R_d R_l C_d C_g V_{dc} + R_e R_l C_c C_d V_{dc} + R_e R_l C_d C_g V_{dc} + R_e R_l C_d C_l V_{dc} + R_e R_l C_c C_g V_g + R_e R_l C_c C_l V_{i1} + \\ & R_d R_l C_c C_g V_{i2} + R_e R_l C_c C_g V_{i2} + R_e R_l C_c C_l V_{i2} + R_d R_l C_g C_l V_{i3} + R_e R_l C_c C_l V_{i3} + R_e R_l C_g C_l V_{i3} + R_e R_l C_l C_l V_{i3} \end{aligned} \quad (3.31)$$

$$c_0 = R_c C_d V_{dc} + R_l C_d V_{dc} + R_l C_c V_{i2} + R_l C_l V_{i3} \quad (3.32)$$

$$d_4 = R_c R_d R_e R_l C_c C_d C_g C_l + R_c R_d R_e R_l C_c C_d C_g C_l + R_c R_d R_e R_l C_d C_g C_l C_l \quad (3.33)$$

$$\begin{aligned} d_3 = & R_c R_d R_e C_c C_d C_g + R_c R_d R_e C_d C_g C_l + R_c R_d R_l C_c C_d C_g + R_c R_d R_l C_d C_g C_l + R_c R_e R_l C_c C_d C_g + R_c R_e R_l C_c C_d C_l + \\ & R_c R_e R_l C_c C_d C_l + R_c R_e R_l C_d C_g C_l + R_c R_e R_l C_d C_l C_l + R_d R_e R_l C_c C_d C_g + R_d R_e R_l C_c C_g C_l + R_d R_e R_l C_d C_g C_l + \\ & R_d R_e R_l C_c C_g C_l + R_d R_e R_l C_g C_l C_l \end{aligned} \quad (3.34)$$

$$\begin{aligned} d_2 = & R_c R_d C_d C_g + R_c R_e R_m C_c C_d + R_c R_e C_d C_g + R_c R_e C_d C_l + R_d R_e C_c C_g + R_d R_e C_g C_l + R_c R_l C_c C_d + \\ & R_c R_l C_d C_l + R_d R_l C_c C_g + R_d R_l C_d C_g + R_d R_l C_g C_l + R_e R_l C_c C_d + R_e R_l C_c C_g + R_e R_l C_d C_g + R_e R_l C_c C_l + \\ & R_e R_l C_d C_l + R_e R_l C_c C_l + R_e R_l C_g C_l + R_e R_l C_l C_l \end{aligned} \quad (3.35)$$

$$d_1 = R_c C_d + R_d C_g + R_e R_m C_c + R_e R_m C_g + R_e C_l + R_l C_c + R_l C_d + R_l C_t \quad (3.36)$$

$$d_0 = 1 \quad (3.37)$$

Appendix D present detailed mathematical deductions of equations applicable for the circuit given in Fig 3.13. It is clear that the mathematical representation of the circuit gives rise to relatively complex relationships. The expressions for the time domain responses of the circuit, obtained through inverse transformation of the above Laplace relationships, are even more cumbersome. Therefore, the variables in the Laplace equations are substituted with numerical circuit values before the time domain relationships are derived through the inverse Laplace transformation. Mathematica software was used to perform these tedious mathematical functions. This has been illustrated in Appendix E

3.6.2.2 Time domain voltage waveforms

The voltage across the test object is a composite waveform that represents an impulse waveform superimposed on a pre-existing dc voltage across the test object. With known circuit variables, equation 3.18 can be transformed to the time domain. Table shows the parameters used in the calculations that follow.

Table 3.3: Summary of circuit parameters used in deriving $V_3(t)$.

<i>Variable</i>	<i>Value</i>	<i>Variable</i>	<i>Value</i>
V_g	800 kV	V_{dc}	300 kV
C_c	10 nF	R_d	375 Ω
C_g	15.625 nF	R_e	1780 Ω
C_l	2500 pF	R_c	1 M Ω
C_d	15.625nF	R_m	20 k Ω
C_t	20 pF	R_t	1 G Ω

For the parameter values given in Table 3.3, R_e excludes R_m .

The actual initial dc voltage (V_{i3}) across the test object is determined by the voltage division between R_c and R_t , i.e.

$$V_{i3} = \left(\frac{R_t}{R_t + R_c} \right) V_{dc} \quad (3.38)$$

which yields

$$V_{i3} = \left(\frac{1 \times 10^9 \Omega}{1 \times 10^9 \Omega + 1 \times 10^6 \Omega} \right) 300 \text{ kV} .$$

The initial voltages V_{i1} and V_{i2} as shown in the Laplace equivalent circuit are set to 0 and 299.572 V respectively. When the above parameters are substituted into the equation 3.19, $V_3(s)$ is given by the relationship

$$V_3(s) = \frac{299572 (150.807 + s)(8868.71 + s)(4.2154 \times 10^6 + s)}{(0.0332963 + s)(149.6 + s)(26706.4 + s)(1.41042 \times 10^6 + s)} . \quad (3.39)$$

Performing the inverse Laplace Transform on equation 3.39, yields the following time domain equation:

$$v_3(t) = 299572 (-2.01345 e^{-1.41042 \times 10^6 t} + 2.02177 e^{-26706.4 t} - 0.00792041 e^{-149.6 t} + 1.00051 e^{-0.03329 t}) \quad (3.40)$$

Figure 3.14 shows a plot of the waveform defined by equation 3.40.

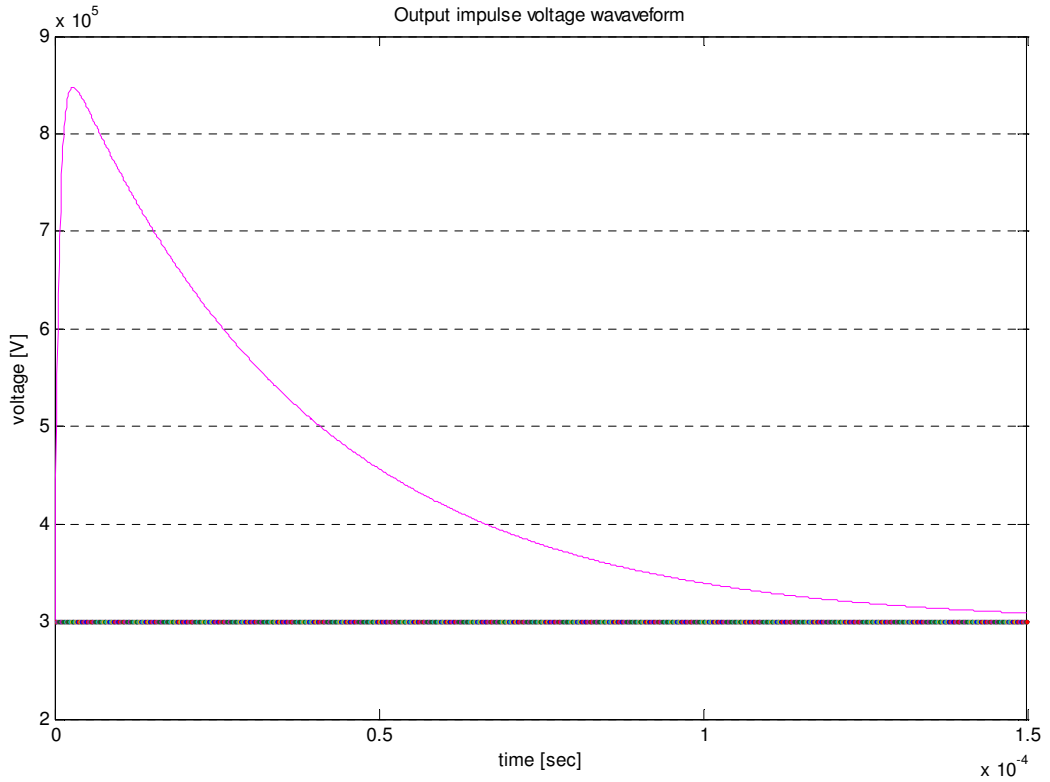


Figure 3.14: Voltage waveform $v_3(t)$ across the test object.

Just as with V_3 , the voltage at the dc terminal node (node 4) is analysed. The impulse component in $v_4(t)$ waveform should ideally be zero. However, there are always some leakage through the coupling resistor. With the parameter values given in Table 3.3, equation 3.29 reduces to:

$$V_4(s) = \frac{300000(149.009 + s)(26807.6 + s)(1.41034 \times 10^6 + s)}{(0.0332963 + s)(149.6 + s)(26706.4 + s)(1.41044 \times 10^6 + s)}. \quad (3.41)$$

To convert the above frequency domain equation into a time-domain format, the inverse Laplace Transform is performed. This yield

$$v_4(t) = 21.3929 e^{-1.41044 \times 10^6 t} - 1136.06 e^{-26706.4 t} + 1191.13 e^{-149.629 t} + 299924 e^{-0.0332963 t}. \quad (3.42)$$

$v_4(t)$ is the actual composite voltage waveform that appears across the dc source. Figure 3.15 shows a plot of the waveform defined by equation 3.42. The figure shows a small spike

coupled to the dc supply side of the circuit as a result of an impulse waveform. The magnitude of the inflicted spike is shown to be just more than $1kV$. It is still small when compared to the $600kV$ impulse wave peak and $300kV$ dc voltage.

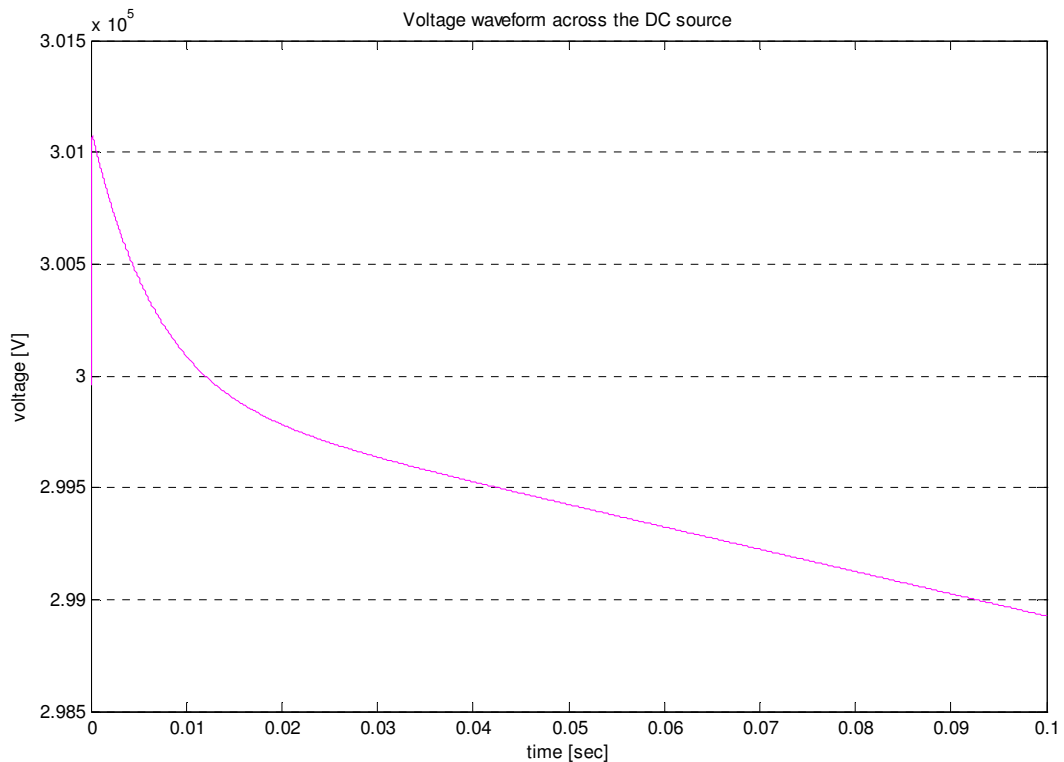


Figure 3.15: Voltage waveform $v_d(t)$ across the dc source.

3.6.3 Effects of circuit variables on the voltage waveforms

3.6.3.1 Introduction

The coupling component values for the composite circuit are selected depending on the desired properties of output waveform and the properties of the impulse generator and dc source used. These coupling components have a direct influence on the performance of the configuration. The test object also forms part of the circuit and its impedances can also have

an influence of the performance of the entire circuit. The effects of the following parameter values on the voltage waveforms applied across the test object and dc source are examined in this section:

- Effects of coupling capacitor value.
- Effects of coupling resistor value.
- Effects of resistance value of the test object.
- Effects of capacitance value of the test object.

3.6.3.2 Effects of coupling capacitor values of the voltage waveform

Using the circuit component values given in Table 3.3 the effect of different coupling capacitor C_c values is studied. Although a wide range of coupling capacitance C_c values will effectively block dc voltage from entering the impulse circuit, the optimum C_c value needs to be calculated.

Since capacitance C_c effectively forms part of the impulse generator circuit, it also has an effect on the efficiency of the impulse circuit. Hence, the voltage across the test object is directly affected. Figure 3.16 shows the effects of C_c on the voltage waveform across the test object $v_3(t)$.

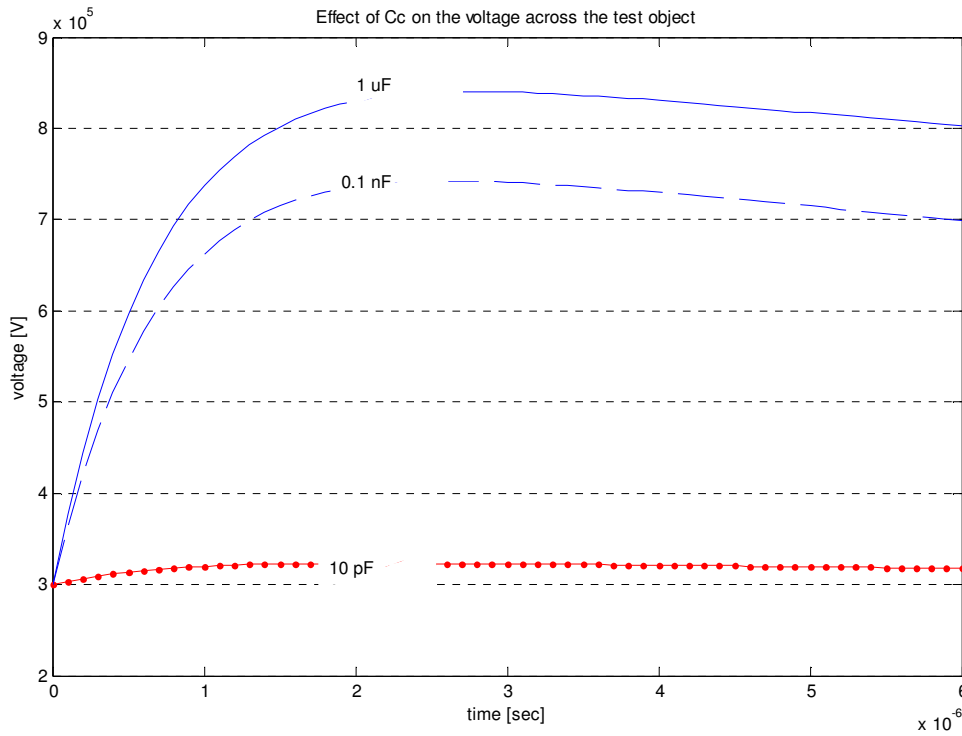


Figure 3.16: Voltage impulse waveforms $v_3(t)$ with different C_c values.

Figure 3.17 plots the peak values of the voltage waveforms $v_3(t)$ and $v_4(t)$ as a function of C_c . It can be observed that both voltage levels ($v_3(t)$ and $v_4(t)$) are proportional to the capacitance C_c . The variation in $v_4(t)$ is however minimal.

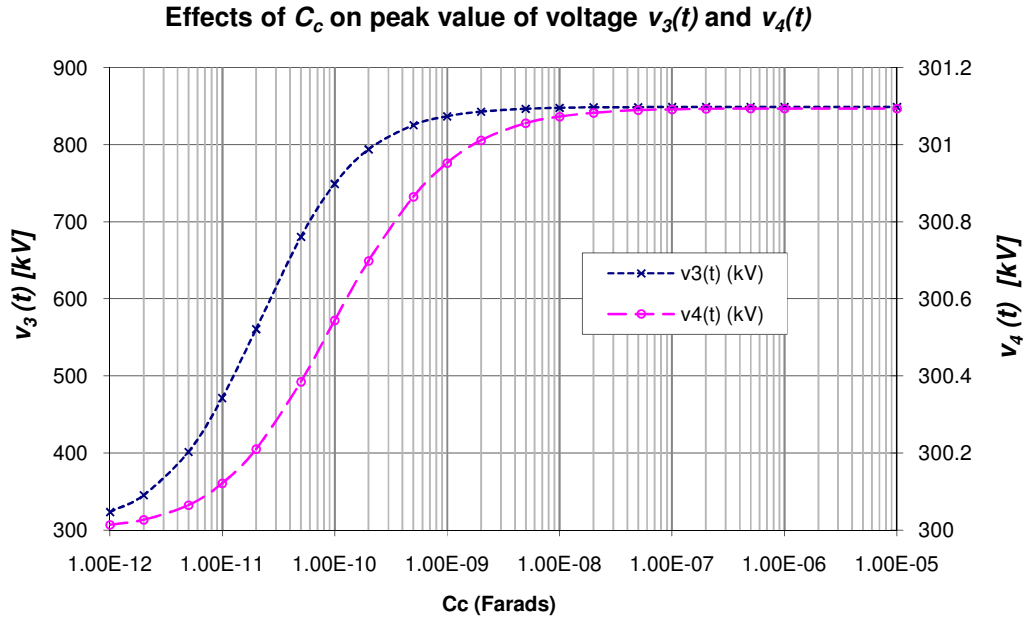


Figure 3.17: Plots of the effect of C_c on the peak values of voltages $v_3(t)$ and $v_4(t)$.

The peak of the impulse part $v_i(t)_{peak}$ of the waveform is defined as the difference between the total voltage peak across test object $v_3(t)$ and the actual dc voltage that appears across the test object before the impulse, V_{i3} . This is expressed by the relationship

$$v_i(t)_{peak} = v_3(t) - V_{i3} \quad (3.43)$$

To determine the efficiency of the impulse circuit, the impulse part of the voltage is expressed as a percentage of the generator input voltage, $(v_i(t)_{peak} / V_g) \%$. A higher $v_i(t)_{peak}$ implies a better efficiency of the circuit. The efficiency plot of this circuit as a function of C_c value is shown in Figure 3.18.

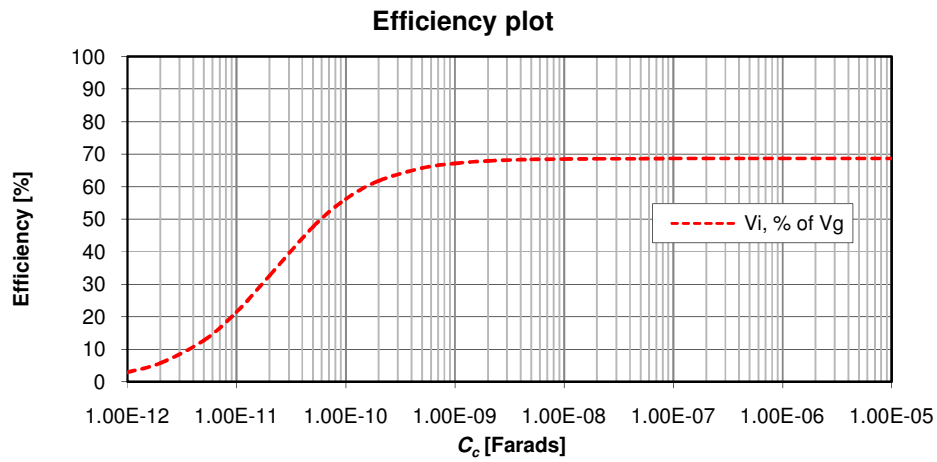


Figure 3.18: Efficiency plot of an impulse generator as a function of C_c .

The efficiency curve follows the same pattern as the peak value of $v_3(t)$. For this particular arrangement, it hardly reaches 70% efficiency. It is clear that for the particular circuit arrangement and variables, the efficiency stabilizes from about $1nF$. Table 3.4 summarises the numerical values for the curves given in Figure 3.17 and Figure 3.18.

Table 3.4: Numerical values for the effects of the value of C_c on peak values of $v_3(t)$, $v_4(t)$ and the efficiency.

C_c	$v_3(t)$		$v_4(t)$	$v_3(t)-V_{i3peak}$	
	<i>Peak voltage</i> [kV]	<i>Time to peak</i> [us]	<i>Peak voltage</i> [kV]	<i>Peak voltage</i> [kV]	% of V_g
1 pF	323563	2.17609	300014	23863	2.983
2 pF	345517	2.19409	300027	45817	5.727
5 pF	401522	2.24432	300065	101822	12.728
10 pF	471368	2.31282	300121	171668	21.459
20 pF	561018	2.41145	300210	261318	32.665
50 pF	680574	2.56773	300385	380874	47.609
0.1 nF	749369	2.67552	300544	449669	56.209
0.2 nF	794145	2.75531	300699	494445	61.806
0.5 nF	825641	2.81717	300865	525941	65.743
1 nF	837068	2.84098	300953	537368	67.171
2 nF	843101	2.8536	301012	543401	67.925
5 nF	846709	2.86142	301056	547009	68.376
10 nF	847922	2.86407	301073	548222	68.528
20 nF	848531	2.8654	301083	548831	68.604
50 nF	848897	2.86621	301090	549197	68.650
0.1 uF	849019	2.86647	301092	549319	68.665
0.2 uF	849080	2.86661	301093	549380	68.673
0.5 uF	849117	2.86669	301094	549417	68.677
1 uF	849129	2.86671	301094	549429	68.679
10 uF	849140	2.86674	301094	549440	68.680

3.6.3.3 Effects of the coupling resistor value

After an optimum C_c range is established, an exercise to perform its resistor counterpart R_c is done. With the given circuit variables in Table 3.3 and C_c value of 10 nF put in table as default, the effect of R_c can be established. The capacitance of 10 nF is chosen because from the Section 3.6.3.4 it was observed that after C_c reaches 1 nF , the efficiency of the impulse circuit is more or less constant, therefore, any reasonable value bigger than that can be used. With these values, the effect of different coupling resistor values can be realized.

The value of R_c should be smaller than the resistance of the test object in order not to lose the dc efficiency across the test object. If the ratio between the two isn't large in favour of the test object, an undesired high value of the dc voltage will end up sitting across the coupling resistor R_c . A low as possible impulse voltage is desired across the test object. The resistance value of the coupling component determines how much of the impulse generator circuit can pass through R_c to dc supply. The effect of different resistor values of R_c on $v_3(t)$ and $v_4(t)$ has been analysed as shown in Figure 3.19.

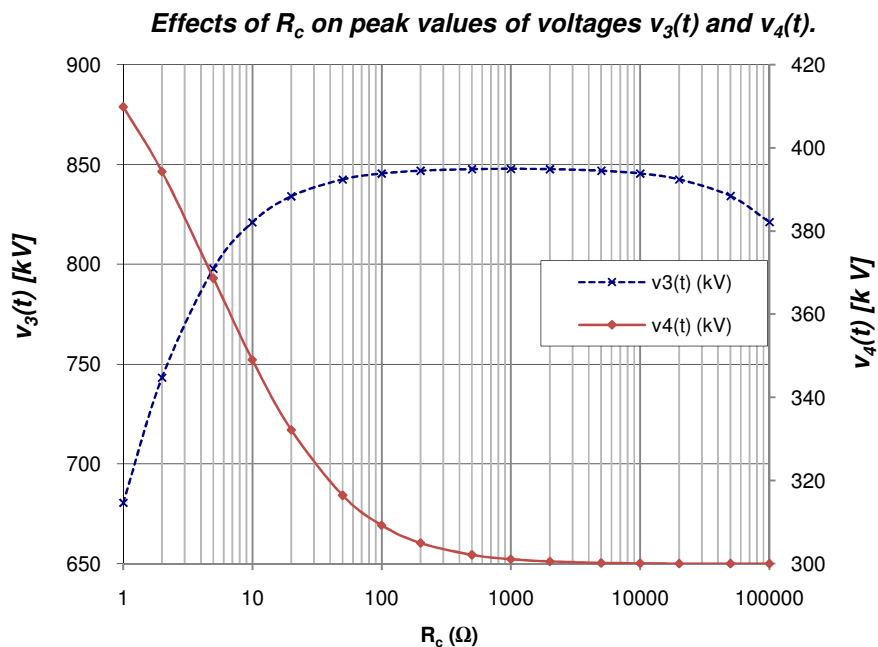


Figure 3.19: Effects of R_c on peak values of voltages $v_3(t)$ and $v_4(t)$.

As shown in Figure 3.19, the lower the R_c resistance, the higher the level of the impulse component of $v_4(t)$ (voltage across dc supply). In this arrangement, it is only with resistance values more than $500\text{ k}\Omega$ that the impulse component on $v_4(t)$ is relatively low. It is also evident that a lower resistor value compromises the total voltage $v_3(t)$ across the test object. However, too high R_c values, more than $10\text{ k}\Omega$ in this arrangement, will see $v_3(t)$ decreasing.

The leakage factor is defined in terms of the impulse voltage component that leak to the dc supply. It is expressed as the impulse part of the $v_4(t)$ waveform over the input voltage to the impulse generator circuit, $\frac{V_4 - V_{i3}}{V_g} \%$. Voltage V_{i3} is the initial dc voltage across the test object (before the application of an impulse). This can also be expressed as the impulse voltage blocked by resistor R_c . The leakage factor curve of R_c is shown in Figure 3.20

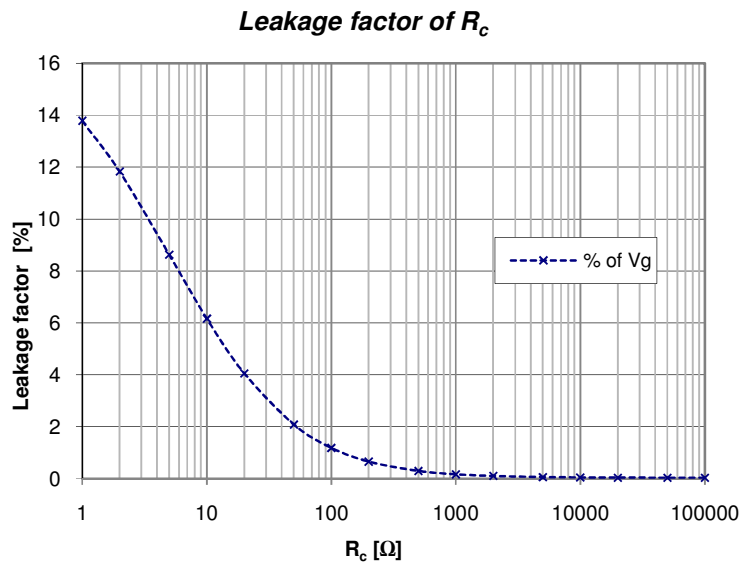


Figure 3.20: Leakage factor as a function of R_c .

It can be observed from the curve that percentage efficiency grows small as R_c value increases. From the results given in Figure 3.19 and Figure 3.20, it can be concluded that the optimum range of R_c value for circuit arrangements at these magnitudes is between $1\text{ M}\Omega$ and $10\text{ M}\Omega$. These waveforms are illustrated in Figure 3.21.

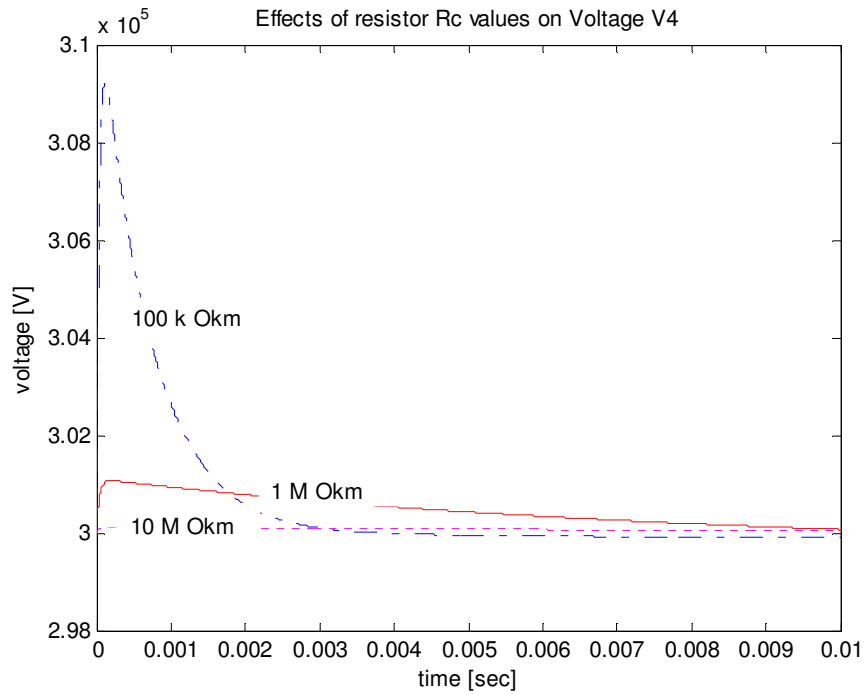


Figure 3.21: Peak $v_4(t)$ voltages with different R_c values for $C_c = 10$ nF.

Table 3.5 summarizes effects of different coupling resistor values on the peak values of $v_3(t)$ and $v_4(t)$, the time to peak of $v_3(t)$ and the leakage factor waveform. The expression $v_4(t) - V_{i3}$ represents an impulse peak that appears across the dc supply as a result of an impulse from the generator. It is desirable to keep the impulse inflicted on the dc source as low as possible.

Table 3.5: Numerical values for the effects of the value of R_c on values of $v_3(t)$, $v_4(t)$ and the efficiency

R_c (k Ω)	$v_3(t)$		$v_4(t)$	$v_4(t) - V_{i3}$	
	Peak voltage [V]	Time to peak [us]	Peak voltage [V]	Peak voltage [V]	% of V_g
1	680470	1.60451	409926	110226	13.778
2	743261	1.93959	394288	94588	11.824
5	797830	2.32712	368688	68988	8.624
10	821096	2.54232	349023	49323	6.165
20	834176	2.68519	332150	32450	4.056
50	842601	2.78886	316414	16714	2.089
100	845509	2.82738	309220	9520	1.190
200	846964	2.84751	304966	5266	0.658
500	847772	2.85989	302101	2401	0.300
1000	847922	2.86407	301073	1373	0.172
2000	847774	2.86617	300542	842	0.105
5000	846970	2.86743	300217	517	0.065
10000	845523	2.86785	300107	407	0.051
20000	842627	2.86806	300052	352	0.044
50000	834232	2.86819	300020	320	0.040
100000	821248	2.86823	300009	309	0.039

From the tables and curves, it is clearly evident that lower values of R_c will allow more impulse voltage onto dc source. In this circuit arrangement, the optimum range is between $1 M\Omega$ and $10 M\Omega$. Thereafter, the higher R_c starts affecting the impulse component of the waveform by the decreasing value of $v_3(t)$ significantly. It is also observed that changing R_c affects the time to peak of the impulse waveform (t_p), hence changing the impulse waveshape. The time-to-peak of the waveshape is directly proportional to the resistance value, R_c .

3.6.3.4 Effects of resistance value of the test object

This resistance is also referred to as R_i . The impedance of the test insulator material consists of very high internal resistance, surface resistance and capacitances. The surface leakage resistance is a variable quantity that depends on the type, geometry of the particular insulator, contamination, as well as on other environmental factors such as temperature, air pressure, etc.

In a good weather, with dc operation, the surface insulation resistance is responsible for voltage distribution as no capacitive current flows. Pollution and wetting is known to reduce the leakage resistance of an insulator and the flashover voltage of the particular insulator.

A polluted and wetted insulator under test does not only affect the flashover voltages, but also affects the operation and output waveforms of the designed test configuration. The effects of the resistance of the test object (R_t) on the peak values of $v_3(t)$ and $v_4(t)$ are shown in Figure 3.22.

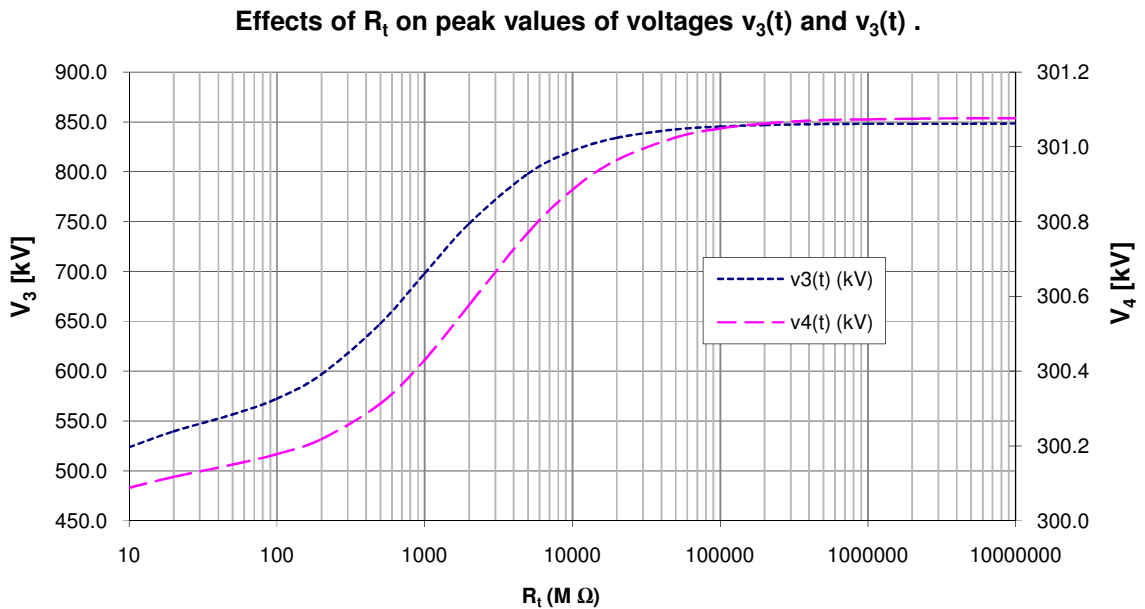


Figure 3.22: Effects of R_t on peak voltages $v_3(t)$ and $v_4(t)$.

It is evident that the total voltage that appears across the test object $v_3(t)$ increases with an increase in R_t . The actual dc voltage (V_{i3}) that appears across the test object against different R_t values is shown in Figure 3.23. Therefore, with a wet insulator arrangement, it is not easy to prestress a dc voltage because, as a result of voltage division, much of the dc voltage will be appearing across resistor R_c .

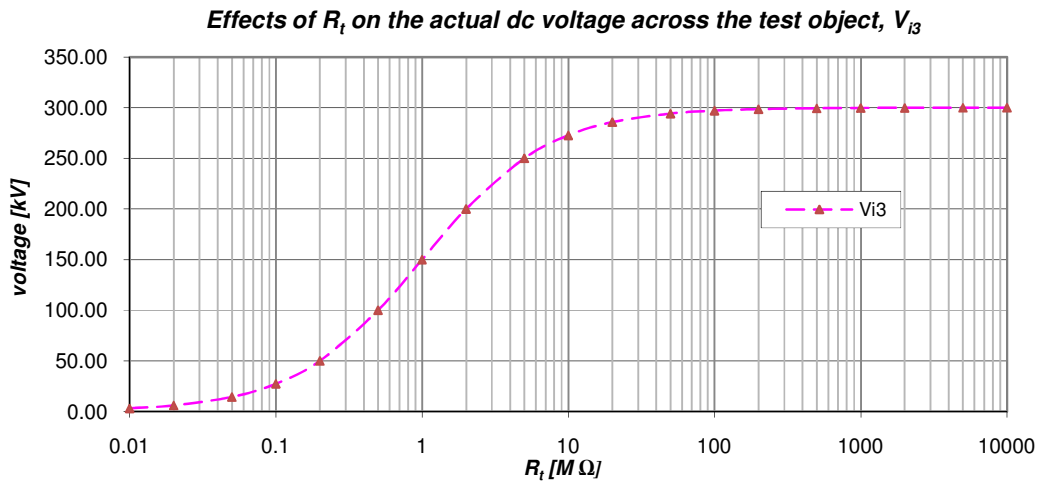


Figure 3.23: DC voltage across the test object as a function of different R_t values.

Table 3.6 summarizes effects of R_t on the circuit performance. This include the peak values of voltages ($v_3(t)$ and $v_4(t)$), time to peak for $v_3(t)$, and dc voltage across the test object V_{i3} . It can be observed that the peak values of $v_3(t)$, $v_4(t)$, V_{i3} and the time-to-peak of the waveform are all directly proportional resistor value R_c , although in the latter case very minimal.

Table 3.6: Numerical values for the effects of the value of R_t on the peak values of $v_3(t)$, $v_4(t)$ and V_{i3} .

$R_t [M\Omega]$	$v_3(t)$		$v_4(t)$	V_{i3}
	<i>Peak voltage</i> [V]	<i>Time to peak</i> [us]	<i>Peak voltage</i> [V]	<i>Peak voltage</i> [V]
0.01	523658	2.536	300088	2970
0.02	539742	2.681	300117	5880
0.05	556609	2.785	300150	14.29
0.10	572512	2.823	300178	27270
0.20	596725	2.843	300218	50000
0.50	647622	2.856	300313	100000
1.00	697922	2.860	300430	150000
2.00	748072	2.862	300577	200000
5.00	798162	2.863	300771	250000
10.0	820923	2.864	300886	272730
20.0	833918	2.864	300965	285700
50.0	842337	2.864	301025	294120
100	845250	2.864	301049	297030
200	846731	2.864	301062	298510
500	847622	2.864	301071	299400
1000	847922	2.864	301073	299700
2000	848072	2.864	301075	299850
5000	848163	2.864	301076	299940
10000	848193	2.864	301076	299970

3.6.3.5 Effects of the capacitance of the test object on the voltage waveforms

The capacitance of the test insulator C_t mainly plays a part in ac and impulses under normal dry conditions. Under wet conditions, however, the leakage resistance is usually the deciding factor in flashover.

The effects that C_t value has on voltages $v_3(t)$ and $v_4(t)$ are illustrated with graphs in Figure 3.24. In the test configuration, the effect of C_t is mainly on the efficiency of the impulse waveform as illustrated in a graph in Figure 3.25.

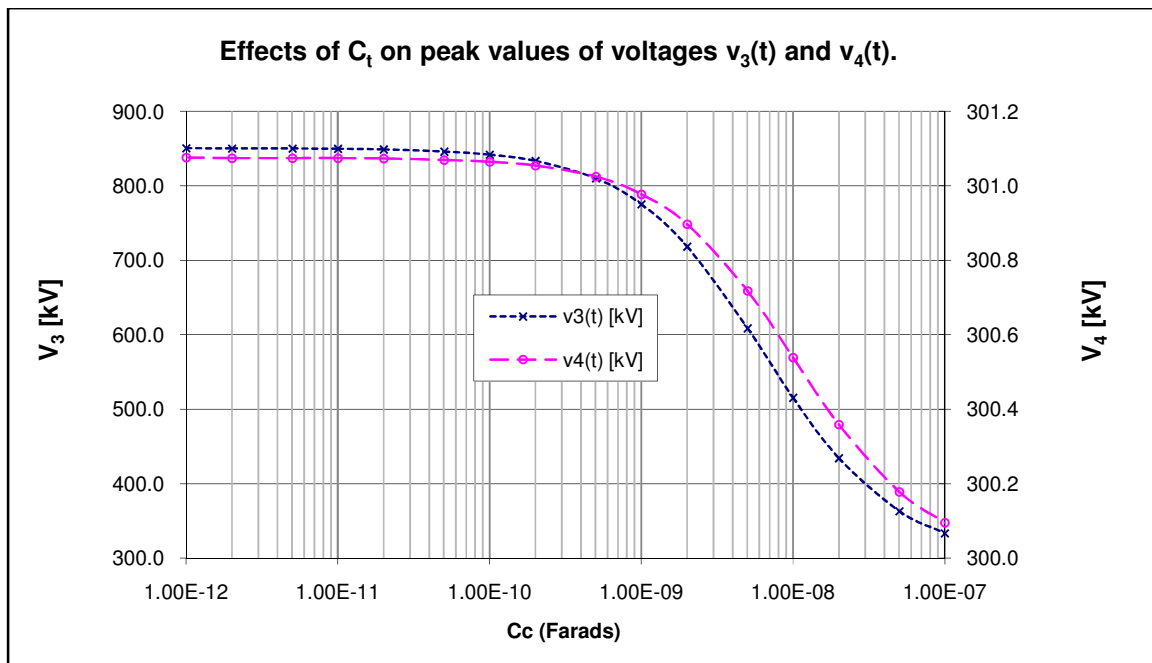


Figure 3.24: Effects of C_t on peak voltage values $v_3(t)$ and $v_4(t)$ voltages

As shown in the figure, $v_3(t)$ is the most affected. For a capacitance of $0.1nF$, the total voltage across test object is about $840kV$ compared to about $330kV$ at $100nF$. The voltage across the dc supply only falls with about $1kV$ or less over the same capacitance range. Figure 3.25 shows the efficiency curve, i.e. the efficiency of the impulse generator as a function of the test object's capacitance.

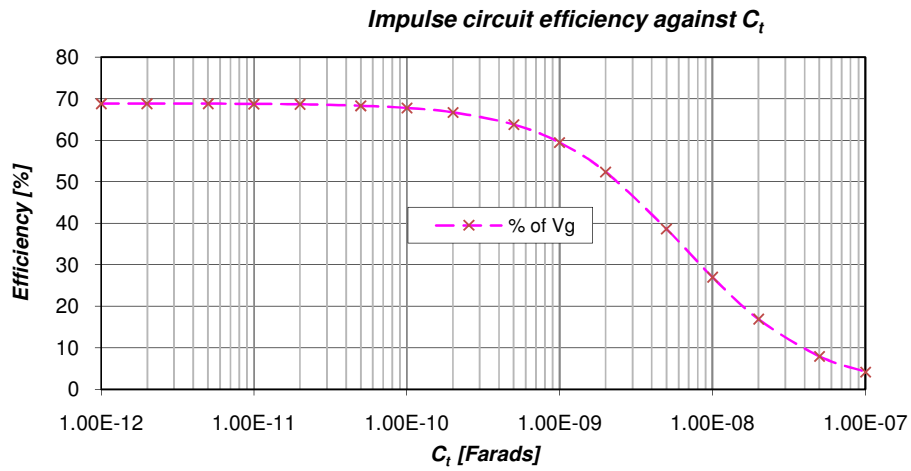


Figure 3.25: Efficiency of impulse circuit as a function of C_t .

The higher the C_t value, the lower the impulse generator’s efficiency. This is opposite to the way C_c affects the impulse circuit. Hence, for this arrangement, the test object’s capacitance can be the limiting factor for the application. Time to peak is proportional to the C_t value. This and all other effects are summarised in Table 3.7.

Table 3.7: Numerical values for the effects of the value of C_t on the peak values of $v_3(t)$, $v_4(t)$ and the efficiency.

C_t (nF)	$v_3(t)$		$v_4(t)$	$v_3(t)-Vi3$	
	<i>Peak voltage</i> [V]	<i>Time to peak</i> [us]	<i>Peak voltage</i> [V]	<i>Peak voltage</i> [V]	<i>% of Vg</i>
0.001	850559	2.825	301076	550859	68.857
0.002	850471	2.826	301075	550771	68.846
0.005	850208	2.828	301075	550508	68.814
0.01	849770	2.832	301075	550070	68.759
0.02	848897	2.840	301074	549197	68.650
0.05	846294	2.864	301070	546594	68.324
0.10	842013	2.903	301065	542313	67.789
0.20	833659	2.980	301055	533959	66.745
0.50	810133	3.194	301025	510433	63.804
1.00	775360	3.510	300978	475660	59.458
2.00	718624	4.022	300897	418924	52.366
5.00	608921	5.011	300718	309221	38.653
10.0	515415	5.861	300539	215715	26.964
20.0	434309	6.609	300359	134609	16.826
50.0	363021	7.280	300178	63321	7.915
100	333343	7.563	300095	33643	4.205

3.7 Conclusions

The standard impulse waveform consists of two components of the same magnitude but different time constants. With dc biasing operation, the voltage waveform $v_3(t)$ can consist of up to 4 exponential components as shown below.

$$v_3(t) = \underset{A}{-603\,173.2} e^{-1.41042 \times 10^6 t} + \underset{B}{605\,655.7} e^{-26706.4t} - \underset{C}{2372.73} e^{-149.6t} + \underset{D}{299\,724.8} e^{-0.03329t}$$

The following observations apply to the waveform equation given above:

- A is a rising part, with 1.41042×10^6 as the time constant and 603173.2 as a peak voltage of the impulse, in volts.
- B is a decaying part, with 26706 as the time constant and 605655.7 as its component in voltage magnitude in volts.
- C is a decaying part, with 149.6 as the time constant and 2372.7 as voltage magnitude in volts.
- D is a decaying part, with 0.03329 as a very long time constant and 299724.8 as dc voltage component of the waveform.

A proper selection of variables is essential to achieve the desired performance. Impulse circuit efficiency is more affected by circuit capacitances than by resistances. Circuit resistances will mainly affect the dc operation of the circuit. The coupling components do have a very significant influence on the circuit performance, where C_c influences impulse efficiency and R_c influences the dc section of the circuit. It is also observed that the waveform times are also affected by these coupling components, with R_c the more influential of the two impedances.

The operation of this circuit is also limited by the resistance of the measured object, as it is not easy to pre-stress a lower resistance insulator because of its insufficient share of voltage since the dc voltage from the supply has to be divided between R_c (coupling resistance) and R_t (test object's resistance).

4. THEORETICAL AND PRACTICAL VALIDATION OF THE COMPOSITE WAVEFORM GENERATOR CIRCUIT

4.1 Introduction

Testing and verification of a design are very important aspects of engineering design and complete the whole design process. This chapter entails an evaluation and validation of the derived mathematical model. By using the available circuit component values of the Messwandler Bau construction kit, the output waveform is simulated using the derived mathematical model. The need for the output prediction is associated to following reasons:

- The safety of personnel and equipment can be at risk with high voltages. It is therefore important to be able to predict the output waveform of the composite waveform generator accurately.
- Understanding the operation of the test circuit and knowing what to expect is an important part of practical testing.
- It is also very important to verify that the test circuit satisfies requirements, namely the accurate generation of a composite waveform to be applied to the test object.

It is against that background that the derived mathematical time-domain model was simulated. This was done with computer software and using the available circuit component values of the used Messwandler Bau kit. The output composite waveform was evaluated against two different approaches in order to help evaluate the accuracy of the mathematical model. These methods are:

- Simulation with HSPICE. In this case, the simulation is performed with HSPICE computer software. The results on HSPICE are then exported to MATLAB software for graphical plotting.

- Practical measurement in the high voltage laboratory. Here, the circuit is constructed in the high voltage laboratory. The results obtained are recorded for analysis.

It is important that the accuracy with which the derived model predicts the output waveform remains consistent for different loading, coupling components and operating voltages.

4.2 Practical test arrangement

In order to test the theoretical model developed for the test arrangement, practical measurements were performed for a representative circuit arrangement. These tests were performed with a Messwandler Bau HV construction kit. Circuit components of the Messwandler Bau kit and their respective impulse generator function are shown in Table 4.1.

Table 4.1: Parameter values for the practical test arrangement.

<i>Impulse generator parameter</i>	<i>Construction kit component (value)</i>	<i>Impulse generator parameter</i>	<i>Construction kit component (value)</i>
$C_c, C_d, C_g,$	$CS (10 nF)$	R_d	$RD(375 \Omega)$
C_l	$CB (1.2 nF)$	R_e	$RE (6100 \Omega)$
V_{dc}	$5 kV$	R_c	$RS (10 M\Omega)$
V_g	$10 kV$		

The full schematic diagram of the circuit configuration is illustrated in Figure 4.1

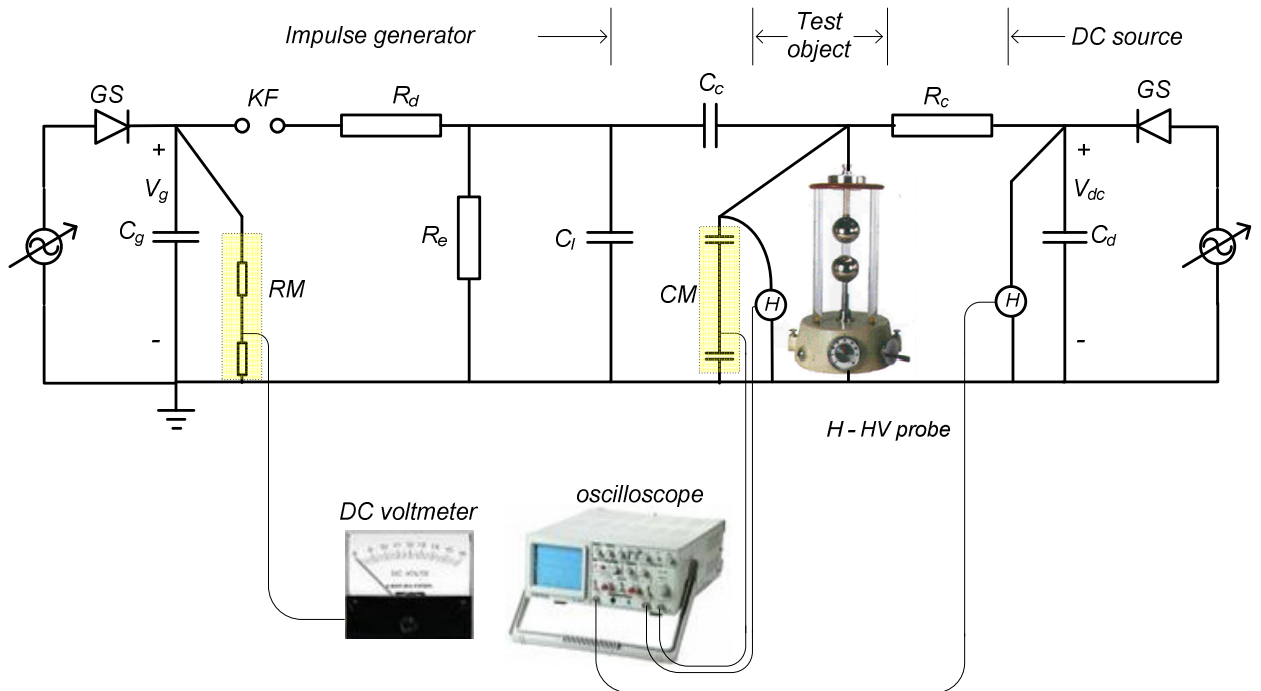


Figure 4.1: Schematic diagram of a test arrangement.

This arrangement consists of two dc circuits, namely the circuit that supplies dc voltage to the impulse generator circuit and the circuit that supplies the dc bias voltage to the composite waveform generator circuit. They are both adjusted with variable ac supplies (VARIACs). Diodes called GS and capacitors C_g and C_i form part of these rectifier circuits. The level of an impulse generator circuit input V_g is monitored with the aid of a dc voltmeter. An oscilloscope is used to monitor the dc bias voltage value. As indicated in Figure 4.1, H represent HV (high voltage) probe. These HV probes are used to measure dc voltages across the test object and across the dc source. The use of HV probes in conjunction with capacitor voltage dividers to measure the output waveform is explained later in this chapter.

Figure 4.2 shows a photograph of the test arrangement's construction made with a Messwandler Bau kit in the high voltage laboratory.



Figure 4.2: Messwandler Bau construction kit arrangement in the high voltage lab.

The test object used in this experiment is a 5 cm sphere-to-sphere air gap with a gap arrangement spacing of 2 cm . This component (sphere-to-sphere air gap arrangement) is part of the construction kit. This component is shown in Figure 4.3.

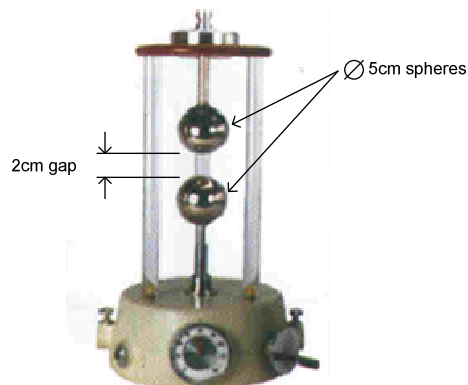


Figure 4.3: A sphere-to-sphere gap arrangement used as test object.

An accurate construction and a close monitoring of the experiment are needed. A careful reading of the results and application of the necessary atmospheric correction factors when interpreting results are the other requirements. Deviation in temperatures and pressure need to be compensated [39]. The process of the entire data capturing and processing are listed below. The full explanation of the data processing is covered in section 4.2.3.

- Practical tests in the high voltage laboratory.
- Capturing of impulse and dc waveform separately.
- Filtering of waveforms.
- Addition of filtered impulse and dc waveforms to obtain the final composite waveform.

The process of obtaining an ultimate output from these experiments is rather lengthy, more especially with the problem of inadequate measuring apparatus. The data is captured with the available equipment as explained in section 4.2.2. The procedures of capturing, processing measurements and interpreting the results are closely explained as in the following sections.

4.2.1 Captured waveforms

The captured waveforms undergo a processing phase before they can be meaningfully interpreted. That includes the filtering of unwanted components i.e. dc offset from impulse measurement and unwanted impulses on the dc measurement. The filtered waveforms are then added together to obtain the final desired composite waveform.

4.2.2 Measuring equipment used

The problem with measuring is not only associated with the magnitude of the voltage, but a combination of high voltage with high frequency contents in the waveform. Lightning happens in microseconds and a fraction of that needs to be captured when doing these waveform analysis. It is a challenge to find an apparatus in practice that can be calibrated to measure both fast transient and the dc part of the composite waveform across the test object simultaneously.

Therefore, the output voltage across the test object was obtained by using two separate measuring equipments for dc and ac (impulse) measurements. The two measured quantities are then added together to obtain the true composite waveform that is supplied across the test object.

With careful calibration, the high voltage probes Tektronix *P6015A* are tuned accurately to measure the dc components in the test circuit, i.e. dc voltage across the dc source terminal and dc voltage across the test object. However, these HV probes can still pick up some high frequency contents of the measured waveform, but rather inaccurately. Therefore, it is needed to get rid of these high frequency contents of the waveform captured with the probes.

A high ohmic ($140\text{ M}\Omega$) resistor was used to measure the impulse generator's input dc voltage V_g . With a good high frequency response, the use of a capacitive component to measure the impulse part of the waveform is necessary. Capacitor CB (1200 pF) of the construction kit was used for impulse measurement.

4.2.3 Processing of data

4.2.3.1 Overview

In section 4.2.1 and 4.2.2 it was stated that one of the challenges in these experiments is measurement. The 75 MHz bandwidth rating of the *P6015A* enables one to capture fast voltage signals. However, fine tuning this apparatus for high frequencies does compromise the accuracy of low frequencies and dc measurements. Hence, in practice it is difficult or almost impossible to calibrate this HV probe for the whole range of frequencies. It is for this reason that a capacitor voltage divider was used to capture the impulse part of the waveform. The probe captures the dc part of the composite waveform.

By using filter functions of MATLAB software, the two waveforms measured with a capacitor voltage divider and a high voltage probe can be filtered. The capacitor voltage divider measured waveform if filtered of the dc offset, while the waveform measured with the probe is filtered of all high frequency components to give the dc voltage. The filtered waveforms are

then added together to produce the actual composite waveform. This procedure is defined below.

4.2.3.2 Measurement of the impulse component of the composite voltage waveform

Voltage measured by the capacitor voltage divider comprises an impulse part of the waveform and dc offset. It is needed to get rid of this dc offset before this result can be interpreted. Figure 4.4 shows waveform as measured by the capacitor voltage divider across the test object.

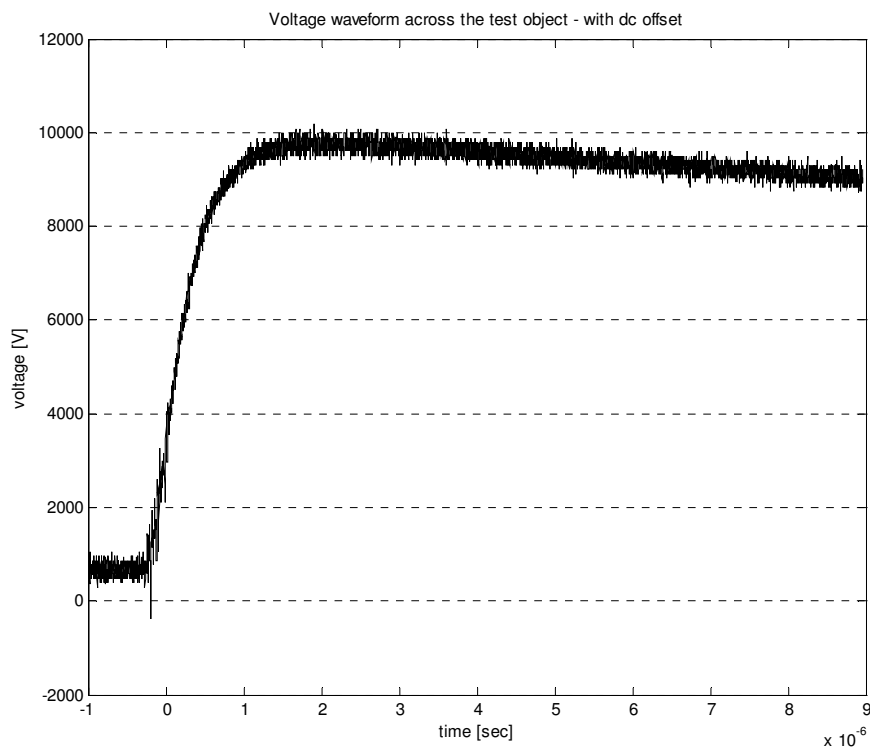


Figure 4.4: The captured waveform from the capacitor voltage divider.

The waveform in Figure 4.4 still contains dc offset voltage. Using MATLAB software's filter functions, the dc offset voltage was filtered out to obtain the voltage waveform shown in Figure 4.5. This is the impulse component of the composite waveform across the test object.

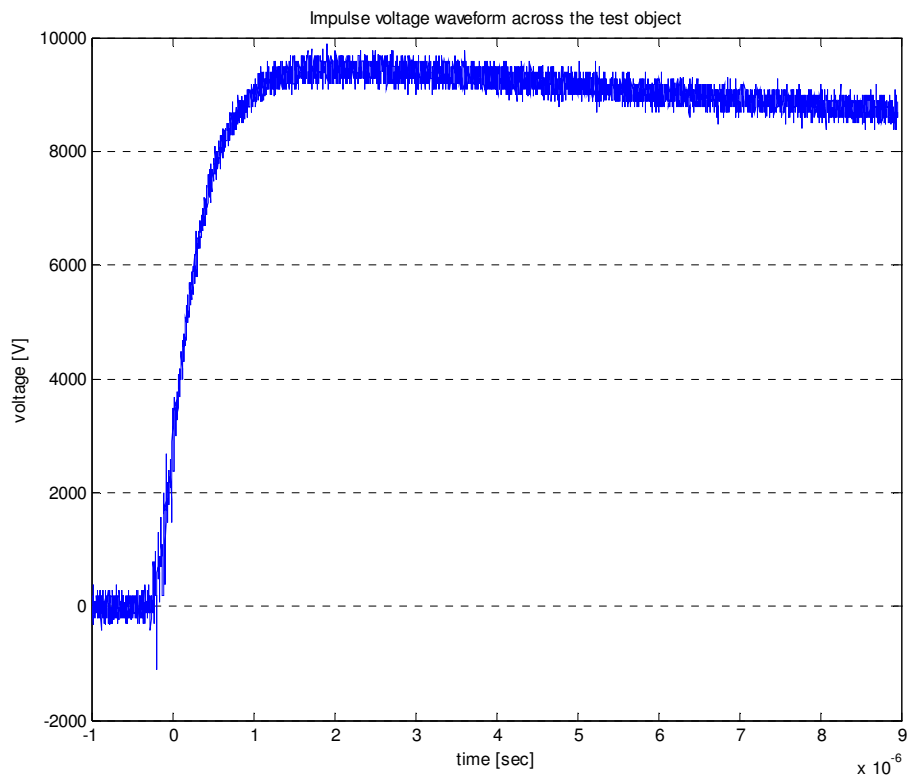


Figure 4.5: A measured impulse signal with dc offset filtered out.

4.2.3.3 Measurement of the dc component of the composite voltage waveform

Because the HV probes were calibrated for better low frequency and dc precision, the entire range of high frequency voltage recorded are compromised and become useless. This high frequency contents need to be filtered out. Figure 4.6 shows a high voltage measured signal across the test object before undergoing filtering process. All impulses and frequency contents of the waveform are then filtered out to leave the dc voltage as shown in Figure 4.7. This is the dc component of the composite voltage waveform that appears across the test object.

CHAPTER 4 – THEORETICAL AND PRACTICAL VALIDATION OF THE COMPOSITE WAVEFORM GENERATOR CIRCUIT

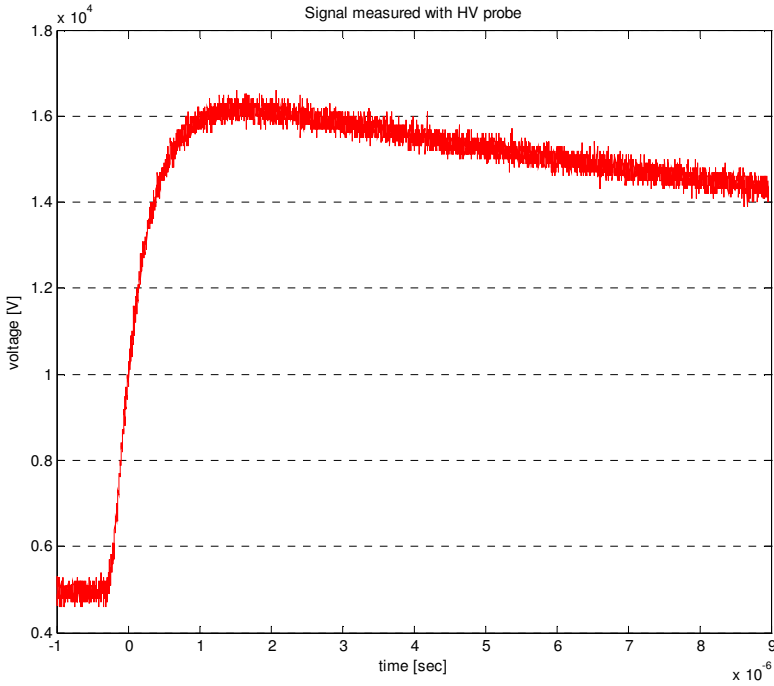


Figure 4.6: A voltage signal measured with high voltage probe.

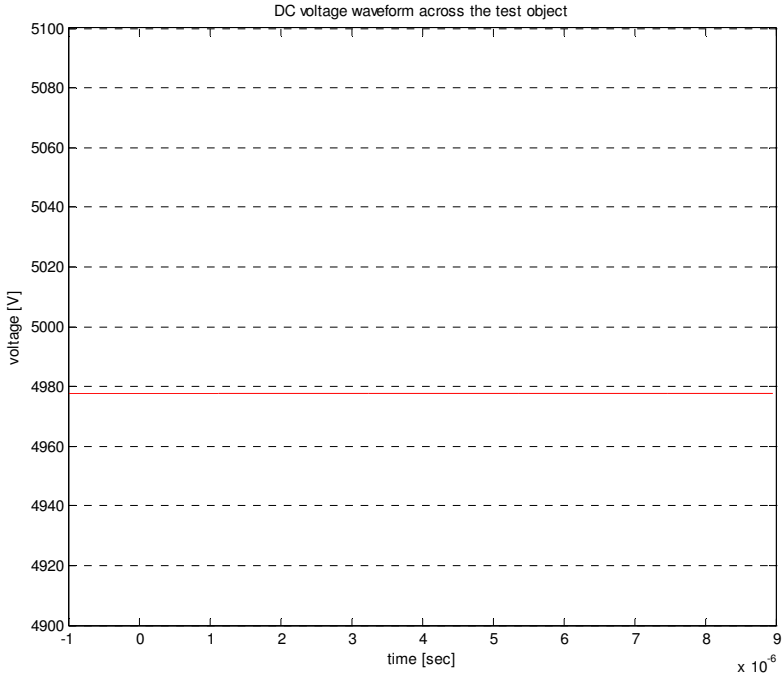


Figure 4.7: The obtained pure dc voltage waveform.

4.2.3.4 Addition of the measured dc and impulse waveforms

After the waveform filtering is completed, the processed waveforms are added together. The applied impulse voltage obtained as shown in Figure 4.5 is superimposed on the measured dc voltage shown in Figure 4.7 to obtain the final waveform. This final (composite) waveform is the actual voltage signal that appears across the test object when there is no flashover. This final composite waveform is shown in Figure 4.8.

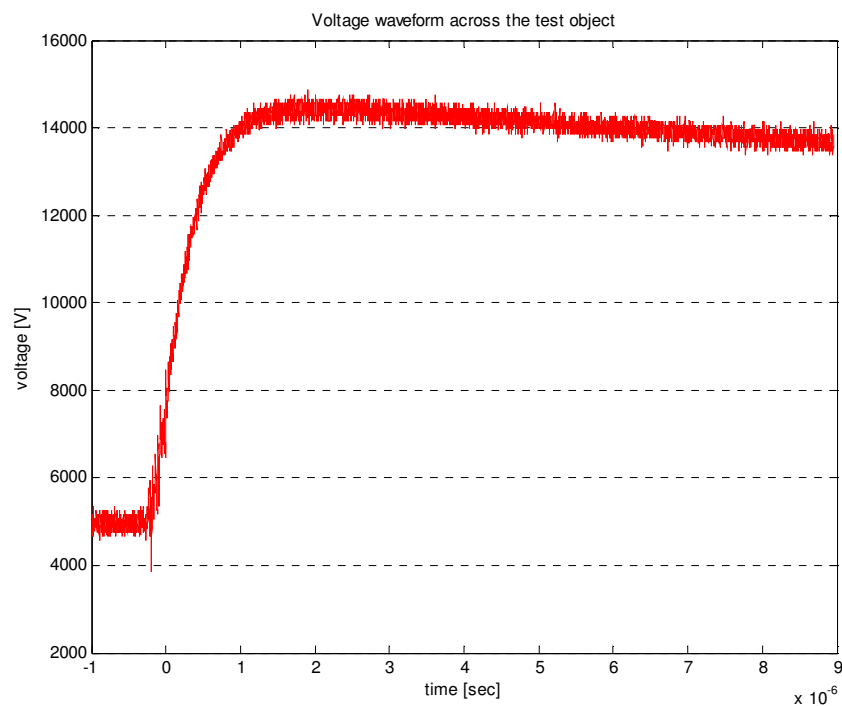


Figure 4.8: The final voltage signal across test object.

It is clearly visible that the front time of this waveform, shown in Figure 4.8, is between the desired 1 to 2 μs , which is the front time for lightning waveshape. The complete waveform is shown in Figure 4.9.

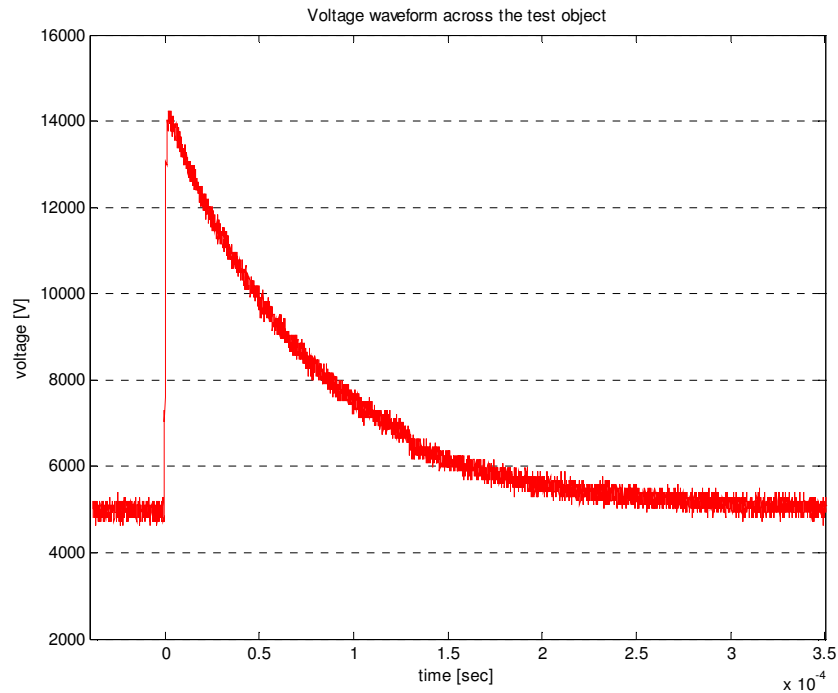


Figure 4.9: The final voltage signal across test object, full waveform.

The tail time in the full waveform figure also shows that it falls within the definitions of a lightning waveform of about $50 \mu s$. The next task is to verify how these measurements compare with the predicted plots of the mathematical model.

4.3 Simulation of the composite waveform generator circuit with the mathematical model

The entire composite waveform generator circuit is simplified as explained in Chapter 3. The measuring devices and test object form part of the overall arrangement, and the respective impedances need to be considered in the circuit representation and simulation. The simulation was performed using the circuit component values used in the practical test as given in section 4.3. The process of modelling and simulation with a mathematical model is highlighted below:

- Deriving the single stage equivalent of the composite waveform generator circuit.
- Substituting circuit variables in equation $V_3(s)$ with actual component values.

- Applying inverse Laplace to equation $V_3(s)$ to obtain equation $v_3(t)$.
- Graphical plotting of equation $v_3(t)$ with MATLAB software.
- Comparing the output voltage waveform with the practical measured waveform.

The derived mathematical (theoretical) model contains all components of this test circuit, i.e. the actual circuit components, test object and measuring equipment impedance parameters. For example, the HV probes used to measure the dc voltages have an input impedance consisting of a 100 MΩ resistors in parallel with a 3 pF capacitance. These impedance components form part of the simplified composite waveform generator circuit. The impedance of the test object can be obtained through direct measurement, or estimated using different tables or formulas. The capacitance of a sphere gap C_t can be determined using the relationship shown in equation 4.1. The letter S denotes the sphere-to-sphere gap spacing and f denotes the geometry factor [[2], [40]].

$$C_t = \frac{S \times 10^{-11}}{36 (f - 1)} [F] \quad (4.1)$$

The geometry factor is derived from the ratio of gap spacing to sphere radius, i.e.

$$\text{Gap to sphere ratio} = \frac{2cm}{5cm} = 0.4$$

The graphical relationship, $f(f_1)$ shown in Figure 4.10 reflects a value of $f = 1.15$ for the ratio of 0.4 [[39], [40]]. This yields

$$C_t = \frac{2 \times 10^{-11}}{36 (1.15 - 1)} = 3.70 \times 10^{-12} F .$$

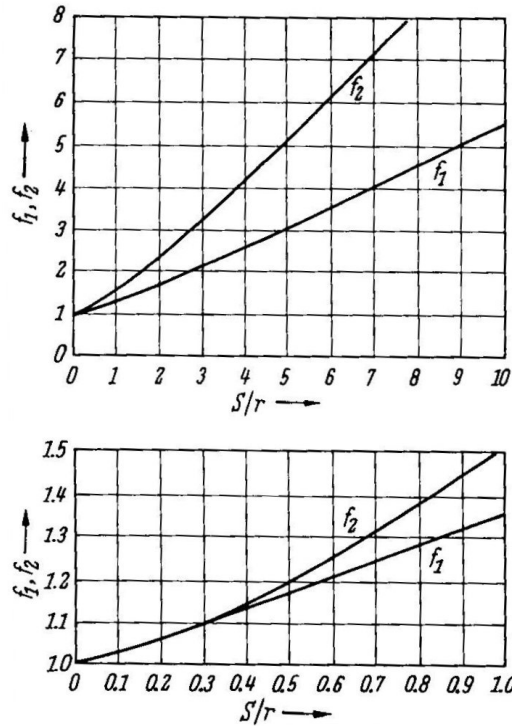


Figure 4.10: Capacitance geometry factor for spaced spheres [40].

In terms of an air gap arrangement, the resistance of the air gap can be represented by a large arbitrary, but reasonable value, e.g. of the order of a hundred megaOhms. In this simulation, 500 M Ω was used as the resistance of the test object.

4.3.1 Results obtained and comparisons with the practical measured results

With C_t of 3.7 pF, R_t of 500 M Ω and the rest of the test circuit parameters given in Figure 4.10, the mathematical model yields the following time domain equation:

$$V_3(t) = 5000 (-1.8999 e^{-2.3616 t} + 1.9014 e^{-13799.6 t} + 0.0237 e^{-20.3462 t} + 0.9747 e^{-0.4842 t}) \quad (4.2)$$

$V_3(t)$ is the voltage waveform to be applied to the test object.

In Figure 4.11, the measured waveform of the composite waveform generator circuit is compared with the response predicted by means of equation 4.2 (mathematical model). Figure 4.12 shows the graphical plot of the same output, but on a longer time scale ($350 \mu s$).

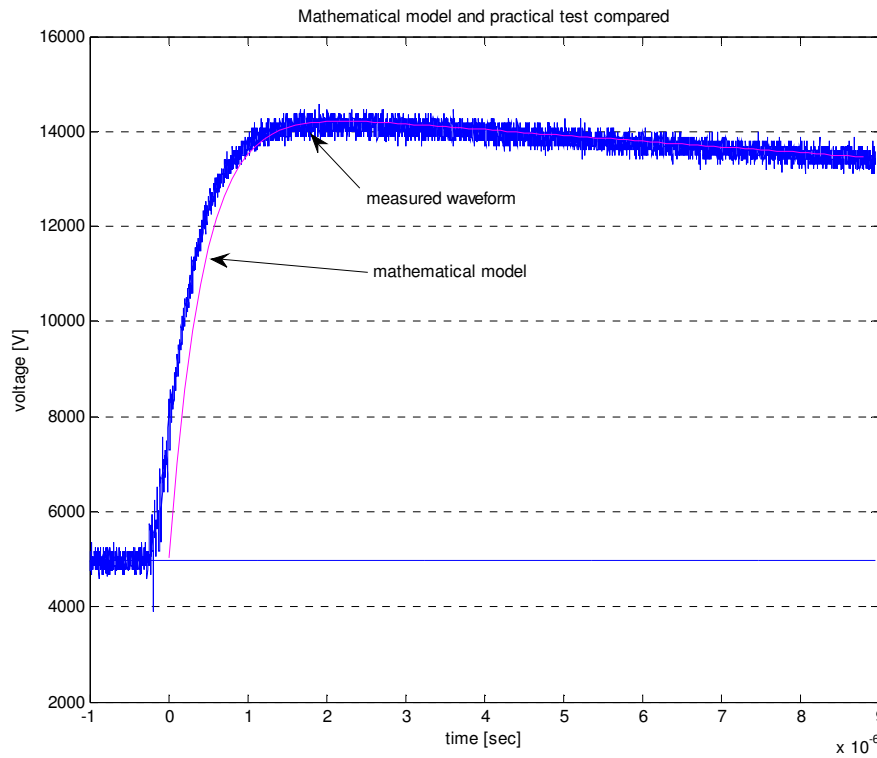


Figure 4.11: Comparison of predicted and measured waveforms, front part.

The results obtained show that the derived model predicts the measured response closely, particularly in view of tolerance uncertainties in the component values used in the simulation. The slight shift of the measured waveform observed in Figure 4.11 is caused by inaccurate triggering of the waveform on the oscilloscope.

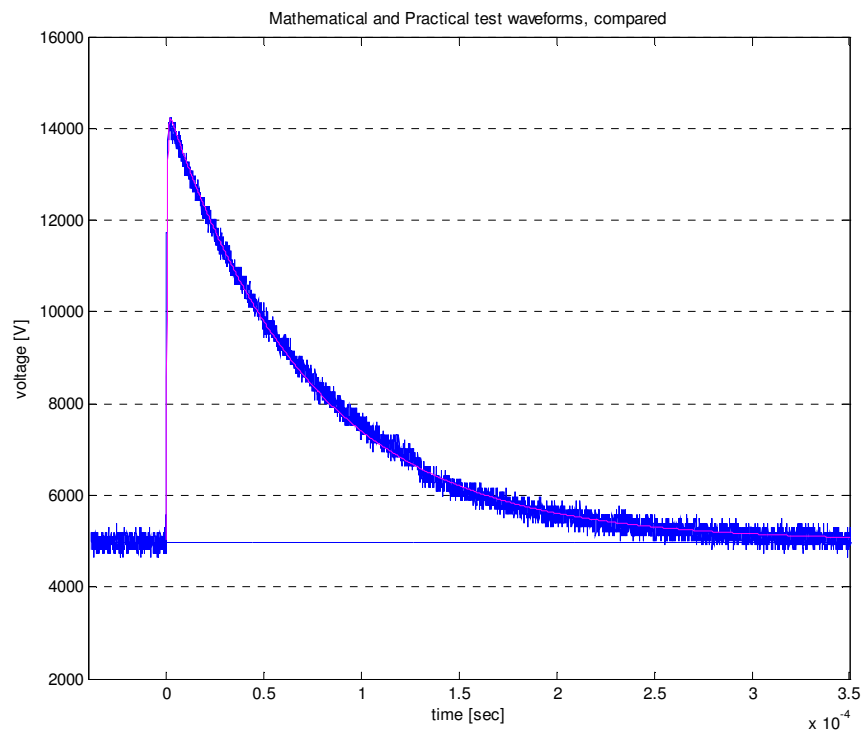


Figure 4.12: Comparison of predicted and measured waveforms, full waveform.

In the full impulse waveform plot shown Figure 4.12, the two waveforms are shown plotted on top of each other. This is an indication of the close prediction of the output waveform with the derived model. The same comparison procedure is also performed with the HSPICE simulation method as explained in Section 4.4

4.4 Modelling the composite waveform generator circuit with HSPICE

This is the other method of assessing the accuracy of the derived mathematical model. Using the component values available with the used Messwandler Bau construction kit, a time response of the composite voltage waveform was simulated with HSPICE software. Just like the previous comparison method (mathematical model and practical measurement), the HSPICE simulation also helps assess the accuracy of the derived mathematical model. The composite waveform obtained in the simulation with the mathematical model is compared to the output waveform obtained when the test is simulated with HSPICE software. This

comparison is also done with graphical plots. The whole process of preparing the circuit and simulating is highlighted below.

- Deriving the single stage equivalent of the composite waveform generator circuit.
- Constructing a net list of the parameters and values in the .sp file.
- Performing a transient analysis of the circuit with the main interest on the voltage across the test object.
- Printing HSPICE results into a CSV file.
- Importing the CSV file into MATLAB and graphical plot the voltage across the test object.
- Comparing the HSPICE waveform with the response obtained with the mathematical model simulation.

A net list is constructed by numbering all circuit nodes. It is then entered into the simulation package by defining each component type and value as well the nodes they are connected to. The initial dc voltages, namely voltage V_g and V_{dc} are defined. Transient analysis is then performed yielding the output voltage after the operation of the switching spark gap at $t = (0)$. The code of this composite waveform simulation is shown in Appendix.E

4.4.1 Results obtained and comparisons with results of the mathematical model

Figure 4.13 and Figure 4.14 compares the responses obtained with equation 4.2 (mathematical model) and the output waveform obtained with HSPICE simulations. It can be observed that a good correlation is obtained. The MATLAB code for plotting these waveforms is shown in G.1 of Appendix.G.

CHAPTER 4 – THEORETICAL AND PRACTICAL VALIDATION OF THE COMPOSITE WAVEFORM GENERATOR CIRCUIT

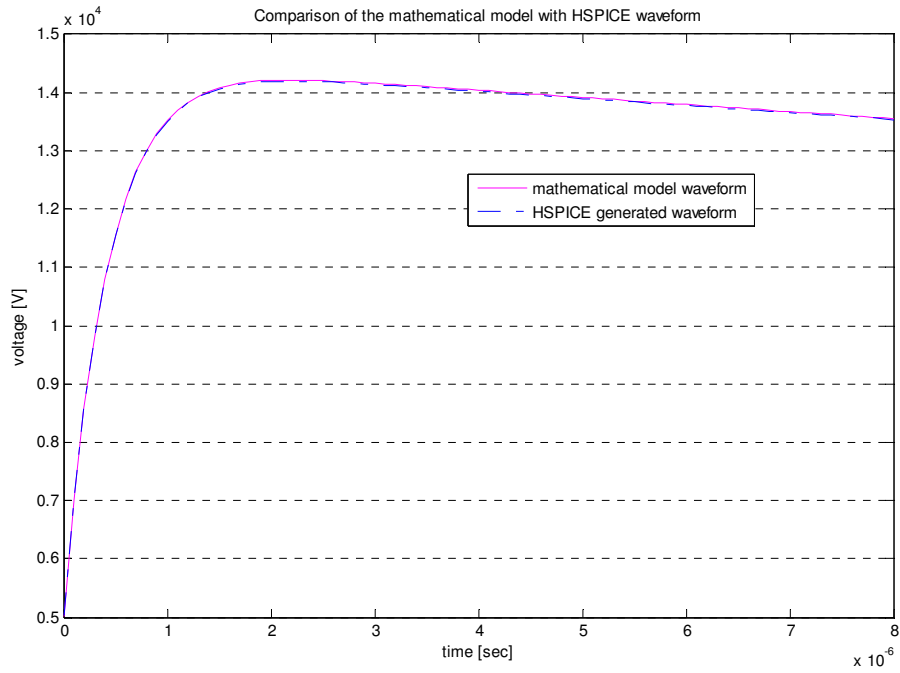


Figure 4.13: Comparison of mathematical model with HSPICE simulation.

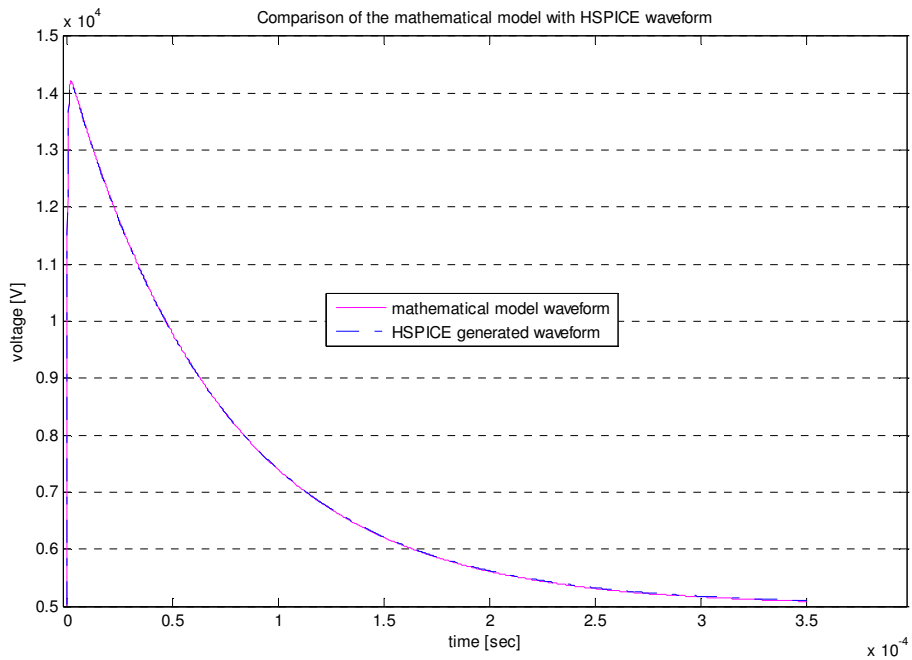


Figure 4.14: Comparison of mathematical model with HSPICE simulation, full waveform.

4.5 The effects of loading, coupling components and operating voltage levels of the performance of the composite waveform generator

The composite waveform generator circuit must be able to perform consistently under the following:

- It must be able to accommodate various loads of different parameter values.
- It must be able to operate effectively with various coupling component values.
- It must be able to operate under different voltage levels depending on the requirements of the test object.

4.5.1 The effects of different load impedances

The successful implementation of this system depends mainly on its aptitude to be used across loads of different impedances. The load (test object) mainly consists of capacitive and resistive components as modelled in the circuit arrangement shown in Figure 4.. In this model, C_t and R_t represent resistance and capacitance of a test object respectively. Insulators come in different types such as composite, porcelain, glass, air gap arrangements, etc. and operate in different conditions, i.e. wet or dry environments. It is therefore imperative to prove use on this proposed arrangement on these typical loading conditions.

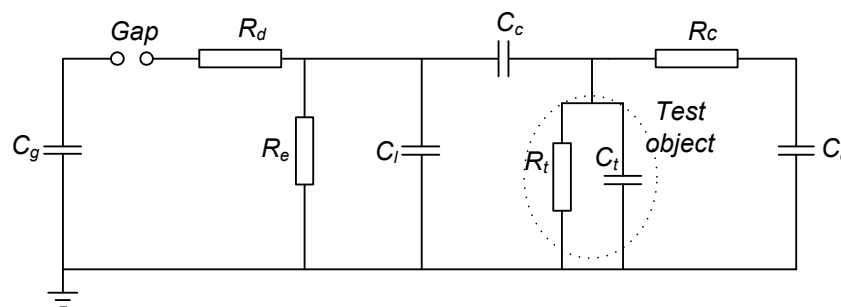


Figure 4.15: Highlights the test object impedance parameters in the circuit.

In this experiment, C_t and R_t values were changed in different tests in order to determine their effects on the output voltage of the composite waveform generator. The experiment was carried out by means of the following methods:

- Simulation with the derived mathematical model.

Practical construction of the circuit in the high voltage laboratory.

Table 4.2 shows a list of parameters used in this experiment. Components C_t and R_t are varied as indicated in Table 4.3.

Table 4.2: List of circuit parameters and variables used in the simulation.

<i>Variable</i>	<i>Value</i>	<i>Variable</i>	<i>Value</i>
V_g	15 kV	V_{dc}	5 kV
C_g	10 000 pF	R_d	375 Ω
C_l	1 200 pF	R_e	6100 Ω
C_c	10 000 pF	R_c	6 M Ω
C_d	20 pF	R_m	20 k Ω
C_t	x	R_t	x

4.5.1.1 Results obtained

The results under different C_t and R_t values are shown in Table 4.3. The results shown are the predicted and measured peak voltage values of the composite waveform across the test object. The differences between the predicted and measured values are also summarised in the form of percentage (%). The used R_t values are 2 M Ω and 6 M Ω and C_t values of 100 pF and 1 300 pF were used.

Table 4.3: Effects of the resistance and capacitances of the test object on the output voltage, V_3 .

$C_t \rightarrow$ $R_t \downarrow$	<i>100 pF</i>			<i>1 300 pF</i>		
	<i>predicted (kV)</i>	<i>Measured (kV)</i>	<i>% deviation from predicted</i>	<i>predicted (kV)</i>	<i>Measured (kV)</i>	<i>% deviation from predicted</i>
<i>2 MΩ</i>	<i>17.17</i>	<i>18.12</i>	<i>5.6</i>	<i>14.90</i>	<i>15.34</i>	<i>3</i>
<i>6 MΩ</i>	<i>17.17</i>	<i>17.36</i>	<i>1.1</i>	<i>14.90</i>	<i>15.51</i>	<i>4.1</i>
<i>12 MΩ</i>	<i>17.17</i>	<i>17.88</i>	<i>4.1</i>	<i>14.90</i>	<i>14.99</i>	<i>0.6</i>
<i>Open Rt</i>	<i>17.17</i>	<i>16.97</i>	<i>-1.2</i>	<i>14.90</i>	<i>15.05</i>	<i>1.0</i>

From the tabulated results, it is shown that the deviation of the measured from the predicted ranges between -1.2% and 5.6%. It is clear that this test circuit and/or arrangement are adequate for application to a wide range of test object impedances.

4.5.2 The effects of different coupling component values

As it was highlighted in Chapter 3, the coupling components play an integral role in this whole test circuit arrangement. Their positions in the circuit are highlighted in Figure 4.16.

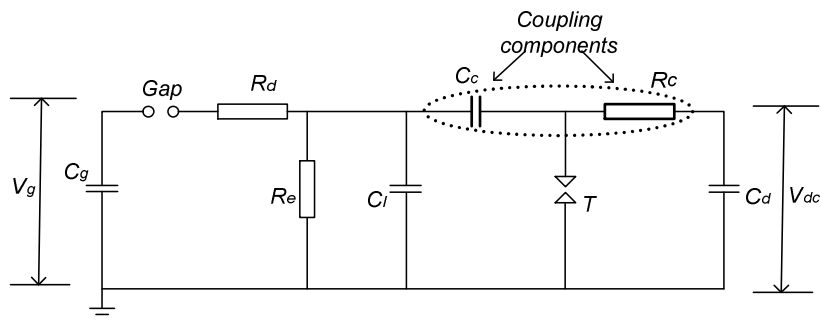


Figure 4.16: Location of coupling components in the test circuit.

It is vital to understand the function of coupling components on the practical test circuit and to establish their effects on the output composite waveform across the test object. Since this test arrangement is assembled with the existing circuit components, finding the exact values of the desired components (coupling) may become a challenge. It is therefore important to know what effect the various coupling resistor and capacitor values have on the output of the composite waveform generator. Tests were performed with a variety of available resistive and capacitive coupling components. Table 4.4 shows a list of circuit parameters used in the simulation.

Table 4.4: List of parameters used in the prediction.

<i>Variable</i>	<i>Value</i>	<i>Variable</i>	<i>Value</i>
V_g	15 kV	V_{dc}	5 kV
C_g	10 000 pF	R_d	375 Ω
C_l	1 200 pF	R_e	6100 Ω
C_c	<i>x</i>	R_c	<i>x</i>
C_d	20 pF	R_m	20 k Ω
C_t	100 pF	R_t	12 M Ω

4.5.2.1 Results obtained

Table 4.5 and Table 4.6 show the results obtained with different coupling and resistor values.

Table 4.5: Results of coupling capacitor effects on voltage V_3 across the test object.

$C_c \rightarrow$	1 200 pF			10 000 pF		
	<i>Predicted</i> (kV)	<i>Measured</i> (kV)	% <i>Deviation</i>	<i>Predicted</i> (kV)	<i>Measured</i> (kV)	% <i>Deviation</i>
$R_c \downarrow$ 6 M Ω	16.25	16.86	-1.8	17.17	17.88	4.1

Table 4.6: of coupling resistor effects on the voltage across test object, V_3 .

$R_c \rightarrow$	$2\text{ M}\Omega$			$12\text{ M}\Omega$		
	<i>Predicted</i> (kV)	<i>Measured</i> (kV)	<i>%</i> <i>Deviation</i>	<i>Predicted</i> (kV)	<i>Measured</i> (kV)	<i>%</i> <i>Deviation</i>
$C_c \downarrow$						
10 000 pF	17.17	17.31	0.8	17.17	17.88	4.1

It can be observed that the percentage deviation of the measured form the predicted is -1.8 and 4.1 for coupling capacitors of 1200 pF and 10 000 pF respectively. For coupling resistors, deviation is at 0.8 and 4.1% for 2 Ω and 6 Ω respectively.

4.5.3 The effects of different operating voltages

The designed test system needs to be able to perform independently of different voltage levels depending on the desired output. Hence, the test system was simulated at different voltage levels to see if voltage levels do influence the efficiency of the circuit. The main aim was to have a different impulse to dc source voltage ratio. At first, the 15 kV voltage was used as V_g (generator's input voltage) and 5 kV dc source voltage V_{dc} , and then a 10 kV as V_g on a 10 kV dc source voltage. Table 4.7 shows a list of used parameters. Voltages V_g and V_{dc} are varied shown in Table 4.8.

Table 4.7 List of circuit variables used in the prediction.

<i>Variable</i>	<i>Value</i>	<i>Variable</i>	<i>Value</i>
V_g	x	V_{dc}	x
C_g	$10\ 000\ pF$	R_d	$375\ \Omega$
C_l	$1\ 200\ pF$	R_e	$6100\ \Omega$
C_c	$10\ 000\ pF$	R_c	$6\ M\Omega$
C_d	$20\ pF$	R_m	$20\ k\Omega$
C_t	$100\ pF$	R_t	$12\ M\Omega$

4.5.3.1 Results obtained

The results of both the predicted and simulated simulations are summarised in Table 4.8.

Table 4.8: Results obtained with different voltages levels of V_g and V_{dc} .

<i>DC Voltage (V_{dc}): 5kV</i>			<i>DC Voltage (V_{dc}): 10 kV</i>		
<i>Impulse generator's input (V_g): 15kV</i>			<i>Impulse generator's input (V_g): 10kV</i>		
<i>Predicted</i> <i>(kV)</i>	<i>Measured</i> <i>(kV)</i>	<i>% Deviation</i>	<i>Predicted</i> <i>(kV)</i>	<i>Measured</i> <i>(kV)</i>	<i>% Deviation</i>
17.17	17.88	4.1	17.17	18.01	4.89

Percentage deviations of 4.1 and 4.89 were obtained for the two different scenarios. This deviation is the difference between measured and predicted expressed in terms of the predicted value.

4.6 Conclusions

This chapter was aimed at testing the model and verifying its accuracy mainly at the voltage across the test object (V_3). This composite waveform comprises of an impulse applied on top of an existing dc voltage.

The responses predicted with the mathematical the model was compared to responses simulated with HSPICE and practical measurements. Good correlations between these results were obtained, thereby validating the accuracy of the model and the associated mathematical relationships.

Although there is a lack of measuring equipment in the market, the practical test results obtained show that good results can be obtained with the use of two separate measuring equipments, i.e. separate dc and ac (impulse) devices, for measurement of the composite output voltage waveform. The two separate measurements just need to be verified and processed correctly.

The last part of the experiment on the robustness and accuracy of the model proves that the derived model performs satisfactorily with different loads, coupling components and operating voltage levels. The small deviations obtained in this experiment are reasonably acceptable and can be attributed to different factors, i.e. analog measurement of waveforms, temperature variations, etc. Otherwise, this series of tests can be deemed a success and they confirm that this circuit can be used to predict the output of the actual circuit arrangement.

5. APPLICATION OF THE COMPOSITE WAVEFORM GENERATOR CIRCUIT TO OBTAIN FLASHOVER LEVELS OF AN INSULATOR

5.1 Introduction

It is in the interest of design engineers to know and understand the requirements of system insulation. Insulator flashover and withstand are some of the main technical attributes that define an insulator. The basic application of the final circuit is insulator testing. Although it was primarily designed to supply impulses superimposed on dc voltage, it can as well solely be used for any of the two voltage types, i.e. dc or impulse.

Understanding the performance of insulators under different operating conditions is so imperative. A good insulator should be able to withstand abnormalities such as internal and external overvoltages. It is therefore important to comprehend the effects these overvoltages will have on our insulators. Switching and lightning are the main causes of overvoltage transients. Pollution and wetting affects the insulator characteristics. The understanding of effects of impulse voltages (overvoltages) on insulators under pre-stressed dc voltage is therefore of practical importance.

This chapter takes the designed composite waveform generator circuit to the real application in the HV laboratory. The composite voltage waveform generated is applied across a dry composite insulator. The impulse component of the composite waveform is of a typical lightning shape. These impulse components were of both positive and negative polarities. The effect on flashover levels was observed as dc bias voltage increased. The experiment was repeated on a polluted wet insulator. The results obtained were tabled, plotted and interpreted. The results were summarised in a way that highlights the effect of dc bias voltage as well as the polarity effect of impulse voltages on dc insulation both under dry and wet conditions.

5.2 Insulator under test

In the last few decades, new materials were developed which in service have proved to be superior to porcelain insulators in combating contamination. However, reported reasons for using these products are primarily the smaller weight ratio, which has permitted compacting and improvement of tower designs and resistance to physical vandalism. These products are commonly called composite or non-ceramic insulators. Because of their weight advantage and superior contamination performance, these non-ceramic insulators are gaining popularity and have been adopted in most new systems including HVDC systems. Silicon rubber (SiR), Ethylene propylene diene monomer (EPDM) and Ethylene propylene monomer (EPM) composite insulators are the types of composite insulators in the market [13]. The Silicon rubber insulator used in this test is shown in Figure 5.1.

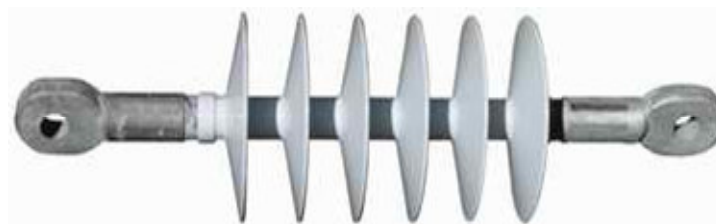


Figure 5.1: Silicon rubber composite insulator which was tested.

The laboratory test conditions were designed to simulate as closely as possible the field conditions. The silicon rubber insulator tested has a creepage distance of 420mm . Testing such an object serves a practical interest because this is the typical type on insulators commonly used on HVDC systems. This 22kV rated insulator was subjected to tests in order to determine its impulse flashover levels when pre-stressed with dc voltage of various levels. The significance is to observe the effect that dc voltage has on the flashover level of the particular insulator.

The impulse flashover tests at different dc values were performed on a dry insulator. The particular insulator was then artificially polluted and wetted. The same series of tests done on a dry insulator were then repeated. This was done in order to observe the influence that wetting would have on the flashover levels. [29]

5.3 Artificial contamination of the insulator

In the practical environment, the insulators of the electrical power lines are often subjected to the deposition of contaminant substances in the environment. This can cause a serious reduction in the efficiency of the insulator. Artificial contamination of the insulator was done in a way that typifies the contamination in polluted and wet field conditions. The insulator was sprayed with an artificial contaminant consisting of Kaolin and salt mixture in water as explained in Section 5.7.3.

The objective of the test was not to see the effect of the severity of contamination, but to observe the difference between dry and wet insulation behaviour and the application of the test circuit arrangement thereof. Therefore, only a light degree of pollution was required. The conductivity volume of 5 mS/cm Kaolin composition was used.

The composition was prepared to the closest accuracy of composition using the substances below:

- A 14 l bowl of distilled water.
- 40 grams of Kaolin powder per litre of water i.e. 280 grams of Kaolin powder was required.
- A very light layer of conductivity of 5 mS/cm was the requirement, therefore, the solution was prepared until the degree of pollution was obtained.
- The conductivity reading was corrected for a temperature of $20 \text{ }^\circ\text{C}$. Laboratory temperatures can be very variant, therefore, it was necessary to have all readings at a standard temperature which is $20 \text{ }^\circ\text{C}$.

5.4 Test arrangement

The test insulator was fixed on a stand with the ground terminal on top and the voltage applied to the bottom terminal of the insulator. The insulator was pre-stressed with dc voltage and

then the impulse voltages were applied is in order to obtain flashover levels of the particular insulator. The results were captured with an analog oscilloscope for observation and analysis.

5.4.1 Test circuit

The impulse flashover voltage rating of the tested insulator is 100 kV . A single stage construction of a Messwandler Bau kit has an output of 90 kV , therefore, a 2-stage which is double that was needed in order to complete this test. Figure 5.2 shows its construction in the HV laboratory at the University of Stellenbosch.



Figure 5.2: A two-stage Messwandler Bau kit arrangement in the HV laboratory.

In order to improve the impulse circuit's operating characteristic, a trigger circuit was used. The operation of a trigger circuit is discussed by Craggs and Meek [36]. It is the triggering of the circuit and the generator's dc voltage that determines the firing of the spark gap.

A Heafely dc circuit, which can supply a voltage of up to 300 kV has a limited current output of 5 mA . Therefore, it was found to be inadequate to prestress the insulator, especially under

wet conditions when the insulator draws a higher amount of surface leakage current. A dc source set shown in Figure 5.3 was therefore used. Although limited to only 15 kV dc voltage, the used dc source has a high current output of up to 700 mA . A water resistor was used as a dc source guard (coupling resistor) against impulses, while an air gap was used as a coupling arrangement for impulse generator and dc circuit in place of a coupling capacitor.

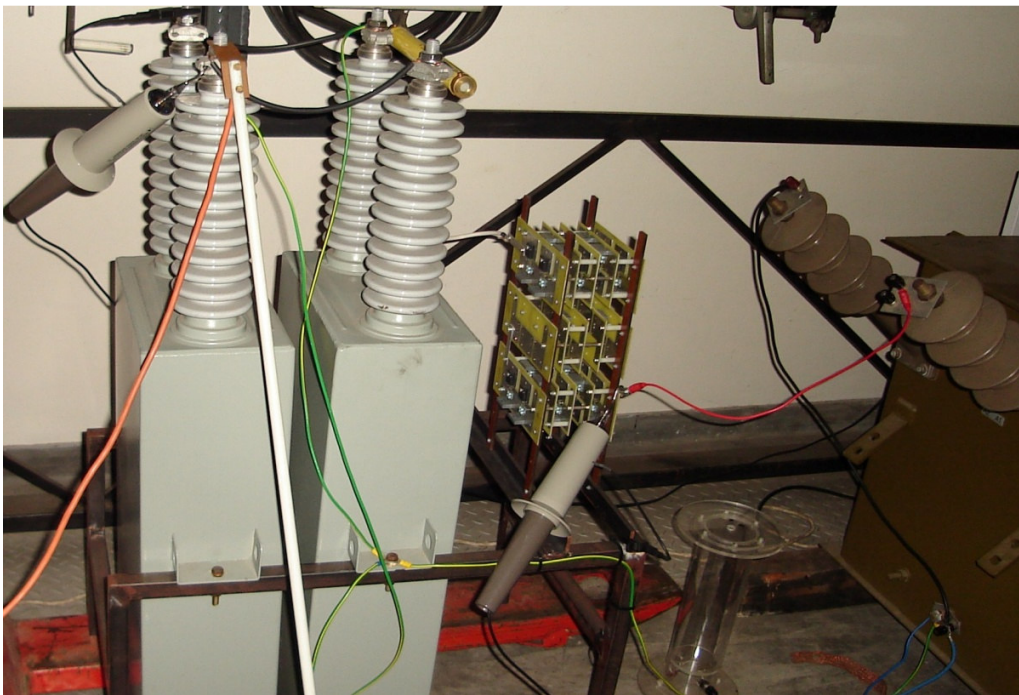


Figure 5.3: The used dc supply set in the HV laboratory.

5.4.2 Description of circuit parameters and operation

One of the aspects that create a challenge in these circuits is measurement. With the high magnitude of voltages used in this experiment, the use of $P6015A$ HV probes for impulse measurement is not possible. Therefore, the probe was restricted to dc measurement on the dc source. The Messwandler Bau kit only provides two measuring capacitor voltage dividers (CB) and a high ohmic resistor ($RM = 140\ \Omega$). In the two-stage impulse circuit constructed in these tests, however, these CB capacitors are already used as tail capacitors or CL as shown in the standard equivalent single-stage circuit. The use of these capacitors to perform both

measuring and tail capacitor functions was investigated. Due to this measurement problem, the circuit was rearranged in a way that allowed the use of capacitor C_B component of the used construction kit as tail capacitors and as impulse measuring equipment. The rearranged circuit is displayed in Figure 5.4. The resistor voltage divider was used to measure dc voltage that supplies the impulse generator.

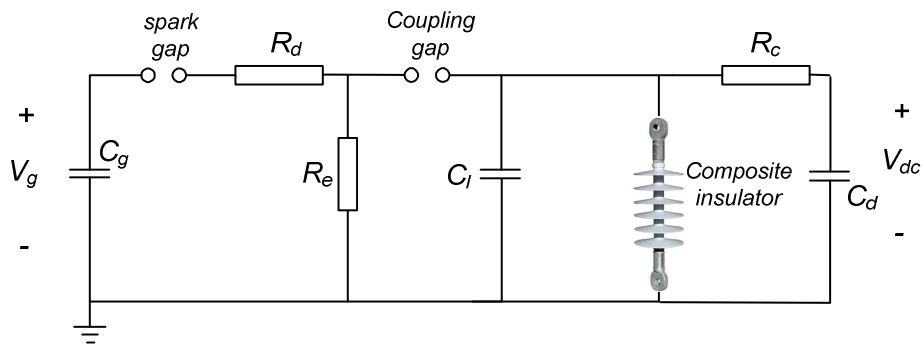


Figure 5.4 Circuit diagram of the test arrangement.

The circuit parameters are defined as follows:

- C_c denotes the coupling capacitor.
- C_d denotes the dc source capacitor.
- C_g denotes the impulse generator charging capacitor.
- R_c denotes the coupling resistor.
- R_d denotes the impulse generator's front resistor.
- R_e denotes the impulse generator's tail resistor.
- V_{dc} denotes the dc source voltage.
- V_g denotes the generator's input dc voltage.

The capacitance and resistance of the test object are be represented by C_t and R_t respectively. Table 5.1 summarizes the value of the circuit parameters.

Table 5.1: Summary of parameter values for the test circuit shown in Figure 5.4

<i>Variable</i>	<i>Value</i>	<i>Variable</i>	<i>Value</i>
C_g	5000 pF	R_d	750Ω
C_l	600 pF	R_e	12.2Ω
C_c	$10\,000 \text{ pF}$	R_c	$6 \text{ M}\Omega$
C_t	20 pF	V_g	150 kV
C_d	$15 \mu\text{F}$	V_{dc}	10 kV

5.4.3 Theoretical simulation

To authenticate the test circuit, a computer simulation on the test circuit arrangement was performed. The circuit diagram shown in Figure 5.4 can be transformed to the Laplace domain equivalent shown in Figure 5.5.

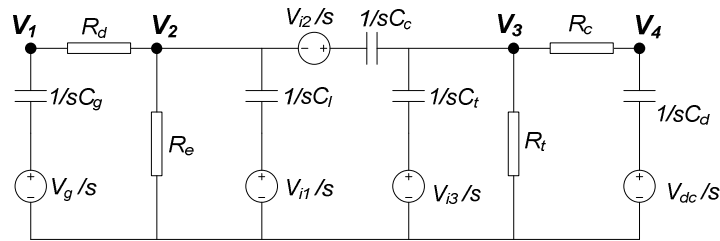


Figure 5.5: Laplace domain equivalent circuit representation of the test arrangement.

With the circuit variables known, an equation can be derived for the voltage waveform that will be applied to the test object. This is achieved through the following procedure:

- The set of nodal equations for the circuit is derived in the Laplace domain.
- The set of nodal equations is solved to yield an expression for $V_3(s)$.
- The circuit variables are replaced by the applicable numerical parameter values and the resulting expression is transformed to the time domain to yield a time-domain expression for $v_3(t)$.

For the circuit parameters given in Table 5.1, the voltage applied to the test object is given by the relationship

$$V_3(t) = 10000(-12.7916e^{-2.53575 \times 10^6 t} + 12.7916e^{-13931.5t} + 0.0000154838e^{-8.31641t} + 0.999988e^{-1.09889 \times 10^{11} t}) \quad (5-1)$$

Figure 5.6 shows graphical representations of the waveform predicted by equation 1. The waveform has a peak voltage V_p and time to peak t_p value of $V_p = 133.608 \text{ kV}$ and $t_p = 2.064 \mu\text{s}$ respectively. The waveform shown in Figure 5.6 exhibits the desired characteristics, i.e. a lightning impulse superimposed on a dc bias voltage.

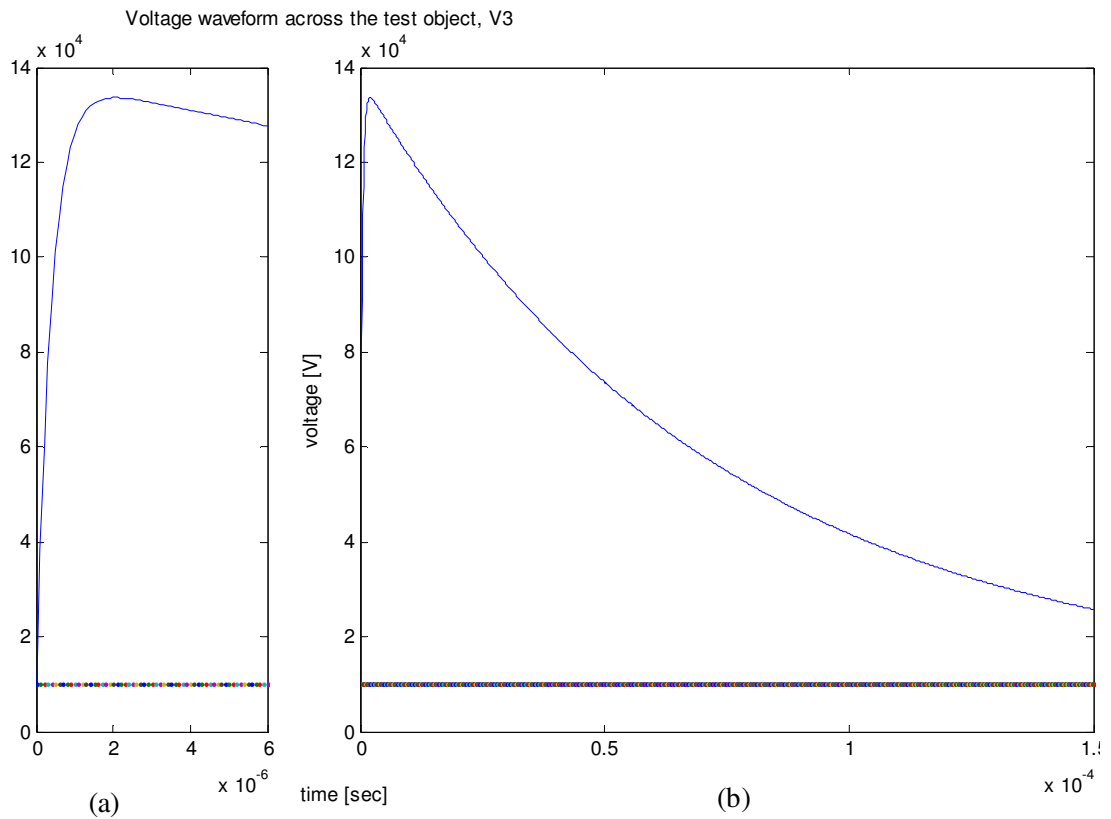


Figure 5.6: Plotted waveform (a) front part, (b) full waveform.

5.5 Test procedure

The main objective of the practical tests was to determine how the presence of a DC bias voltage affects the flashover voltage of the insulator for a standard lightning impulse. Due to the statistical nature, this breakdown voltage is typically specified as the voltage level that yields a 50% change of flashover, designated by U_{50} [18]. This up and down exercise is done for about 20 impulses and, according to statistics, about half of the impulse should result in flashovers and the other half in withstands. V_{50} or U_{50} as commonly known can then be determined as follows:

$$U_{50} = \frac{(V_1+V_2+V_3+\dots+V_n)}{n} \quad (5.2)$$

The letter n represents the number of up and down voltage impulses applied, V_1 to V_n are the applied peak voltage impulses that resulted either in flashover or withstand. U_{50} represents the Critical Flashover voltage (CFO) of the particular insulation material.

5.6 Data capturing and processing

After the verification of the circuit connections, impulse voltages were applied to an insulator under test which was pre-stressed with dc voltage as explained in section 5.5. In order to determine flashover values, the up and down methodology was used. On each test, a minimum of 20 impulse shots were performed in search of the flashover level [18]. The impulse waveform can be recorded in different ways:

- The total voltage required to break down the insulation, this is overall strength of the insulator under respective bias and impulse conditions, $V_{dc} + V_{impulse}$ in the case of positive impulse and $V_{impulse}$ in the case for negative impulse. This principle of interpreting is illustrated in Figure 5.7 (a) for positive impulses and (b) for negative impulse voltages.

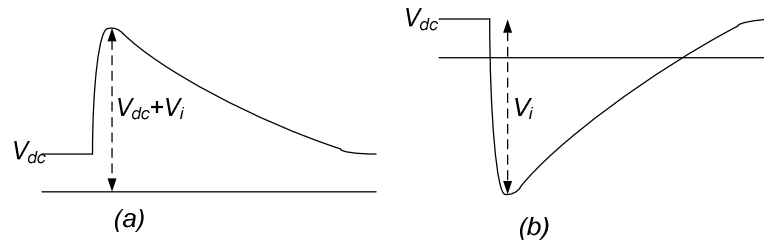


Figure 5.7: Magnitudes of impulses (a) $V_{dc}+V_i$ for positive and (b) V_i for negative impulses.

- The impulse voltage needed to break down the insulation. This is the impulse, $V_{impulse}$, voltage that is needed to break down the dc biased insulator, as illustrated in Figure 5.8. A smaller impulse is required in positive case and a larger one in negative case.

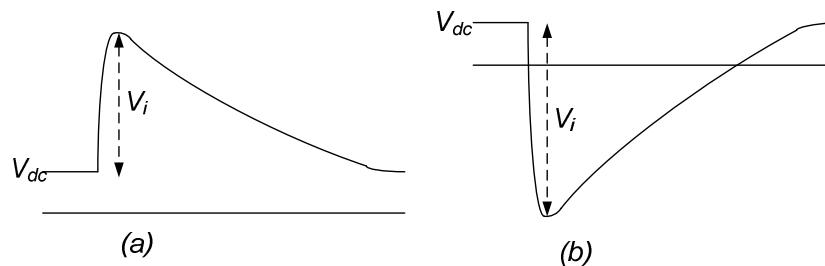


Figure 5.8: Magnitudes of impulses (a) V_i for positive and (b) V_i for negative impulses.

The method illustrated in Figure 5.7 was used in this test.

When performing the tests, the atmospheric values in the laboratory, i.e. temperature and pressure were recorded. The values were recorded just before the test and verified soon after the test had been completed. These atmospheric factors were used in the processing of results as explained later in this section.

The impulse part of the waveform was captured by using CB (C_l) capacitors. In the case of positive impulse, the actual impulse part (V_i) was added to the pre-stressing voltage (V_{dc}) to complete the actual voltage potential that appeared across the tested insulator and referred to as V_3 in the theoretical part of this thesis. Voltage values recorded in these tests are the actual crest values of the full waveforms. Figure 5.9 shows a waveform that resulted in a flashover

on a dry insulator pre-stressed with 20 kV dc voltage. The trace was captured during the test by using an oscilloscope.

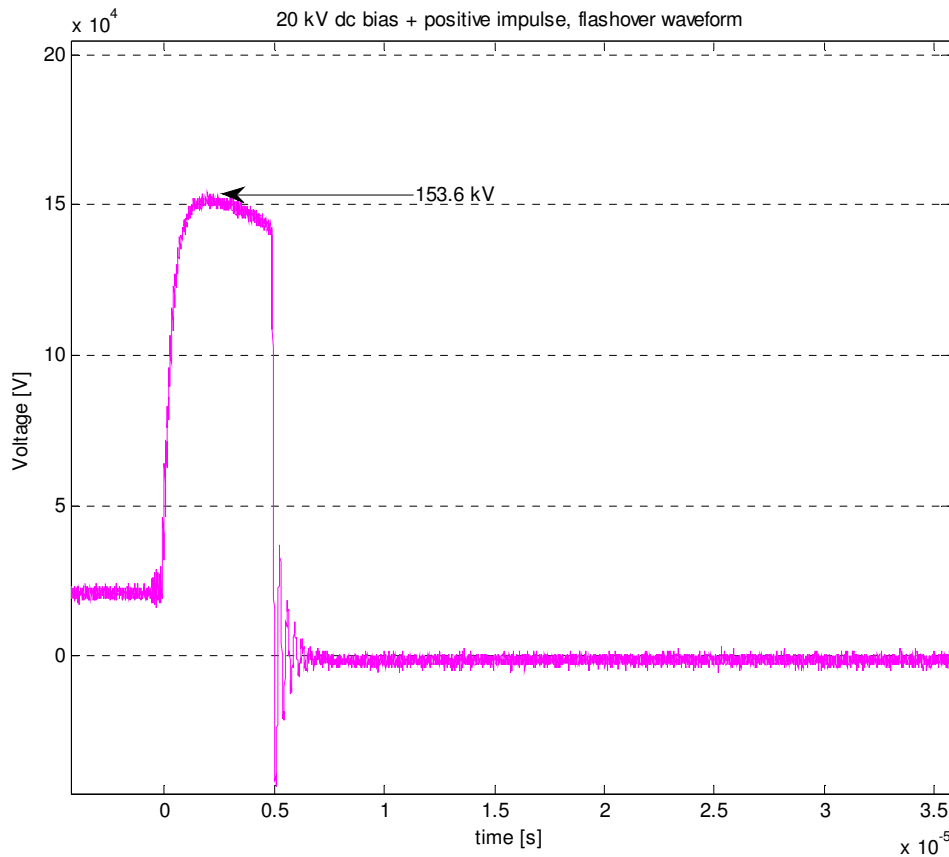


Figure 5.9: An illustration of a flashover positive waveform with dc bias voltage.

In a voltage waveform above, a flashover shot of 153.6 kV is recorded, and that particular impulse shot resulted in a flashover.

Twenty (20) single positive impulses (up and down) were applied on the composite insulator in an effort to obtain flashover level. The example below illustrates the process performed on a dry insulator with 10 kV dc bias. The results of the impulses and calculation of U_{50} are shown below. This is the process applied in all the performed cases. Table 5.2 shows the applied voltage impulses and whether the applied impulses resulted in flashover or withstand.

CHAPTER 5 – APPLICATION OF THE COMPOSITE WAVEFORM GENERATOR CIRCUIT TO OBTAIN FLASHOVER LEVELS OF AN INSULATOR

The letter X represents flashover impulses while O represents withstands Table 5.3 summarises the results by adding up the voltage impulses before the mean value is determined.

Table 5.2: Determination of CFO, the 20 recorded impulses.

<i>Voltage</i>	<i>Flashover/Withstand</i>	<i>Voltage</i>	<i>Flashover/Withstand</i>
79	X	78	X
75	O	75	O
79	X	78	X
76	O	76	O
78	X	78	X
75	O	75	X
78	X	72	O
75	O	77	X
78	O	73	O
82	X	78	X

Table 5.3: Summary of the recorded impulses.

$\sum v$	1534
<i>Flashovers (X)</i>	10
<i>Withstands (O)</i>	10

$$\begin{aligned} \text{Mean} &= 1/20(\sum v) \\ &= 76.68 \end{aligned}$$

$$\text{voltage ratio} = 1667/1$$

$$\begin{aligned} V &= 76.68 \times 1667 \\ &= 127.83 \text{ kV} \end{aligned}$$

The obtained result is the voltage flashover level under laboratory environmental conditions. To standardise this result, atmospheric correction factors are implemented as per IEC standards [39]. This is illustrated below.

The factor expressed by d reduces the influence of temperature and air pressure variations. The IEC standard conditions are temperature (T) of 20°C and an atmospheric pressure (P) of 760mmHg . Factor d is determined using actual readings taken before the test and confirmed again after a particular test [39]. With this particular test, the following readings were taken, and the correction factor obtained. The letters t and p represent the actual room temperature and pressure respectively.

$$t = 13.5^{\circ}\text{C}$$

$$p = 759 \text{ mm Hg}$$

$$d = \frac{p}{P} \times \frac{273 + T}{273 + t}$$

$$d = \frac{759}{760} \times \frac{(273 + 20)}{(273 + 13.5)}$$

$$= 1.021$$

With the correction factor, d , obtained, the final value U_{50} is then determined as follows:

$$U_{50} = \frac{V}{d}$$

$$U_{50} = \frac{127.83 \text{ kV}}{1.021}$$

$$= 125.2 \text{ kV}$$

5.7 Tests performed

5.7.1 Overview

The main objective of the investigation was to determine how the relative magnitude of a dc bias voltage affects the flashover voltage of a composite insulator for a standard lightning impulse, allowing for different surface conditions, i.e. dry and polluted wet, and both positive and negative polarities of the impulse compared to the dc bias voltage. The following series of tests were performed:

- Positive impulse with a positive dc bias voltage of 0 kV (no dc bias), 5 kV and 10 kV.
- Negative impulse with a positive dc bias voltage of 0 kV (no dc bias), 5 kV and 10 kV.

The tests were performed for both dry and wet insulator surfaces.

5.7.2 Tests under dry conditions

To represent a polluted insulator under dry conditions, the test insulator was immersed in the light pollution contaminant and dried. The light solution's specifications are shown in Table 5.4. The composite insulator was pre-stressed with a dc voltage and then an impulse voltage applied. Using the up-down method [18], the flashover voltage is obtained.

5.7.3 Tests under wet conditions

It is important to observe the behaviour of polluted and wetted insulator against flashover performance. The composite insulator was sprayed with a kaolin composition and then pre-stressed with a respective dc bias voltage. Impulse voltages were then applied to the wet insulator and flashover level determined using the up-down method. The specifications of the used Kaolin composition are shown in the table below [[24], [28]]:

Table 5.4: Kaolin composition used as an insulator contaminant.

<i>Conductivity</i>	<i>Contents</i>		
	<i>Kaolin (g)</i>	<i>Water (l)</i>	<i>salt</i>
<i>5 mS/cm</i>	<i>280 g</i>	<i>7</i>	<i>Until the 5mS/cm is obtained</i>

To represent a polluted insulator under wet condition, the test insulator was immersed in the light pollution contaminant and the dc bias voltage and impulse voltage were applied to the wet insulator. However, the heating effect of the leakage current induced by the bias voltage gives rise to dry band formation. This process is well illustrated by the response of the leakage current across the insulator after application of the bias voltage. Figure 5.10 shows measured examples of this leakage current profile. The gradual reduction in leakage current due to the initial dry-out process is clearly visible, followed by the dry-band formation after which the leakage current reduces to zero. This introduces another variable, namely the state of dry band formation when the impulse is applied. The objective of tests were to apply the impulse at the critical point of dry band formation [41], as this condition represents the most vulnerable point for an overvoltage-induced flashover.

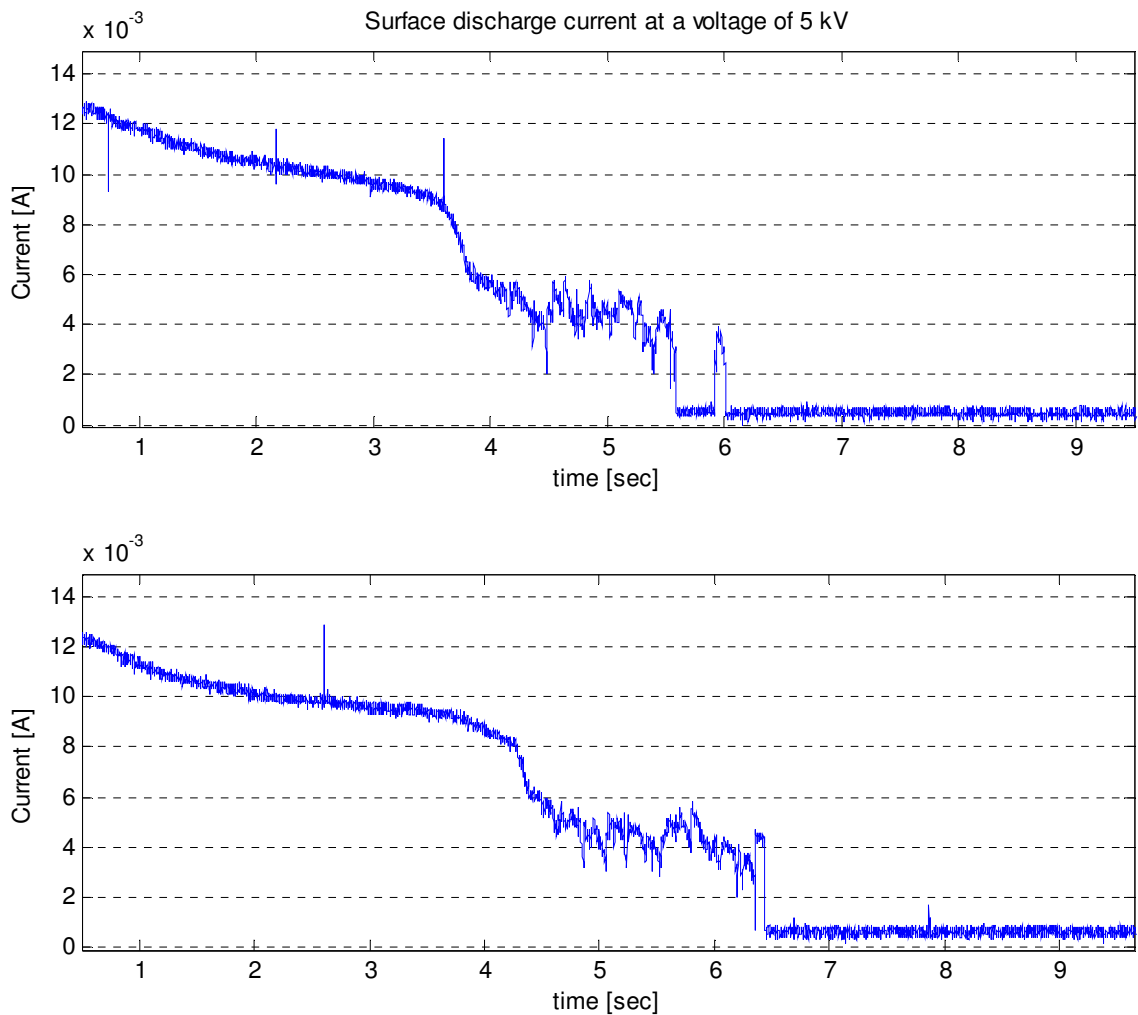


Figure 5.10: Drying process of a composite insulator surface.

The drying process is influenced by leakage current, which is dependent on the voltage magnitude and resistance of the pollution layer. Hence, the higher the surface conductivity, the faster the surface drying.

To evaluate the effect of the surface drying process, the graph that represents the typical drying process is divided into three stages (I, II and III) as shown in Figure 5.11. Stage I is when the surface is completely wet, therefore, a relatively higher continuous current flow is observed on the surface. During stage II, dry bands start forming, hence, the surface current

flow is far from being even. During stage III dry bands have formed, hence a zero to very small current flows on the surface.

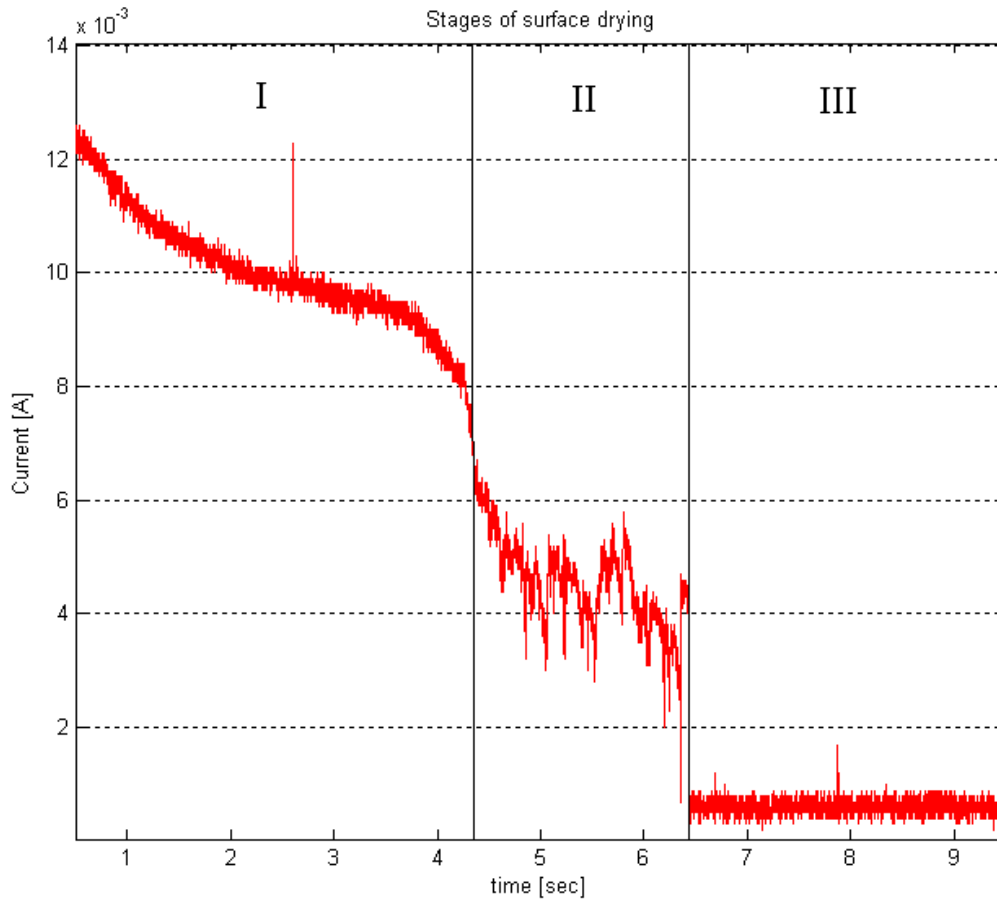


Figure 5.11: Three drying stages of a composite.

It was observed that under wet-drying periods (stage I, II and III), the insulator produces virtually the same flashovers at all three stages when impulse voltages are applied. Results of these comparison tests are presented in Table 5.5.

CHAPTER 5 – APPLICATION OF THE COMPOSITE WAVEFORM GENERATOR CIRCUIT TO OBTAIN FLASHOVER LEVELS OF AN INSULATOR

Table 5.5: Flashover tests at different stages of insulator drying.

<i>Drying Process</i>	<i>Impulse Voltage (V)</i>		<i>U₅₀ (V)</i>
		<i>X / O</i>	
Stage I	133360	X	129268.27
	127298	O	
	133360	X	
	128814	O	
	133360	O	
	137906	X	
	131845	X	
	127298	O	
	121236	O	
	118205	O	
Stage II	127298	X	127752.82
	124267	X	
	121236	O	
	118205	O	
	124267	X	
	130329	X	
	133360	X	
	137906	X	
	133360	O	
	127298	O	
Stage III	131845	X	129874.45
	127298	O	
	131845	X	
	128814	O	
	133360	X	
	136391	X	
	130329	X	
	127298	X	
	122752	O	
	128814	O	

5.8 Results on the determination of flashover levels of the insulator

5.8.1 Impulse flashover tests at different dc bias voltages

This section presents the results as they were recorded in the HV laboratory during flashover tests. The contents of the tables are highlighted below:

- Table 5.6 contains results of the tests performed with positive impulses under dry condition.
- Table 5.7 contains results of the tests performed with positive impulses under wet condition.
- Table 5.8 contains results of the tests performed with negative impulse under dry condition.
- Table 5.9 contains results of the tests performed with negative impulses under wet condition.

The impulses recorded either flashover (X) or withstand (O), when determining U_{50} values are shown in Figure 5.12 to Figure 5.15. The description of the figures is highlighted below:

- Figure 5.12 contains results of the tests performed with positive impulses under dry condition.
- Figure 5.13 contains results of the tests performed with positive impulses under wet condition.
- Figure 5.14 contains results of the tests performed with negative impulse under dry condition.
- Figure 5.15 contains results of the tests performed with negative impulses under wet condition.

In these figures and tables, the recorded X and O represent flashover and withstand impulses respectively.

5.8.1.1 Dry insulator, Positive impulses

Table 5.6: Positive impulse tests on a dry composite insulator at different dc bias voltages.

<i>DC bias voltage (V)</i>	<i>Impulse Voltage (V)</i>		<i>U50 (V)</i>
	<i>O</i>	<i>X</i>	
0	137147.89	142046.03	136821.35
	130617.04	140413.32	
	137147.89	135515.18	
	133882.47	140413.32	
	133882.47	138780.61	
	130617.04	140413.32	
	135515.18	140413.32	
	130617.04	135515.18	
	137147.89	140413.32	
		135515.18	
		140413.32	
5000	120820.76	127351.62	128657.79
	124086.19	128984.33	
	124086.19	130617.04	
	130617.04	137147.89	
	122453.48	132249.76	
	127351.62	127351.62	
	125718.90	132249.76	
	127351.62	132249.76	
	128984.33	133882.47	
	127351.62	132249.76	
	1258821.74	1314333.99	
10 000	122453.48	128984.33	125229.09
	124086.19	128984.33	
	122453.48	127351.62	
	122453.48	128984.33	
	127351.62	133882.47	
	122453.48	127351.62	
	124086.19	128984.33	
	117555.34	127351.62	
	119188.05	124086.19	
	120820.76	125718.90	
	1222902.06	1281679.73	

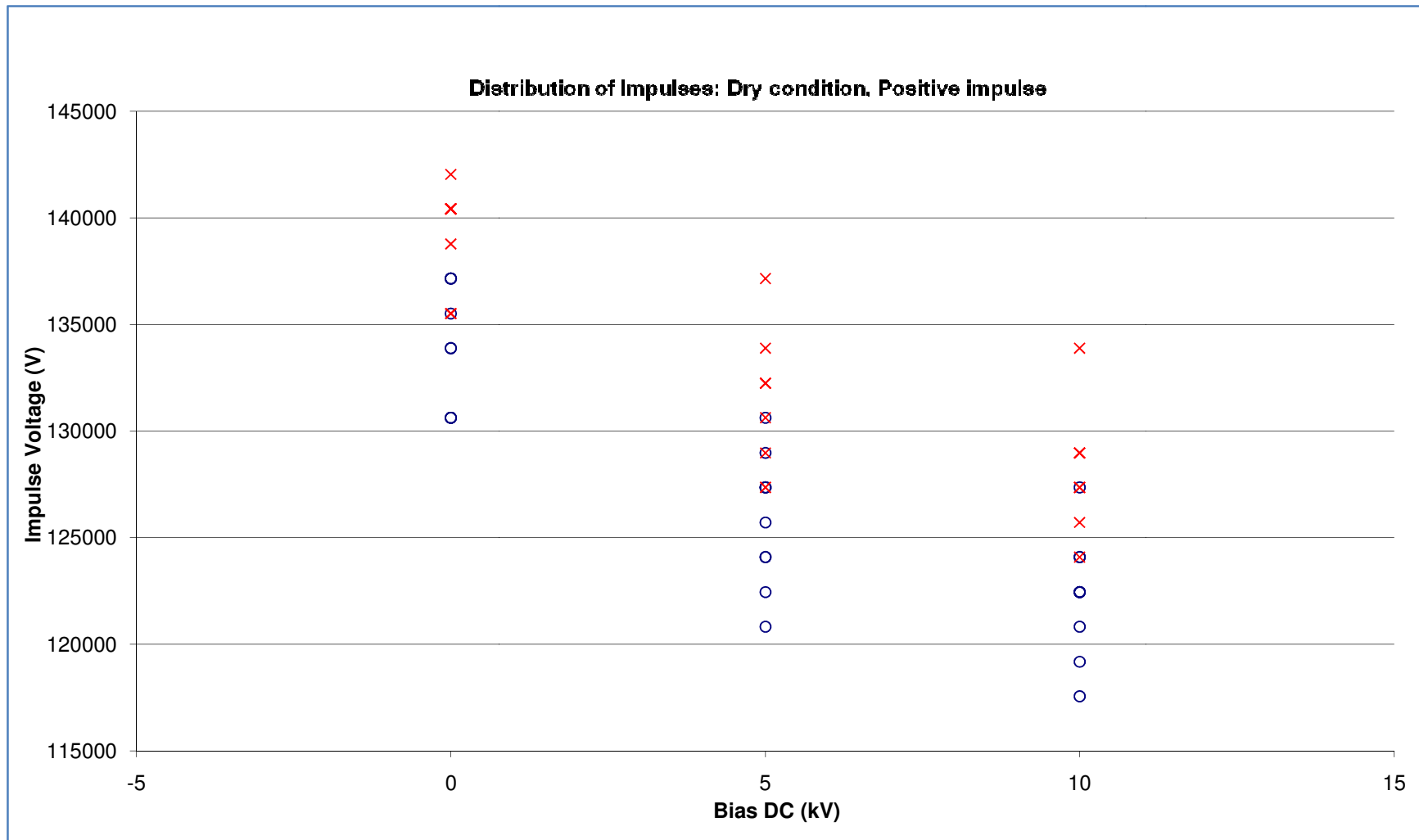


Figure 5.12: Distribution of impulses during positive impulse flashover tests on a dry composite insulator

5.8.1.2 Wet insulator, positive impulses

Table 5.7: Positive impulse tests on a wet composite insulator at different dc bias voltages.

<i>DC bias voltage (V)</i>	<i>Impulse Voltage (V)</i>		<i>U50 (V)</i>
	<i>O</i>	<i>X</i>	
0	115649.16	120605.55	124240.24
	118953.42	123909.81	
	122257.68	125561.94	
	122257.68	127214.07	
	120605.55	125561.94	
	125561.94	132170.47	
	120605.55	128866.20	
	122257.68	127214.07	
	122257.68	128866.20	
	123909.81	130518.33	
5000	104084.24	120605.55	115649.16
	110692.77	113997.03	
	109040.63	109040.63	
	110692.77	118953.42	
	117301.29	112344.90	
	112344.90	115649.16	
	115649.16	123909.81	
	120605.55	117301.29	
	115649.16	118953.42	
	120605.55	125561.94	
10 000	105736.37	113997.03	113501.39
	104084.24	112344.90	
	107388.50	109040.63	
	107388.50	115649.16	
	110692.77	115649.16	
	110692.77	117301.29	
	115649.16	122257.68	
	115649.16	122257.68	
	112344.90	117301.29	
	115649.16	118953.42	

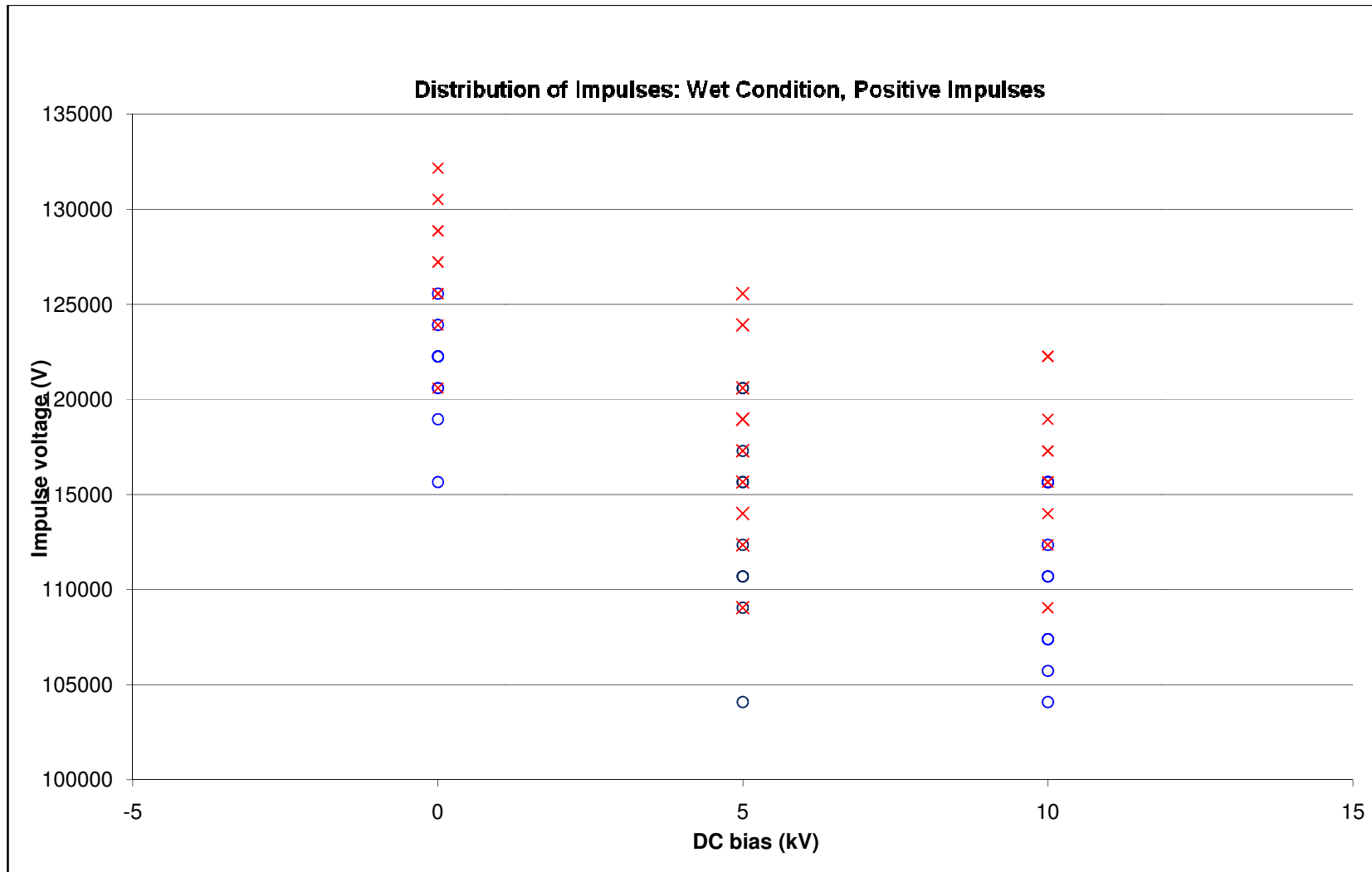


Figure 5.13: Distribution of impulses during positive impulse flashover tests on a wet composite insulator.

5.8.1.3 Dry insulator, negative impulses

Table 5.8: Negative impulse tests on a dry composite insulator at different dc bias voltages.

<i>DC bias voltage (V)</i>	<i>Impulse Voltage (V)</i>		<i>U50 (V)</i>
	<i>O</i>	<i>X</i>	
0	189394.71	192660.14	
	189394.71	192660.14	
	192660.14	205721.84	
	197558.28	200823.70	
	202456.42	194292.85	
	186129.29	195925.56	
	189394.71	195925.56	
	189394.71	189394.71	
	187762.00	192660.14	
	186129.29	194292.85	
5 000	187762.00	194292.85	
	189394.71	195925.56	
	192660.14	195925.56	
	191027.42	197558.28	
	194292.85	194292.85	
	186129.29	197558.28	
	192660.14	192660.14	
	186129.29	189394.71	
	189394.71	195925.56	
		191027.42	
		192660.14	
10 000	186129.29	192660.14	
	189394.71	199190.99	
	194292.85	199190.99	
	192660.14	195925.56	
	189394.71	194292.85	
	191027.42	195925.56	
	191027.42	202456.42	
	194292.85	202456.42	
	194292.85	197558.28	
	192660.14	197558.28	

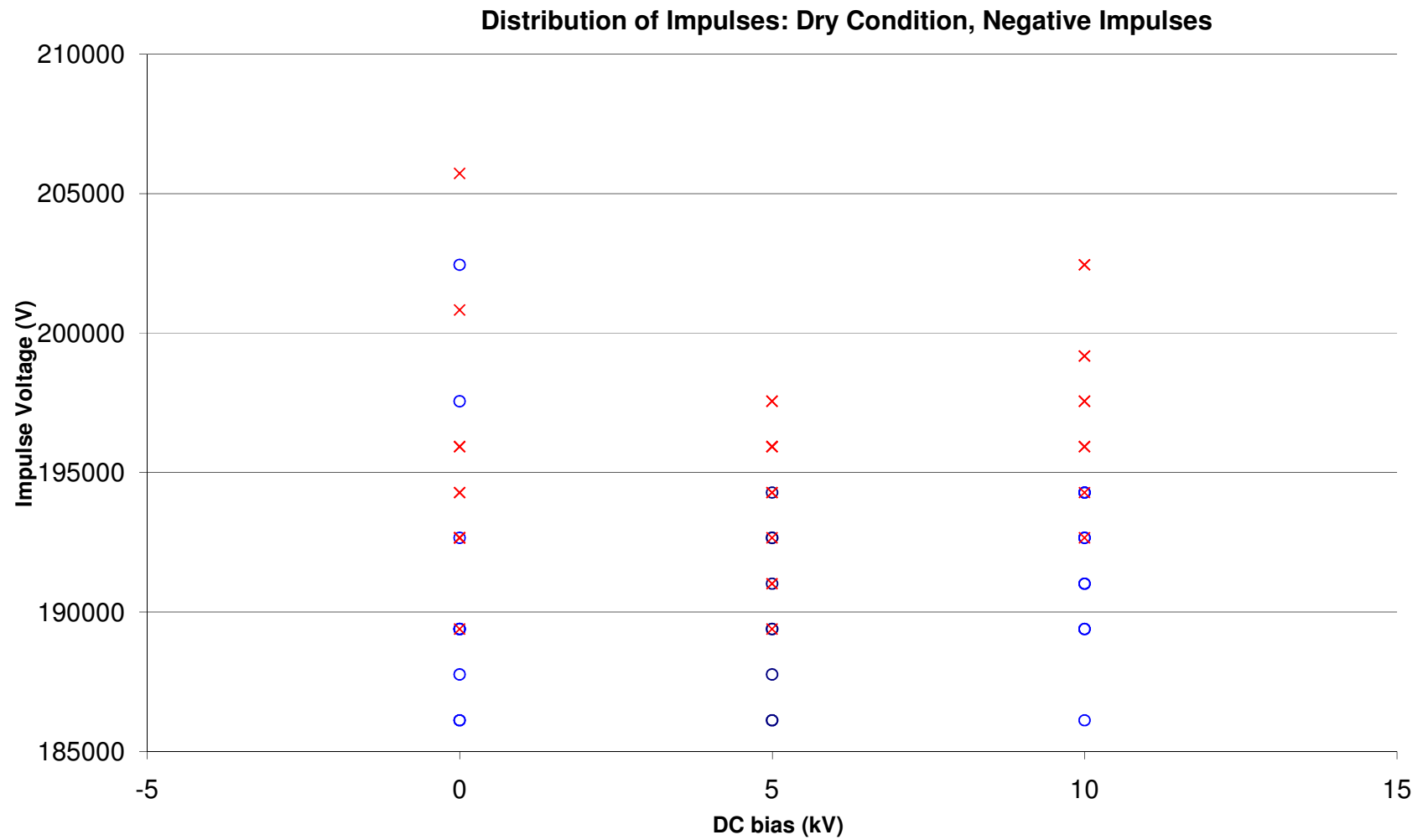


Figure 5.14: Distribution of impulses during negative impulse flashover tests on a dry composite insulator

5.8.1.4 Wet conductor, negative impulse

Table 5.9: Negative impulse tests on a wet composite insulator at different dc bias voltages.

<i>DC bias voltage (V)</i>	<i>Impulse Voltage (V)</i>		<i>U50 (V)</i>
	<i>O</i>	<i>X</i>	
0	130617.04	135515.18	128821.06
	127351.62	133882.47	
	132249.76	137147.89	
	128984.33	133882.47	
	132249.76	137147.89	
	125718.90	132249.76	
	122453.48	132249.76	
	117555.34	127351.62	
	122453.48	127351.62	
	117555.34	122453.48	
5 000	130617.04	137147.89	130453.77
	132249.76	137147.89	
	125718.90	135515.18	
	130617.04	130617.04	
	125718.90	135515.18	
	132249.76	130617.04	
	130617.04	135515.18	
	119188.05	125718.90	
	125718.90	132249.76	
	125718.90	130617.04	
10 000	120820.76	124086.19	130372.14
	125718.90	133882.47	
	122453.48	127351.62	
	127351.62	133882.47	
	127351.62	138780.61	
	132249.76	132249.76	
	125718.90	133882.47	
	128984.33	140413.32	
	130617.04	135515.18	
	135515.18	130617.04	

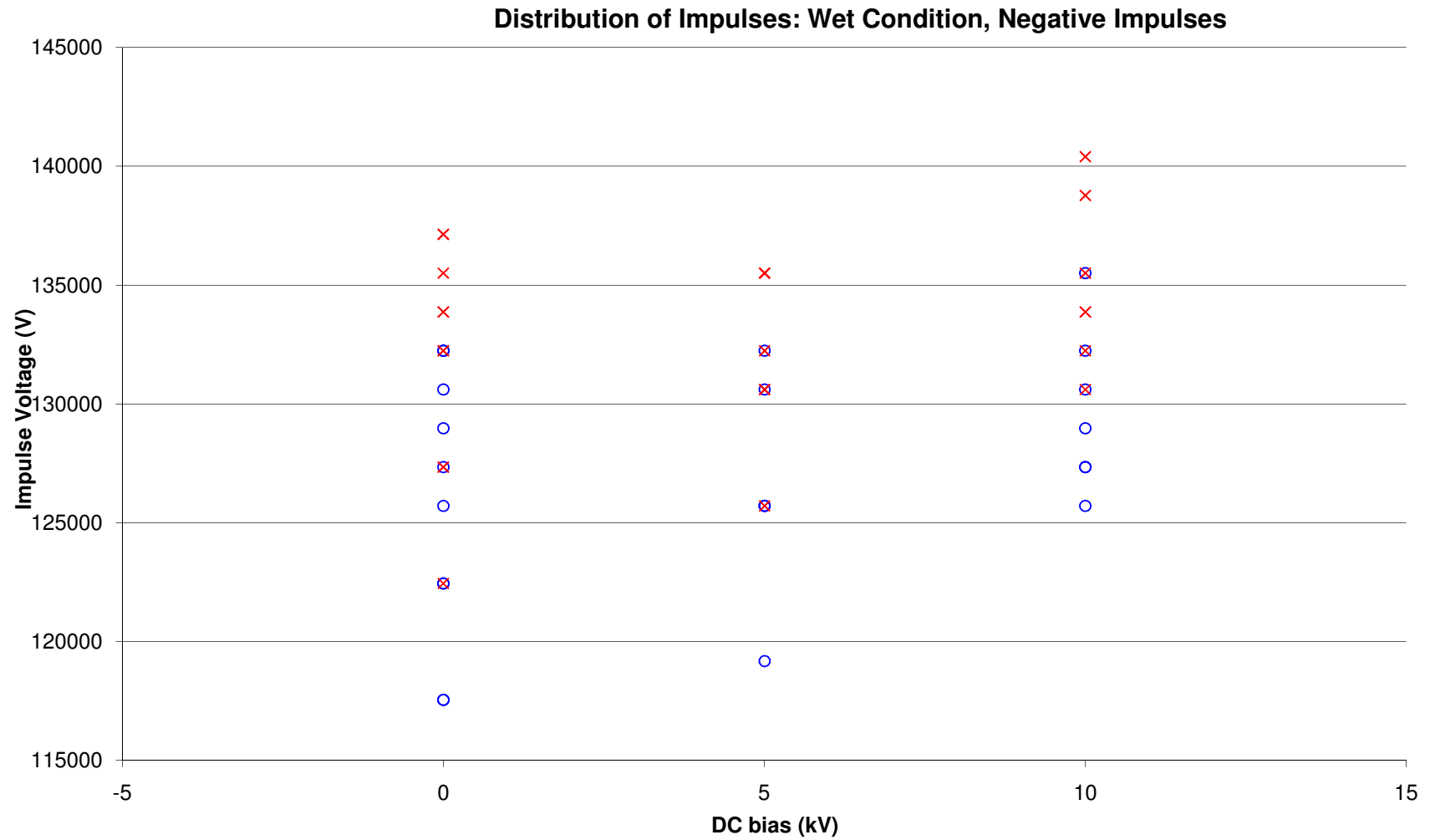


Figure 5.15: Distribution of impulses during negative impulse flashover tests on a wet composite insulator.

5.8.2 Summary of flashover results

The complete obtained results of the explained tests are summarised. Table 5.10 and Table 5.11 for dry and wet conditions respectively. These are the final results that are already corrected against respective atmospheric variations explained in Section 5.6. These results summarise the effects of dc bias (positive) on impulse flashover levels with different polarities (positive and negative impulses). The effect of wetting on the insulation strength against impulse voltages is also summarised. Although the main aim of the chapter is to authenticate the application of the test arrangement, these results have been presented in a way that demonstrates:

- The effect of dc bias voltage on the impulse flashover level of the insulator under dry and wet condition.
- The effects of insulator wetting on the flashover levels with positive and negative impulse voltages.

5.8.3 Dry conditions

Results of dry insulator flashover tests are summarised in Table 5.10. The differences between positive and negative impulse flashovers at various bias voltages are indicated.

Table 5.10: Recorded voltage CFO values at dry condition.

<i>DC bias</i>	<i>U₅₀</i>		
<i>Positive DC [kV]</i>	<i>Positive impulse [kV]</i>	<i>Negative impulse [kV]</i>	<i>Difference [%]</i>
0	136.8	193.3	41
5	133.7	192.3	44
10	135.2	194.7	44

Comments

- For positive impulse condition, the impulse flashover levels recorded at 5 and 10kV dc bias are both within 2% of the impulse flashover level at no dc bias.
- For negative impulse condition, the impulse flashover levels recorded at 5 and 10kV dc bias are both measured to be within 1% of the impulse flashover level at no dc bias.

5.8.4 Wet conditions

Results of dry insulator flashover tests are summarised in Table 5.11. The differences between positive and negative impulse flashovers at various bias voltages are indicated.

Table 5.11: Recorded CFO voltage values at wet condition.

<i>DC bias</i>	<i>U₅₀</i>			
	<i>Positive DC [kV]</i>	<i>Positive impulse [kV]</i>	<i>Negative impulse [kV]</i>	<i>Difference [%]</i>
0		124.22	128.8	4
5		115.5	130.5	13
10		114.0	130.2	14

Comments

- For positive impulse condition, the impulse flashover levels recorded at 5 and 10kV dc bias are both within 3% of the no-dc bias impulse flashover.
- For negative impulse condition, the impulse flashover levels recorded at 5 and 10kV dc bias are both measured to be within 1% of the no-dc bias impulse flashover

For comparisons and assessment, the results are plotted in one graph as shown in Figure 5.16. The plotted results are for impulse flashover tests performed at 0 , 5 and 10kV dc bias voltages. Four graphs, i.e. positive and negative withstand levels under dry conditions, and positive and negative flashovers under wet conditions are presented.

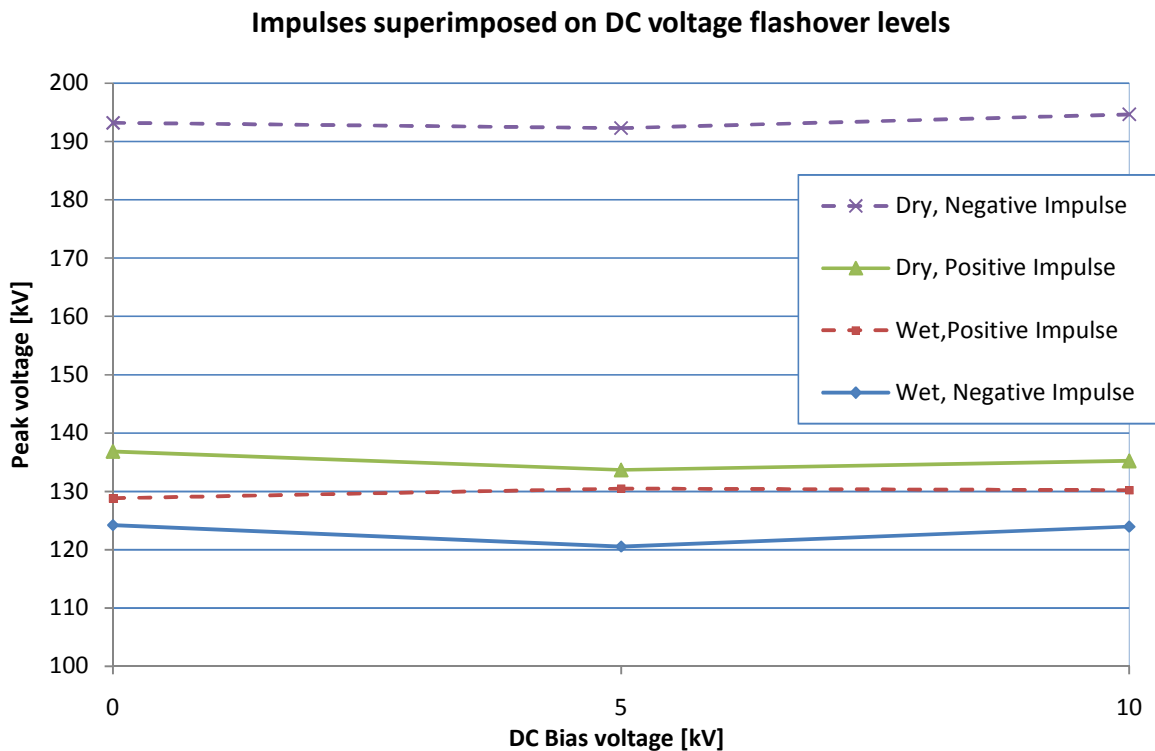


Figure 5.16: Compared series of results, for series of tests are all shown.

It is observed that under normal (dry condition) the insulator’s highest flashover is with negative impulse. The lowest impulse flashovers were observed with positive impulses in both dry and wet categories. However, it is the negative impulse level that wetting affects the most.

From the obtained test results, it can be observed that, with the negative impulse polarity (impulse voltage opposite the dc bias voltage), the impulse voltage (ΔV) required to break the insulation down remains the same regardless of the bias voltage level. These analyses were done for all the tested cases. They are presented with the aid of bar charts in Figure 5.17 to Figure 5.20. Figure 5.17 and Figure 5.18 present the results at dry and wet conditions with positive impulse flashovers respectively. Figure 5.19 and Figure 5.20 show the negative impulse flashover at dry and wet conditions respectively. In the series of these figures, the bar diagrams contain different portions of voltage components, i.e. dc bias and impulse voltage. The effect of different bias voltages can therefore be seen on how much impulse will be needed to break down the insulation at the respective bias level.

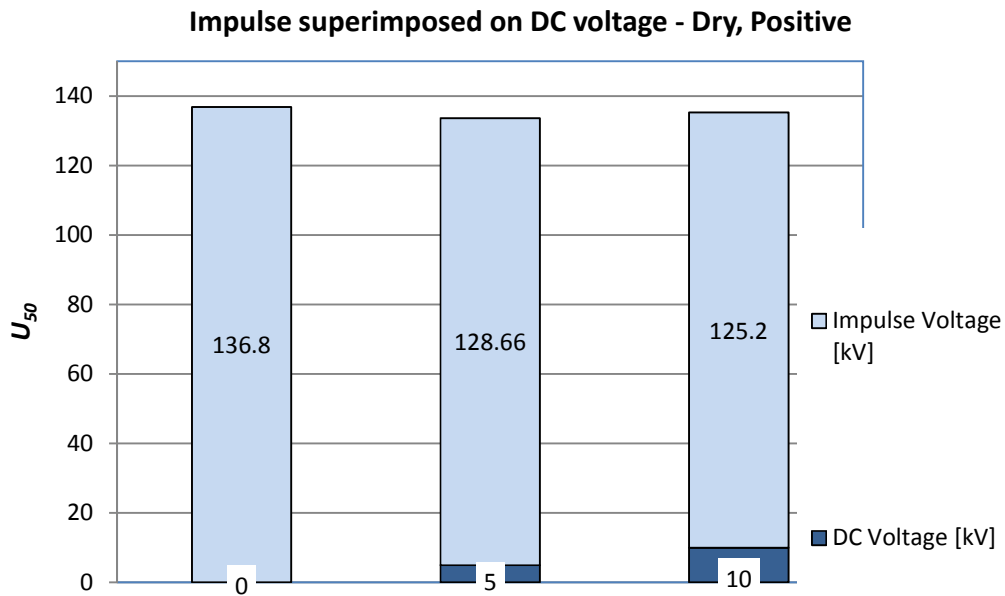


Figure 5.17: Voltage components of the composite waveforms, positive flashovers under dry condition.

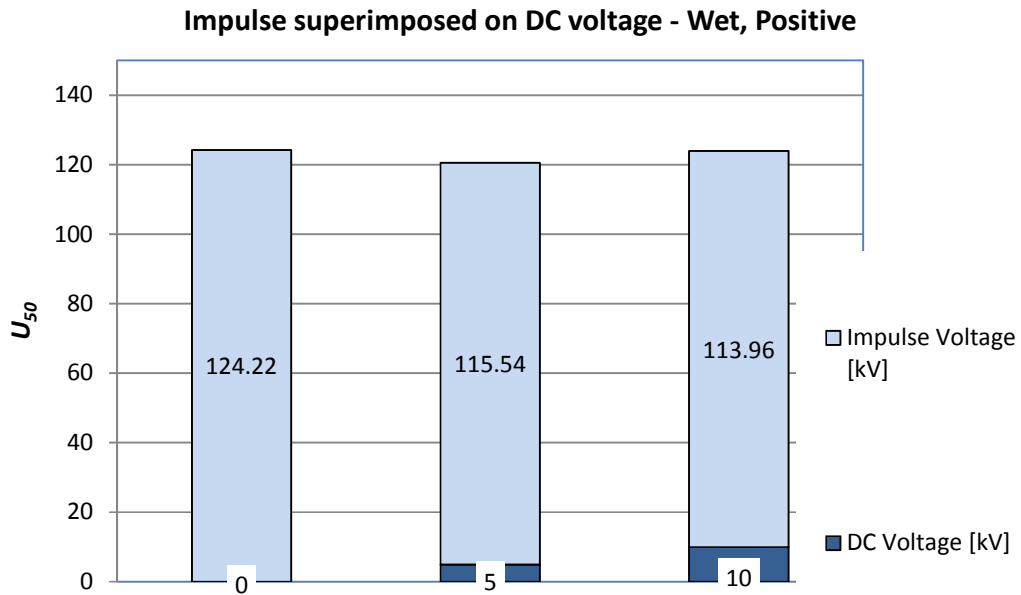


Figure 5.18: Voltage components of the composite waveforms, positive flashovers under wet condition.

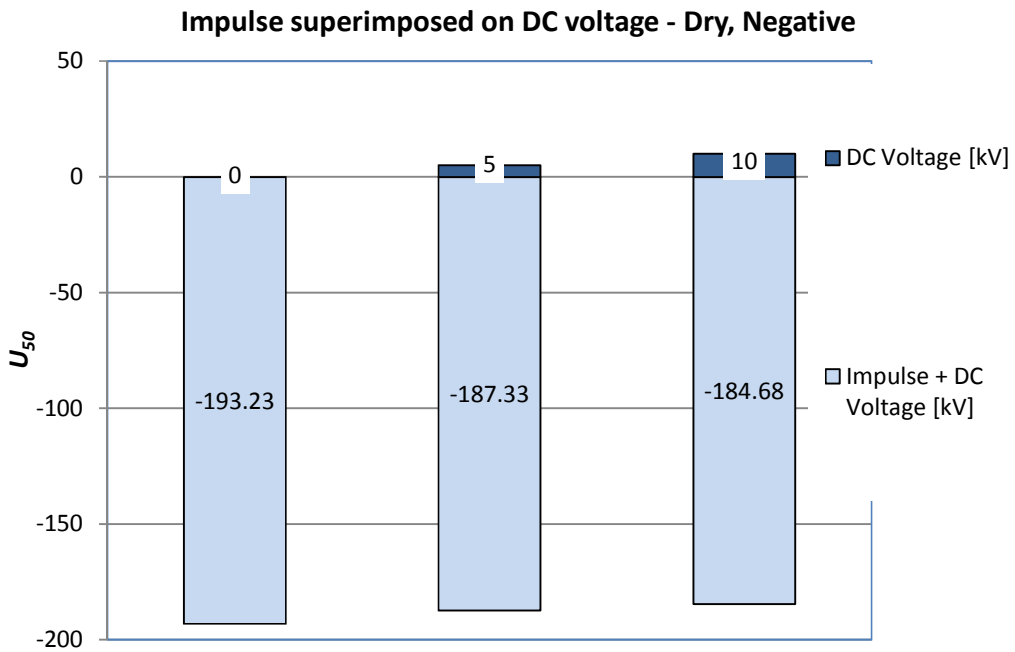


Figure 5.19: Voltage components of the composite waveforms, negative flashovers under dry condition.

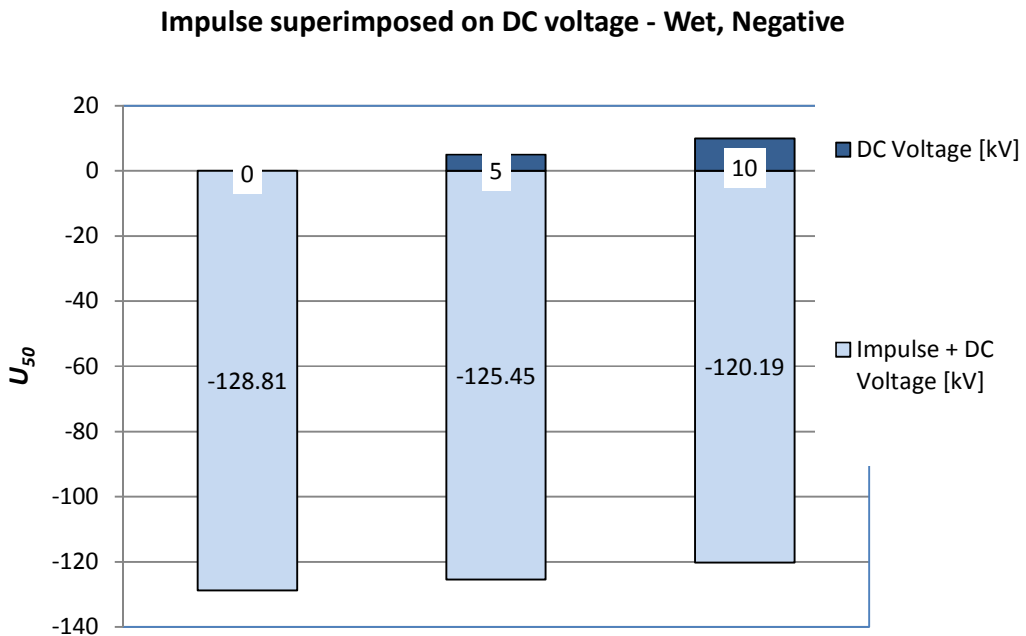


Figure 5.20: Voltage components of the composite waveforms, negative flashovers under wet condition.

5.8.5 Discussions of results

The interpretation and understanding of results is always the ultimate objective of a scientific research. A basic discussion of the overall results is given below. The effects of Polarity, bias voltage and wetting have been particularly addressed.

5.8.5.1 The effect of impulse polarity

Under normal conditions (dry), the negative flashover level is higher than the positive level. In this test configuration, up to 45% difference was observed between the two. This is due to different characteristics of positive and negative coronas [20]. The flashover level difference is however reduced with wetting. Negative impulse flashover is the worst affected by wetting.

5.8.5.2 The effect of dc bias voltage

For the used test object configuration, the effect of dc bias is minimal for both positive and negative withstands. This means that the impulse critical flashover (CFO) level without dc and critical flashover with dc is the same in magnitude ($V_{DC} + V_i \approx V_i$). Therefore, for a particular environmental condition, it can be said that an impulse alone can be used as a good approximation for surges superimposed on dc voltages for practical transmission line conditions. This is in agreement with various results obtained in previous studies [20], [39].

5.8.5.3 The effect of insulator wetting

Although the lowest flashover voltage was recorded with positive impulse condition, it is the negative withstand that is greatly affected by pollution and wetting. In these tests, the positive flashover level is only reduced by less than 10% after wetting, compared to around 35% in case of negative. It is believed that if the severity of pollution is increased, the negative and positive withstand levels will move closer to one another. It is also understood that the severity of this effect is also dependant on the geometry of an insulator [[20], [39]].

5.9 Conclusions

The proposed test circuit for conducting impulse tests with a dc bias voltage performed well in the practical tests conducted with polluted insulators. The mathematical model predicted the test waveforms correctly, thereby validating the test circuit topology.

The results obtained for the insulator tests show that the presence of a dc bias voltage does not affect the total flashover voltage of the insulator, whether dry or wet and for both positive and negative impulses, to a significantly degree. This is in agreement with various results obtained in previous studies for air-gaps [[20], [39]]. It was also observed that wetting affects the flashover at negative impulse more severely. The influence of wetting is minimal with positive impulse voltages.

6. CONCLUSIONS AND RECOMMENDATIONS

6.1 Overview

This chapter summarises conclusions from the major results obtained in the overall study. It also presents recommendations for future work.

6.2 Conclusions

The following are the summarised conclusions for this study:

Past research and related studies on the performance of insulators with composite waveforms mainly covered the aspect of air gaps. However, these results are essential to this study. Air is an integral part of a composite insulator and it becomes the crucial part is determining the insulation breakdown of a composite insulator under dry condition. It is only under wet conditions that the effect of surface leakage comes into main play.

The test circuit configurations, used for these types of composite waveform flashover tests are basically the same. They consist of an impulse generator, a dc source and components to integrate those two. However, it is the circuit variables and component values that need proper calculation in order to obtain the desired output of the composite waveform generator circuit. The equivalent circuit model and the associated mathematical expressions derived to represent the precise design of the test circuit configuration and comparison of results with different methods, i.e. practical and HSPICE simulations, proved this model to be accurate. Therefore, this model can be deemed as a success given the accuracy as proved in the figures of comparisons.

The analytical model enhances understanding of the test arrangement in the sense that the mathematical structure of the time domain of the composite voltage waveform applied to the

test object, i.e. a waveform consisting of four exponential terms, is exposed. The main application of the model for future work is the efficient development of a series of graphical relationships from which the output voltage parameters of the test circuit can be determined as a function of circuit parameters and the initial dc voltage levels. The performed test on the robustness and accuracy of the derived model proves that the derived model performs satisfactorily with different loads, coupling components and operating voltage levels.

In the test arrangement, dc voltage across the test object is a function of voltage division between test object resistance and the coupling resistor. Therefore, a lower coupling resistor with respect to the test object's resistance is needed in order to have sufficient dc voltage across the test object.

In the experiments presented in Chapter 5, it is observed that the effect on the CFO of the composite insulator under both dry and wet conditions of dc bias voltage could not be established. The effect of wetting on composite insulator for positive impulse flashover levels was observed to be insignificant. It is the negative flashover levels that are significantly reduced by insulator wetting. Under any condition, the lowest impulse observed was that of a positive impulse. It shows that this impulse can be used as the determining factor for insulation rating against impulse voltages.

It was observed that it doesn't really matter at which stages of dry band formation (Stage I, II and III shown in Figure 5.11) the impulse is applied, the insulator produces virtually the same voltage flashovers at all three stages when the same impulse voltage is applied.

When performing the practical testing, measurement proved to be one the most crucial aspects in high voltage testing. The high voltages at high frequency involved in these experiments make it very challenging. Therefore, it is necessary to select the accurate measurement method from the available technologies. This experiment, involved composite waveforms that comprise of dc and up to a few megahertz frequencies. Therefore, a combination of measuring equipment was needed. The measured waveforms were then processed and summed up for interpretation. The results obtained prove this method to be accurate.

6.3 Recommendations

After the completion of this study, few recommendations have been summarised for consideration in future work. They are as follows:

- As This study was rather wide, but fundamental, it would be appreciated if advanced analyses are undertaken in the different sections covered in this study.
- Switching surges produce insulator flashovers at lower voltages than lightning surges. Therefore, they are used to determine the insulator rating during design. It is therefore necessary to perform practical impulse experiments with switching surges.
- Measuring equipment was one of the shortcomings in this experimental study. The acquisition of high voltage measuring equipment for low and high frequency will increase the competence of the test circuit in terms of voltage magnitude.
- To perform better tests on insulators under wet conditions, a proper steam generator or rain chamber is needed. This will help to maintain dry band condition for a longer period and keep the wetting even as it might be desired.
- A high power high voltage dc source is needed. This will enable tests with dc bias voltage to be performed at high voltages.
- For practical reasons, i.e. measurement and dc source, these tests were performed at lower voltages where some of the effects may not be clearly significant on the results obtained. It is believed that if these tests are performed on larger scales i.e. bigger insulators and higher voltage magnitudes, some effects might start showing.

References

- [1] F.S. Edwards, A.S. Husbands, F.R. Perry, "*Development and Design of High Voltage Impulse Generators*", Proc. IEE 98 (1951), p155-180.
- [2] S.K Shifidi, H.J. Vermeulen, P. Pieterse "*Modelling of a High Voltage Impulse Test Generator with HVDC DC Bias*" Proceedings of the 17th Southern African Universities Power Engineering Conference, Durban University of Technology, 2008.
- [3] P Pieterse, *Impulse Voltage Testing Scheme with DC Bias Thesis*, Cape Peninsula University of Technology, 2004.
- [4] K. Feser, "*Breakdown Behaviour of Air Spark-Gaps with Non-Homogenous Field at Bias Voltage*", Bulletin ASE 62, pp 320 – 329, 1971.
- [5] A. Bradwell, R. Cooper, B. Varlow "*Conduction in Polythene with Strong Electric Fields and the Effect of Prestressing on the Electric Strength*" PROC. IEEE, Vol 118 No. 1, January 1971.
- [6] Siemens AG, *HVDC Proven Technology for power Exchange pamphlet*, Power Transmission and Distribution, Germany, website: www.siemens.com/hvdc.
- [7] R. Rudervall¹, J.P. Charpentier², R. Sharma³, "*High Voltage Direct Current (HVDC) Transmission Systems Technology Review Paper*"; ¹ABB power Systems, Sweden, ²World Bank, United States of America, ³ABB Financial Services, Sweden, Presented at Energy Week 2000, Washington, D.C, USA, March 7-8, 2000.
- [8] J.D. Glover, M.S. Sarma, *Power Systems Analysis and Design handbook*, 3rd Edition, Books/Cole Thomson Learning.

REFERENCES

- [9] P. Tuson, “*HVDC Strengthening in Southern Africa*”, IEEE PES PowerAfrica 2007 Conference and Exposition, Johannesburg, South Africa, 16-20 July 2007.
- [10] IEC 60815, “*Guide for the Selection of Insulators in Respect of Polluted Conditions*”, 1st Edition, 1996.
- [11] N.M. Ijumba, A.C. Britten, L Rajpal, L. Pillay, “*Development of research capacity in HVDC technology in southern Africa*”, AFRICON, 2004. 7th AFRICON Conference in Africa, Vol. 2, Page(s): 765 - 768 Vol.2, 15-17 Sept. 2004.
- [12] C. Adamson, N.G. Hingorani, *High Voltage Direct Current Power Transmission handbook*, published by Garraway, Original form University of Michigan, 1960.
- [13] A.R. Hileman, “*Insulation coordination for Power Systems handbook*”, Published by CRC Press, 1999.
- [14] F.W. Peek, *Dielectric Phenomena in High Voltage Engineering handbook*, Published and reprinted by Read Books, 2007.
- [15] J.Holtzhausen, W. Vosloo, *Practical High Voltage Engineering handbook/ notes*, University of Stellenbosch, 2006.
- [16] M. Abdel-Salam, *High Voltage Engineering Theory and Practice handbook*, Published by CRC Press, 2000.
- [17] E. Kuffel, W.S. Zaegel, J. Kuffel, *High Voltage Engineering: Fundamentals handbook*, 2nd Edition, Newness Press.
- [18] J.A. Bakken, “*Determination of Characteristic Voltages in Impulse Switching Surge Testing*”, IEEE Transactions on Power Apparatus and Systems, Vol 86, No. 8, August 1967.

REFERENCES

- [19] L.E Zafanella, A.W Antiwood et al, “*Guide for Application of Insulators to Withstand Switching Surges*”, IEEE Transaction Paper No. T24 347-1.
- [20] N. Knudsen, “*Flashover Tests on Large Air Gaps with DC Voltage and with Switching Surges Superimposed on DC Voltage*”, IEEE Transactions on Power Apparatus and Systems, PAS vol 89, June 1970.
- [21] Y. Watanabe, “*Influence of Pre-existing DC Voltage on Switching Surge Flashover Characteristics*”, IEEE Transactions on Power Apparatus and Systems, PAS vol 87, April 1968.
- [22] L. Paris, R. Cortina, “*Switching and Lightning Impulse Discharge Characteristics of Large Air Gaps and Long Insulator Strings*”, IEEE, Transaction on Power Apparatus and Systems, Vol. PAS-87 No.4, April 1968.
- [23] L.Paris, “*Influence of Air Gap Characteristics on Line-to-Ground Switching Surge Strength*”, IEEE, Transaction on Power Apparatus and Systems, Vol. PAS-86 No.8, August 1967.
- [24] H. Ramos¹ A. Jose¹, M. Campayo¹, J. Jose¹, G. Motrico¹, Zamora Belver² “*Insulator Pollution in Transmission Lines*”, ¹Escuela Univestaria de Ingenieria, Spain, ²Escuela Tecnica Superior de Ingenieria.
- [25] L.J. Williams, J.H. Kim, Y.B. Kim, N. Arai, O. Shimoda, K.C. Holte, “*Contaminated Insulators Chemical Dependence of Flashover voltages and salt migration*”, IEEE Transaction on Power Apparatus and Systems, Vol. PAS-93 No.5, 1974.
- [26] IEEE working group: K.C. Holte, D.E Alexander, D.M. Baker, et al “*Application of insulators in a contaminated environment*” IEEE Transaction on Power Apparatus and Systems, Vol. PAS-98 No.5, Sept/Oct 1979.

REFERENCES

- [27] A.R Hileman, *Insulation Coordination for Power Systems*, Published by Marcel Dekker, New York, 1999
- [28] IEC507, “*Artificial Pollution Tests on High Voltage Insulators to be Used on AC systems*”, 2nd Edition 1991.
- [29] M. Kawai, D. Milone, “*Flashover Tests at Project UHV on Salt-Contaminated Insulators*”, IEEE, Transaction on Power Apparatus and Systems, Vol. PAS-89 No.5/6, May/June 1970
- [30] J. John, et al; “*Field and Laboratory Tests of Contaminated Insulators for the Design of the State Electricity Commission of Victoria’s 500kV System*”, IEEE, Transaction on Power Apparatus and Systems, Vol. PAS-87 No.5, May 1968.
- [31] C.L Wadhwa, *High Voltage Engineering handbook*, New Age International Limited, Publishers, 1999.
- [32] M.S, Naidu, V. Kamaraju, *High Voltage Engineering*, 2nd Edition, Tata McGraw-Hill Publishing Company Limited.
- [33] Philips eight-stage impulse generator manual.
- [34] F.C. Creed, N.M.C. Collins, “*Shaping circuits for high voltage impulses*”, IEEE Winter Power Meeting, September 1970.
- [35] D. Kind, K. Feser, Translated by Y. Narayana Rao, *High Voltage Test techniques handbook*, Published by Newnes, 2001.
- [36] J. D. Craggs, J.M. Meek, *High Voltage laboratory Technique*, London Butterworths Scientific Publications, 1954.
- [37] Haefely, *Haefely dc source set manual*.

REFERENCES

- [38] Messwandler-Bau GMBH, *High Voltage construction kit manual*, Messwandler-Bau GMBH Bamberg, Germany.
- [39] IEEE Working Group, “*Guide for applications of insulators to withstand switching surges*”, IEEE, Transaction on Power Apparatus and Systems, 1975.
- [40] A.J Schwab, *High Voltage Measurement Techniques handbook*, M.I.T. Press, 1972.
- [41] E. Nasser, “*Some Physical Properties of Electrical Discharges on Contaminated Surfaces on Contaminated Surfaces*”, IEEE, Transaction on Power Apparatus and Systems, Vol. PAS-7 No. 4, April 1968.

Appendix.A Mathematical analysis of a single-stage impulse generator circuit

To obtain the general voltage equations at circuit nodes, the circuit is converted into a Laplace domain equivalent as shown in Figure A.1.

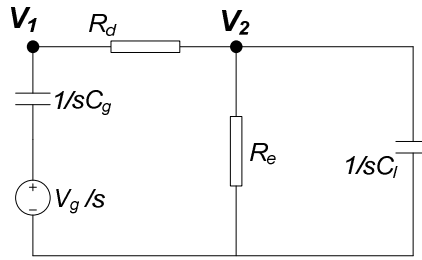


Figure A.1: Laplace equivalent circuit of a standard impulse generator.

The nodal voltage equation for node V_1 is given by the relationship

$$\frac{V_1 - \frac{V_g}{s}}{(1/sC_g)} + \frac{(V_1 - V_2)}{R_d} = 0. \quad (A.1)$$

The above expression can be simplified as follows:

$$V_1 s C_g + \frac{V_1}{R_d} = \frac{V_2}{R_d} + \frac{V_g}{s} \times s C_g \quad (A.2)$$

$$V_1 s C_g + \frac{V_1}{R_d} - \frac{V_2}{R_d} = V_g C_g \quad (A.3)$$

$$V_1 \left(s C_g + \frac{1}{R_d} \right) = \frac{V_2}{R_d} + C_g V_g \quad (A.4)$$

This yields the following expression for V_1 :

$$V_l = \frac{\frac{V_2}{R_d} + C_g V_g}{sC_g + \frac{I}{R_d}} \quad (\text{A.5})$$

which can be simplified to give

$$V_l = \frac{V_2 + R_d C_g V_g}{sR_d C_g + I}. \quad (\text{A.6})$$

The nodal voltage equation for node V_2 is given by the relationship

$$\frac{V_2 - V_l}{R_d} + \frac{V_2}{(I/sC_l)} + \frac{V_2}{R_e} = 0. \quad (\text{A.7})$$

The above expression can be simplified as follows:

$$\frac{V_2}{R_d} - \frac{V_l}{R_d} + V_2 sC_l + \frac{V_2}{R_e} = 0 \quad (\text{A.8})$$

$$\frac{V_2}{R_d} - \left[\frac{V_2 + R_d C_g V_g}{(sR_d C_g + I)R_d} \right] + V_2 sC_l + \frac{V_2}{R_e} = 0 \quad (\text{A.9})$$

$$\frac{V_2}{R_d} - \frac{R_d C_g V_g}{(sR_d C_g + I)R_d} - \frac{V_2}{(sR_d C_g + I)R_d} + V_2 sC_l + \frac{V_2}{R_e} = 0 \quad (\text{A.10})$$

$$V_2 \left[\frac{I}{R_d} - \frac{I}{(sR_d C_g + I)R_d} + \frac{I}{R_e} + sCl \right] = \frac{C_g V_g}{(sR_d C_g + I)} \quad (\text{A.11})$$

$$V_2 \left[\frac{I}{R_d} + \frac{sR_d C_g}{R_d} + sC_l + s^2 R_d C_g C_l - \frac{I}{R_d} + \frac{I}{R_e} + \frac{sR_d C_g}{R_e} \right] = C_g V_g \quad (\text{A.12})$$

$$V_2 \left[sC_g + sC_l + s^2 R_d C_g C_l + \frac{I}{R_e} + \frac{sR_d C_g}{R_e} \right] = C_g V_g \quad (\text{A.13})$$

This yields the following expression for V_2 :

$$V_2 = \frac{C_g V_g}{\left[sC_g + sC_l + s^2 R_d C_g C_l + \frac{I}{R_e} + \frac{sR_d C_g}{R_e} \right]} \quad (\text{A.14})$$

The above relationship can be simplified as follows:

$$V_2 = \frac{V_g}{R_d C_l \left[\frac{s}{R_d C_l} + \frac{s}{R_d C_g} + s^2 + \frac{s}{R_e C_l} + \frac{I}{R_d R_e C_g C_l} \right]} \quad (\text{A.15})$$

$$= \frac{V_g}{R_d C_l \left[s^2 + s \left(\frac{I}{R_d C_l} + \frac{I}{R_d C_g} + \frac{I}{R_e C_l} \right) + \frac{I}{R_d R_e C_g C_l} \right]} \quad (\text{A.16})$$

The roots of the general relationship $ax^2 + bx + c$ is given by the expression

$$\text{roots}(x) = \frac{-b \pm \sqrt{b^2 - 4ac}}{2a}. \quad (\text{A.17})$$

Applying the above expression for the roots to the denominator of equation A.16 yield

$$\text{roots}(x) = -\frac{I}{2} \left(\frac{I}{R_d C_l} + \frac{I}{R_d C_g} + \frac{I}{R_e C_l} \right) \pm \sqrt{\left(\frac{I}{R_d C_l} + \frac{I}{R_d C_g} + \frac{I}{R_e C_l} \right)^2 - 4 \left(\frac{I}{R_d R_e C_g C_l} \right)}. \quad (\text{A.18})$$

Let

$$\alpha = \frac{I}{2} \left(\frac{I}{R_d C_l} + \frac{I}{R_d C_g} + \frac{I}{R_e C_l} \right) \quad (\text{A.19})$$

and

$$\beta = \frac{I}{2} \left[\sqrt{\left(\frac{I}{R_d C_l} + \frac{I}{R_d C_g} + \frac{I}{R_e C_l} \right)^2 - 4 \left(\frac{I}{R_d R_e C_g C_l} \right)} \right]. \quad (\text{A.20})$$

The roots given by equation A.18 can then be then expressed as

$$-\alpha + \beta$$

and

$$-\alpha - \beta.$$

Substituting the roots into equation A.16 yields the relationship

$$V_2 = \frac{V_g}{R_d C_l} \left[\frac{I}{(s + \alpha - \beta) + (s + \alpha + \beta)} \right]. \quad (A.21)$$

By using the principle of partial fractions expansion the term in the bracket in equation A.21 yields

$$\begin{aligned} \frac{I}{(s + \alpha - \beta) + (s + \alpha + \beta)} &= \frac{I}{(s + \alpha - \beta)} + \frac{I}{(s + \alpha + \beta)} \\ &= \frac{A(s + \alpha + \beta) + B(s + \alpha - \beta)}{(s + \alpha - \beta)(s + \alpha + \beta)} \\ &= \frac{As + A\alpha + A\beta + Bs + B\alpha - B\beta}{(s + \alpha - \beta)(s + \alpha + \beta)}. \end{aligned} \quad (A.22)$$

By comparing coefficients, A and B can be obtained as follows:

$$A + B = 0 \quad (A.23)$$

$$A = -B \quad (A.24)$$

$$A\alpha + A\beta + Bs + B\alpha - B\beta = 1 \quad (A.25)$$

Replacing coefficient B with A gives yields the relationship

$$A\alpha + A\beta - A\alpha + A\beta = 1 \quad (A.26)$$

$$2A\beta = 1. \quad (A.27)$$

This yields the following expressions for A and B:

$$A = \frac{1}{2\beta} \quad (A.28)$$

$$B = -\frac{1}{2\beta} \quad (A.29)$$

When the above expression for A and B are substituted into equation A.22, the following equation in frequency domain format is obtained.

$$V_2(s) = \frac{V_g}{R_d C_l} \times \frac{1}{2\beta} \left[\frac{1}{s+(\alpha-\beta)} - \frac{1}{s+(\alpha+\beta)} \right] \quad (A.30)$$

Applying inverse Laplace to $V_2(s)$, equation $V_2(t)$ is obtained.

$$V_2(t) = \frac{V_g}{2\beta R_d C_l} \left[e^{-(\alpha-\beta)t} - e^{-(\alpha+\beta)t} \right] \quad (A.31)$$

$$v_2(t) = \frac{V_g}{k} \left[e^{-(\alpha-\beta)t} - e^{-(\alpha+\beta)t} \right] \quad (A.32)$$

Constant k is expressed as

$$k = \frac{1}{2\beta R_d C_l}. \quad (A.33)$$

$V_2(t)$ is the time domain voltage that appears at node. It is the standard equation of impulse waveform.

Appendix.B Deriving the peak value of an impulse waveform

This is an important step of design. It enables one to obtain the time at which voltage waveform reaches maximum voltage. Recalling equation A.32 and then substituting t with t_p (time to peak) in order to obtain the peak voltage value, the following expression is obtained.

$$v_p(t) = \frac{V_g}{k} [e^{-(\alpha-\beta)t_p} - e^{-(\alpha+\beta)t_p}] \quad (B.1)$$

Time t_p is the time when the maximum voltage is obtained. It is when $\frac{dv}{dt} = 0$. This is illustrated in Figure B.1.

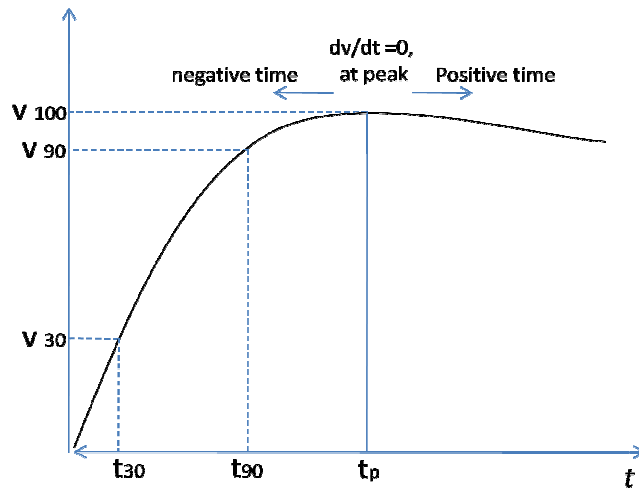


Figure B.1: The graph used to define and calculate the front time of the waveshape.

Expressing equation B.1 in the format $\frac{dv}{dt} = 0$, the following equation is obtained.

$$\frac{d}{dt} \left[\frac{V_g}{k} [e^{-(\alpha-\beta)t_p} - e^{-(\alpha+\beta)t_p}] \right] = 0 \quad (B.2)$$

The differentiation of the above equation yields the following:

APPENDIX B – DERIVING THE PEAK VALUE OF AN IMPULSE WAVEFORM

$$\frac{V_g}{k}(\alpha + \beta)e^{-(\alpha+\beta)t_p} - \frac{V_g}{k}(\alpha - \beta)e^{-(\alpha-\beta)t_p} = 0 \quad (B.3)$$

$$(\alpha + \beta)e^{-(\alpha+\beta)t_p} = (\alpha - \beta)e^{-(\alpha-\beta)t_p} \quad (B.4)$$

$$\frac{\alpha + \beta}{\alpha - \beta} = e^{-(\alpha-\beta)t_p - [-(\alpha+\beta)t_p]} \quad (B.5)$$

$$\frac{\alpha + \beta}{\alpha - \beta} = e^{-\alpha t_p + \beta t_p + \alpha t_p + \beta t_p} \quad (B.6)$$

$$\frac{\alpha + \beta}{\alpha - \beta} = e^{2\beta t_p} \quad (B.7)$$

$$\ln \left[\frac{\alpha + \beta}{\alpha - \beta} \right] = 2\beta t_p \quad (B.8)$$

This yields the following expression for t_p :

$$t_p = \frac{1}{2\beta} \ln \left[\frac{\alpha + \beta}{\alpha - \beta} \right] \quad (B.9)$$

Appendix.C Deriving the front and tail times of an impulse waveform

C.1 Overview

Figure C.1 illustrates the definition of times of an impulse waveform.

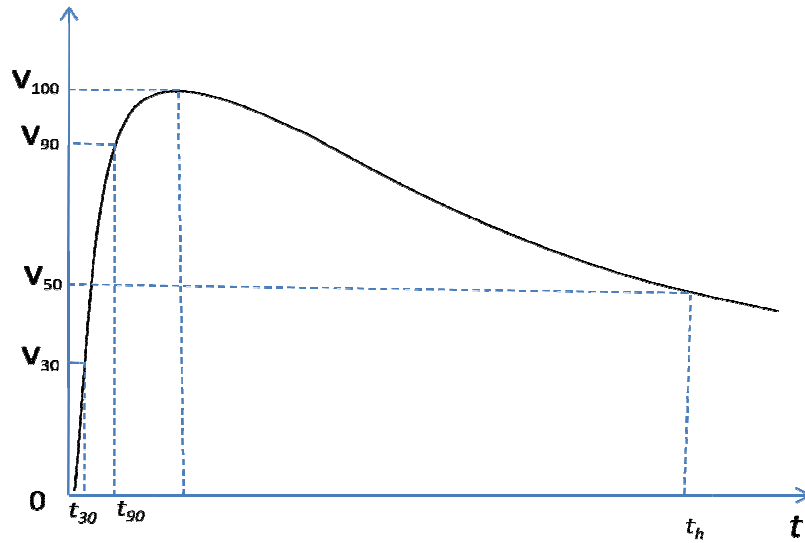


Figure C.1: Definition of front and tail times.

The standard principle of expressing an impulse waveform is t_1/t_2 time, t_1 being the front time while as, t_2 is the tail time of the particular waveform.

$$t_1 = (t_{90} - t_{30}) \times 1.67 \quad (C.1)$$

Time t_2 is also referred as t_h .

The voltages on the waveform are defined as follows:

$$V_{30} = V_{peak} \times 30\% \quad (C.3)$$

$$V_{90} = V_{peak} \times 90\% \quad (C.4)$$

and

$$V_{100} = V_{peak} \quad (C.5)$$

C.2 Deriving the front time

The expressions below indicate when the voltage is at 30% of the peak value.

$$\frac{V_g}{k} [e^{-(\alpha-\beta)t_{30}} - e^{-(\alpha+\beta)t_{30}}] = \frac{V_g}{k} \times \frac{3}{10} [e^{-(\alpha-\beta)t_p} - e^{-(\alpha+\beta)t_p}] \quad (C.6)$$

$$[e^{-(\alpha-\beta)t_{30}} - e^{-(\alpha+\beta)t_{30}}] = \frac{3}{10} [e^{-(\alpha-\beta)t_p} - e^{-(\alpha+\beta)t_p}] \quad (C.7)$$

Since the above equation is too complex to solve for time values, it can be broken down into parts as shown in the Figure C.2. The expression $-(\alpha+\beta)$ being the positive gradient (charging time constant) and $-(\alpha-\beta)$ is the negative gradient (discharging time constant). This graph is divided in its exponential section as shown in the figure, i.e. the charging and the decaying sections.

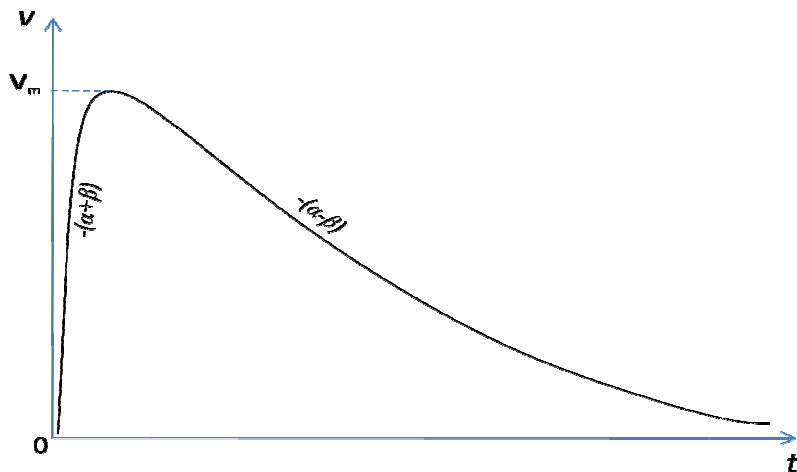


Figure C.2: The two exponential terms of an impulse waveform.

To obtain the rise times in a simplified way, the waveform graph is treated as a separate exponential curve, with a makeshift y-axis as indicated with 0 in Figure C.3. From the rising part of the waveform, t_{30} and t_{90} can be obtained as shown in equations below. The front time is then established.

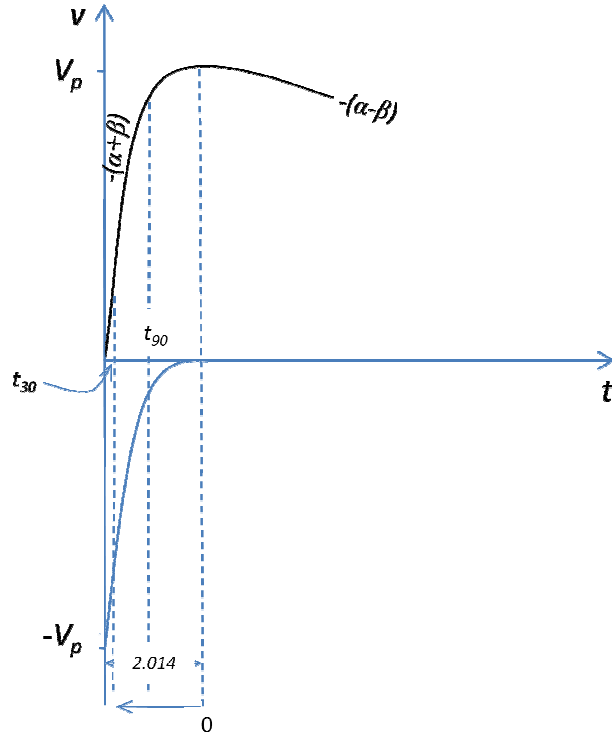


Figure C.3: Illustration of the method used to calculate front time, t_f .

The following mathematical equations show the process of obtaining the front time t_f . It starts with t_{30} . The simplification process is also shown.

$$-e^{-(\alpha+\beta)(t_{30}-t_p)} = -\frac{(10-3)}{10} e^{-(\alpha+\beta)t_p} \quad (C.8)$$

$$e^{-(\alpha+\beta)(t_{30}-t_p)} = \frac{7}{10} e^{-(\alpha+\beta)t_p} \quad (C.9)$$

$$\ln e^{-(\alpha+\beta)(t_{30}-t_p)} = \ln \left[\frac{7}{10} e^{-(\alpha+\beta)t_p} \right] \quad (C.10)$$

$$-(\alpha + \beta)(t_{30} - t_p) = \ln \left[\frac{7}{10} e^{-(\alpha + \beta)t_p} \right] \quad (C.11)$$

$$(\alpha + \beta)(t_{30} - t_p) = \ln \left[\frac{10}{7} e^{-(\alpha + \beta)t_p} \right] \quad (C.12)$$

This yields the following expression for t_{30} :

$$t_{30} = t_p - \left[\frac{1}{\alpha + \beta} \ln \left(\frac{10}{7} e^{-(\alpha + \beta)t_p} \right) \right]. \quad (C.13)$$

The time between t_{30} and t_p is can be expressed as follows:

$$\frac{1}{\alpha + \beta} \ln \left(\frac{10}{7} e^{-(\alpha + \beta)t_p} \right)$$

and time between t_{30} and t_p is given by

$$\frac{1}{\alpha + \beta} \ln \left(\frac{10}{1} e^{-(\alpha + \beta)t_p} \right).$$

With circuit constants known,

$$\alpha = 1312750$$

$$\beta = 1298800$$

times t_p and t_{30} are obtained as shown below:

$$t_p = \frac{1}{2\beta} \ln \left[\frac{\alpha + \beta}{\alpha - \beta} \right]$$

$$t_p = 2.014 \mu s$$

$$t_{30} = 2.014 + (-1.737) \mu s$$

$$= 0.0403 \mu s$$

Similarly, time t_{90} is obtained as shown below:

$$t_{90} = t_p - \left[\frac{1}{\alpha + \beta} \ln \left(\frac{10}{(10-9)} e^{-(\alpha+\beta)t_p} \right) \right] \quad (C.14)$$

$$t_{90} = t_p - \left[\frac{1}{\alpha + \beta} \ln \left(\frac{10}{1} e^{-(\alpha+\beta)t_p} \right) \right] \quad (C.15)$$

$$\begin{aligned} t_{90} &= 2.014 + (-1.132)\mu s \\ &= 0.882\mu s \end{aligned}$$

With t_{30} and t_{90} known, the *front time* t_f can be obtained.

$$\begin{aligned} t_f &= (t_{90} - t_{30}) \times 1.67 \\ &= (0.745\mu s) \times 1.67 \\ &= 1.245\mu s \end{aligned}$$

C.3 Deriving the tail time

On the discharge phase, the voltage decreases to half the peak voltage in a time t_h (also referred to t_2 in this thesis), so that

$$v_2(t) = \frac{V_g}{k} [e^{-(\alpha-\beta)t_2} - e^{-(\alpha+\beta)t_2}] = \frac{V_g}{2k} [e^{-(\alpha-\beta)t_p} - e^{-(\alpha+\beta)t_p}]. \quad (C.16)$$

If t_h is expressed in terms of t_p ,

$$t_2 = c t_p, \quad (C.17)$$

c is the constant, the following is obtained:

$$v_2(t) = \frac{V_g}{k} [e^{-(\alpha-\beta)ct_p} - e^{-(\alpha+\beta)ct_p}] = \frac{V_g}{2k} [e^{-(\alpha-\beta)t_p} - e^{-(\alpha+\beta)t_p}] \quad (C.18)$$

For a short front impulse, the charging section of the impulse can be neglected, so the above equation simplifies to give [32]:

$$e^{-(\alpha-\beta)ct_p} = \frac{1}{2}[e^{-(\alpha-\beta)t_p} - e^{-(\alpha+\beta)t_p}] \quad (C.19)$$

$$2e^{-(\alpha-\beta)ct_p} = e^{-(\alpha-\beta)t_p} - e^{-(\alpha+\beta)t_p} \quad (C.20)$$

$$2e^{-(\alpha-\beta)(c-1)t_p} = 1 - e^{-2\beta t_p} \quad (C.21)$$

$$\alpha - \beta = \frac{1}{t_p(c-1)} \cdot \ln\left(\frac{2}{1 - e^{-2\beta t_p}}\right) \quad (C.22)$$

If $2\beta t_p > 4$ the above equation simplifies to

$$\alpha - \beta = \frac{0.7}{t_p(c-1)} \quad (C.23)$$

$$\alpha - \beta = \frac{0.7}{t_h - t_p} \quad (C.24)$$

This yields the following expression for t_2 :

$$t_2 = \frac{0.7}{\alpha - \beta} + t_p \quad (C.25)$$

Appendix.D Nodal voltage analysis of the composite waveform generator circuit

Figure D.1 shows the Laplace equivalent representation of the composite waveform generator circuit.

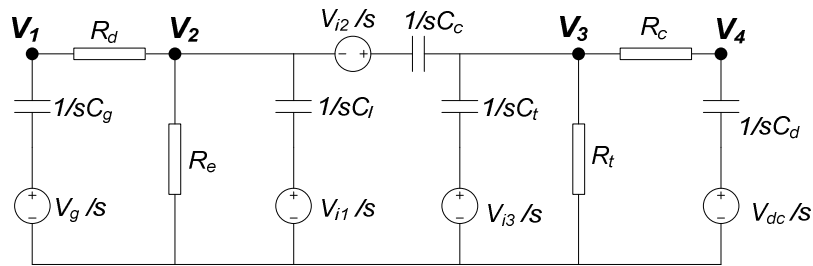


Figure D.1: Laplace equivalent representation of the composite waveform generator circuit.

The impulse generator parameters in Figure D.1 are defined as follows:

- V_g : Impulse generator's input dc voltage [V]
- C_g : Generator capacitance [F]
- C_l : Load capacitance [F]
- R_d : Wave shaping resistance / control of wavefront [Ω]
- R_e : Wave tail resistance [Ω]
- V_{i1} : Initial voltage across the load capacitor[V]

The dc source parameters are defined as follows:

- V_{dc} : DC source voltage [V]
- C_d – DC source capacitor [F]

The test object parameters are defined as follows:

- C_t : Capacitance of the test object [F]

- R_t : Resistance of the test object [Ω]
- V_{i3} : Initial voltage across the test test object [V]

The coupling component parameters are defined as follows:

- C_c : Coupling capacitance [F]
- R_c : Coupling resistance [Ω]
- V_{i2} : Initial voltage across the coupling capacitor [V]

The circuit in Figure D.1 gives rise to the following nodal equations in the Laplace domain:

The nodal voltage equation for node V_1 is given by the relationship

$$\frac{V_1 - \frac{V_g}{s}}{(1/sC_g)} + \frac{(V_1 - V_2)}{R_d} = 0. \quad (D.1)$$

The above expression can be simplified as follows:

$$V_1 s C_g + \frac{V_1}{R_d} = \frac{V_2}{R_d} + \frac{V_g}{s} \times s C_g \quad (D.2)$$

$$V_1 s C_g + \frac{V_1}{R_d} - \frac{V_2}{R_d} = V_g C_g \quad (D.3)$$

$$V_1 \left(s C_g + \frac{1}{R_d} \right) = \frac{V_2}{R_d} + C_g V_g \quad (D.4)$$

This yields the following expression for V_1 :

$$V_1(s) = \frac{\frac{V_2}{R_d} + C_g V_g}{s C_g + \frac{1}{R_d}} \quad (D.5)$$

which can be simplified to give

$$V_1(s) = \frac{V_2 + R_d C_g V_g}{s R_d C_g + 1} \quad (D.6)$$

The nodal voltage equation for node V_2 is given by the relationship

$$\frac{V_2 - V_1}{R_d} + \frac{V_2 + \frac{V_{i2}}{s} - V_3}{(1/sC_c)} + \frac{V_2 - \frac{V_{i1}}{s}}{(1/sC_l)} + \frac{V_2}{R_e} = 0 \quad (D.7)$$

The above equation is simplified as follows:

$$\frac{V_2}{R_d} - \frac{V_1}{R_d} + sC_c V_2 + C_c V_{i2} - sC_c V_3 + sC_l V_2 - C_l V_{i1} + \frac{V_2}{R_e} = 0 \quad (D.8)$$

$$\frac{V_2}{R_d} - \frac{1}{R_d} \left(\frac{V_2 + C_g V_g}{sC_g + \frac{1}{R_d}} \right) + sC_c V_2 + sC_l V_2 + \frac{V_2}{R_e} = C_l V_{i1} - C_c V_{i2} + sC_c V_3 \quad (D.9)$$

$$\frac{V_2}{R_d} - \frac{\frac{V_2 + C_g V_g}{R_d}}{sR_d C_g + 1} + sC_c V_2 + sC_l V_2 + \frac{V_2}{R_e} = C_l V_{i1} - C_c V_{i2} + sC_c V_3 \quad (D.10)$$

$$\frac{V_2}{R_d} - \frac{\frac{V_2}{R_d}}{sR_d C_g + 1} + sC_c V_2 + sC_l V_2 + \frac{V_2}{R_e} = C_l V_{i1} - C_c V_{i2} + sC_c V_3 + \frac{C_g V_g}{sR_d C_g + 1} \quad (D.11)$$

$$\left[\frac{V_2 (sR_d C_g + 1) - \frac{V_2}{R_d} (R_d)}{R_d (sR_d C_g + 1)} \right] + sC_c V_2 + sC_l V_2 + \frac{V_2}{R_e} = C_l V_{i1} - C_c V_{i2} + sC_c V_3 + \frac{C_g V_g}{sR_d C_g + 1} \quad (D.12)$$

$$\frac{sC_g V_2}{sR_d C_g + 1} + sC_c V_2 + sC_l V_2 + \frac{V_2}{R_e} = C_l V_{i1} - C_c V_{i2} + sC_c V_3 + \frac{C_g V_g}{sR_d C_g + 1} \quad (D.13)$$

This yields the following expression for V_2 :

$$V_2(s) = \frac{C_l V_{i1} - C_c V_{i2} + sC_c V_3 + \frac{C_g V_g}{sR_d C_g + 1}}{\frac{sC_g}{sR_d C_g + 1} + sC_c + sC_l + \frac{1}{R_e}} \quad (D.14)$$

which can be simplified to give

$$V_2(s) = \frac{R_e \left(s^2 R_d C_c C_g V_3 + sC_c V_3 + sR_d C_g C_l V_{i1} - sR_d C_c C_g V_{i2} + C_g V_g + C_l V_{i1} - C_c V_{i2} \right)}{s^2 R_d R_e C_c C_g + s^2 R_d R_e C_g C_l + sR_d R_e C_g + sR_e C_c + sR_e C_g + sR_e C_l + 1} \quad (D.15)$$

The nodal voltage equation for node V_3 is given by the relationship

$$\frac{V_3 - \frac{V_{i2}}{s} - V_2}{(1/sC_c)} + \frac{V_3 - \frac{V_{i3}}{s}}{(1/sC_t)} + \frac{V_3}{R_t} + \frac{V_3 - \frac{V_{dc}}{s}}{(R_c + 1/sC_d)} = 0. \quad (D.16)$$

The above expression can be simplified as follows:

$$\frac{V_3}{R_t} + \frac{C_d \left(sV_3 - \frac{V_{dc}}{s} \right)}{R_c + sC_d} + sC_c \left(-V_2 + V_3 - \frac{V_{i2}}{s} \right) + sC_t \left(V_3 - \frac{V_{i3}}{s} \right) = 0 \quad (D.17)$$

$$-sC_c V_2 + sC_c V_3 + sC_t V_3 + \frac{V_3}{R_t} + \frac{sC_d V_3}{sR_c C_d + 1} = C_c V_{i2} + C_t V_{i3} - \frac{C_d V_{dc}}{sR_c C_d + 1} \quad (D.18)$$

$$\begin{aligned}
 & \frac{V_3}{R_t} + \frac{C_d \left(sV_3 - \frac{V_{dc}}{s} \right)}{R_c + sC_d} + sC_c \left(- \left(\frac{C_l V_{i1} - C_c V_{i2} + sC_c V_3 + \frac{C_g V_g}{sR_d C_g + 1}}{\frac{sC_g}{sR_d C_g + 1} + sC_c + sC_l + \frac{1}{R_e}} \right) + V_3 - \frac{V_{i2}}{s} \right) + \\
 & sC_t \left(V_3 - \frac{V_{i3}}{s} \right) = 0
 \end{aligned} \tag{D.19}$$

This yields the following expression for V_3 :

$$\begin{aligned}
 V_3(s) = & \left(\frac{V_{dc}}{\left(R_c + \frac{1}{sC_d} \right) s} + \frac{sC_c C_g V_g}{(1 + sC_g R_d) + \left(\frac{1}{R_e} + sC_c + sC_l + \frac{sC_g}{1 + sC_g R_d} \right)} + \right. \\
 & \left. \frac{sC_c C_l V_{i1}}{\frac{1}{R_e} + sC_c + sC_l + \frac{sC_g}{1 + sC_g R_d}} + C_c V_{i2} - \frac{sC_c^2 V_{i2}}{\frac{1}{R_e} + sC_c + sC_l + \frac{sC_g}{1 + sC_g R_d}} + C_t V_{i3} \right) / \\
 & \left(\frac{s^2 C_c^2}{\frac{1}{R_c + \frac{1}{sC_d}} + \frac{1}{R_t} + sC_c + sC_l + \frac{sC_g}{1 + sC_g R_d}} \right)
 \end{aligned} \tag{D-20}$$

which can be simplified to give

$$\begin{aligned}
 & (R_t (s^3 R_c R_d R_e C_c C_d C_g C_l V_{i1} + s^3 R_c R_d R_e C_c C_d C_g C_l V_{i2} + s^3 R_c R_d R_e C_c C_d C_g C_l V_{i3} + \\
 & s^3 R_c R_d R_e C_d C_g C_l C_t V_{i3} + s^2 R_c R_e C_c C_d C_l V_{i1} + s^2 R_d R_e C_c C_g C_l V_{i1} + s^2 R_c R_d C_c C_d C_g V_{i2} + \\
 & s^2 R_c R_e C_c C_d C_g V_{i2} + s^2 R_c R_e C_c C_d C_l V_{i2} + s^2 R_d R_e C_c C_g C_l V_{i2} + s^2 R_c R_d C_c C_d C_g V_{i3} + \\
 & s^2 R_c R_e C_c C_d C_l V_{i3} + s^2 R_c R_e C_d C_l C_t V_{i3} + s^2 R_d R_e C_d C_l C_t V_{i3} + s^2 R_d R_e C_c C_g C_l V_{i3} + \\
 & s^2 R_d R_e C_g C_l C_t V_{i3} + s^2 R_d R_e C_c C_d C_g V_{dc} + s^2 R_d R_e C_d C_g C_l V_{dc} + s^2 R_c R_e C_c C_d C_g V_g + s R_e C_c C_l V_{i1} + \\
 & s R_c C_c C_d V_{i2} + s R_d C_c C_g V_{i2} + s R_e C_c C_g V_{i2} + s R_e C_c C_l V_{i2} + s R_e C_d C_l V_{i3} + s R_d C_g C_l V_{i3} + R_e C_c C_l V_{i3} + \\
 & s R_e C_g C_l V_{i3} + s R_e C_l C_t V_{i3} + s R_d C_d C_g V_{dc} + s R_e C_c C_d V_{dc} + s R_e C_d C_g V_{dc} + s R_e C_d C_l V_{dc} + s R_e C_c C_g V_g + \\
 & C_c V_{i2} + C_l V_{i3} + C_d V_{dc}) \\
 V_3(s) = & \frac{C_c V_{i2} + C_l V_{i3} + C_d V_{dc})}{(s^4 R_c R_d R_e R_t C_c C_d C_g C_l + s^4 R_c R_d R_e R_t C_c C_d C_e C_t + s^4 R_c R_d R_e R_t C_d C_g C_l C_t + s^3 R_c R_d R_e C_c C_d C_g + \\
 & s^3 R_c R_d R_e C_d C_g C_l + s^3 R_c R_d R_t C_c C_d C_g + s^3 R_c R_d R_t C_d C_g C_t + s^3 R_c R_e R_t C_c C_d C_g + s^3 R_c R_e R_t C_c C_d C_l + \\
 & s^3 R_c R_e R_t C_c C_d C_t + s^3 R_c R_e R_t C_d C_g C_t + s^3 R_c R_e R_t C_d C_l C_t + s^3 R_d R_e R_t C_c C_d C_g + s^3 R_d R_e R_t C_c C_g C_l + \\
 & s^3 R_d R_e R_t C_d C_g C_l + s^3 R_d R_e R_t C_c C_g C_t + s^3 R_d R_e R_t C_g C_l C_t + s^2 R_c R_d C_d C_g + s^2 R_c R_e C_c C_d + \\
 & s^2 R_c R_e C_d C_g + s^2 R_c R_e C_d C_l + s^2 R_d R_e C_c C_g + s^2 R_d R_e C_g C_l + s^2 R_c R_t C_c C_d + s^2 R_c R_t C_d C_t + \\
 & s^2 R_d R_t C_c C_g + s^2 R_d R_t C_d C_g + s^2 R_d R_t C_g C_t + s^2 R_e R_t C_c C_d + s^2 R_e R_t C_c C_g + s^2 R_e R_t C_d C_g + \\
 & s^2 R_e R_t C_c C_l + s^2 R_e R_t C_d C_l + s^2 R_e R_t C_c C_t + s^2 R_e R_t C_g C_t + s^2 R_e R_t C_l C_t + s R_c C_d + s R_d C_g + s R_e C_c + \\
 & s R_e C_g + s R_e C_l + s R_t C_c + s R_t C_d + s R_t C_t + 1) }
 \end{aligned}
 \tag{D.21}$$

The above expression can be reordered is to give the following equation:

$$\begin{aligned}
 & s^3(R_c R_d R_e R_t C_c C_d C_g C_l V_{i1} + R_c R_d R_e R_t C_c C_d C_g C_l V_{i2} + R_c R_d R_e R_t C_c C_d C_g C_l V_{i3} + \\
 & R_c R_d R_e R_t C_c C_d C_l C_t V_{i3}) + \\
 & s^2(R_c R_e R_t C_c C_d C_l V_{i1} + R_d R_e R_t C_c C_g C_l V_{i1} + R_c R_d R_t C_c C_d C_g V_{i2} + R_c R_e R_t C_c C_d C_g V_{i2} + \\
 & R_c R_e R_t C_c C_d C_l V_{i2} + R_d R_e R_t C_c C_g C_l V_{i2} + R_c R_d R_t C_c C_d C_g C_l V_{i3} + R_c R_e R_t C_c C_d C_l V_{i3} + \\
 & R_c R_e R_t C_c C_d C_g C_l V_{i3} + R_c R_e R_t C_d C_l C_t V_{i3} + R_d R_e R_t C_c C_g C_l V_{i3} + R_d R_e R_t C_g C_l C_t V_{i3} + \\
 & R_d R_e R_t C_c C_d C_g V_{dc} + R_d R_e R_t C_d C_g C_l V_{dc} + R_c R_e R_t C_c C_d C_g V_g) + \\
 & s(R_e R_t C_c C_l V_{i1} + R_c R_t C_c C_d V_{i2} + R_d R_t C_c C_g V_{i2} + R_e R_t C_c C_g V_{i2} + R_e R_t C_c C_l V_{i2} + \\
 & R_c R_t C_d C_l V_{i3} + R_d R_t C_g C_l V_{i3} + R_e R_t C_c C_t V_{i3} + R_e R_t C_g C_t V_{i3} + R_e R_t C_l C_t V_{i3} + \\
 & R_d R_t C_d C_g V_{dc} + R_e R_t C_c C_d V_{dc} + R_e R_t C_d C_g V_{dc} + R_e R_t C_d C_l V_{dc} + R_e R_t C_c C_g V_g) + \\
 V_3(s) = & \frac{R_t C_c V_{i2} + R_t C_l V_{i3} + R_t C_d V_{dc}}{s^4(R_c R_d R_e R_t C_c C_d C_g C_l + R_c R_d R_e R_t C_c C_d C_e C_t + R_c R_d R_e R_t C_d C_g C_l C_t) +} \\
 & s^3(R_c R_d R_e C_c C_d C_g + R_c R_d R_e C_d C_g C_l + R_c R_d R_t C_c C_d C_g + R_c R_d R_t C_d C_g C_t + \\
 & R_c R_e R_t C_c C_d C_g + R_c R_e R_t C_c C_d C_l + R_c R_e R_t C_c C_d C_t + R_c R_e R_t C_d C_g C_t + \\
 & R_c R_e R_t C_d C_l C_t + R_d R_e R_t C_c C_d C_g + R_d R_e R_t C_c C_g C_l + R_d R_e R_t C_d C_g C_l + \\
 & R_d R_e R_t C_c C_g C_t + R_d R_e R_t C_l C_t) + \\
 & s^2(R_c R_d C_d C_g + S^2 R_c R_e C_c C_d + R_c R_e C_d C_g + R_c R_e C_d C_l + R_d R_e C_c C_g + R_d R_e C_g C_l + \\
 & R_c R_t C_c C_d + R_c R_t C_d C_t + R_d R_t C_c C_g + R_d R_t C_d C_g + R_d R_t C_g C_t + R_e R_t C_c C_d + \\
 & R_e R_t C_c C_g + R_e R_t C_d C_g + R_e R_t C_c C_l + R_e R_t C_d C_l + R_e R_t C_c C_t + R_e R_t C_g C_t + \\
 & R_e R_t C_l C_t) + \\
 & s(R_c C_d + R_d C_g + R_e C_c + R_e C_g + R_e C_l + R_t C_c + R_t C_d + R_t C_t) + \\
 & 1
 \end{aligned} \tag{D.22}$$

Equation D.22 can be expressed in the format:

$$V_3(s) = \frac{a_3 s^3 + a_2 s^2 + a_1 s + a_0}{b_4 s^4 + b_3 s^3 + b_2 s^2 + b_1 s + b_0} \tag{D.23}$$

where

$$a_3 = R_c R_d R_e R_t C_c C_d C_g C_l V_{i1} + R_c R_d R_e R_t C_c C_d C_g C_l V_{i2} + R_c R_d R_e R_t C_c C_d C_g C_l V_{i3} + R_c R_d R_e R_t C_c C_d C_l C_t V_{i3}, \tag{D.24}$$

$$\begin{aligned}
 a_2 = & R_c R_e R_t C_c C_d C_l V_{i1} + R_d R_e R_t C_c C_g C_l V_{i1} + R_c R_d R_t C_c C_d C_g V_{i2} + R_c R_e R_t C_c C_d C_g V_{i2} + R_c R_e R_t C_c C_d C_l V_{i2} + \\
 & R_d R_e R_t C_c C_g C_l V_{i2} + R_c R_d R_t C_d C_g C_l V_{i3} + R_c R_e R_t C_c C_d C_l V_{i3} + R_c R_e R_t C_d C_g C_l V_{i3} + R_c R_e R_t C_d C_l C_l V_{i3} + \\
 & R_d R_e R_t C_c C_g C_l V_{i3} + R_d R_e R_t C_g C_l C_l V_{i3} + R_d R_e R_t C_c C_d C_g V_{dc} + R_d R_e R_t C_d C_g C_l V_{dc} + R_c R_e R_t C_c C_d C_g V_g ,
 \end{aligned} \tag{D.25}$$

$$\begin{aligned}
 a_1 = & R_e R_t C_c C_l V_{i1} + R_c R_t C_c C_d V_{i2} + R_d R_t C_c C_g V_{i2} + R_e R_t C_c C_g V_{i2} + R_e R_t C_c C_l V_{i2} + R_c R_t C_d C_l V_{i3} + \\
 & R_d R_t C_g C_l V_{i3} + R_e R_t C_c C_l V_{i3} + R_e R_t C_g C_l V_{i3} + R_e R_t C_l C_l V_{i3} + R_d R_t C_d C_g V_{dc} + R_e R_t C_c C_d V_{dc} + \\
 & R_e R_t C_d C_g V_{dc} + R_e R_t C_d C_l V_{dc} + R_e R_t C_c C_g V_g ,
 \end{aligned} \tag{D.26}$$

$$a_0 = R_t C_c V_{i2} + R_t C_l V_{i3} + R_t C_d V_{dc} , \tag{D.27}$$

$$b_4 = R_c R_d R_e R_t C_c C_d C_g C_l + R_c R_d R_g R_t C_c C_d C_e C_t + R_c R_d R_e R_t C_d C_g C_l C_t , \tag{D.28}$$

$$\begin{aligned}
 b_3 = & R_c R_d R_e C_c C_d C_g + R_c R_d R_e C_d C_g C_l + R_c R_d R_t C_c C_d C_g + R_c R_d R_t C_d C_g C_t + R_c R_e R_t C_c C_d C_g + \\
 & R_c R_e R_t C_c C_d C_l + R_e R_e R_t C_c C_d C_t + R_c R_e R_t C_d C_g C_t + R_c R_e R_t C_d C_l C_t + R_d R_e R_t C_c C_d C_g + \\
 & R_d R_e R_t C_c C_g C_l + R_d R_e R_t C_d C_g C_l + R_d R_e R_t C_c C_g C_t + R_d R_e R_t C_g C_l C_t ,
 \end{aligned} , \tag{D.29}$$

$$\begin{aligned}
 b_2 = & R_c R_d C_d C_g + R_c R_e C_c C_d + R_c R_e C_d C_g + R_c R_e C_d C_l + R_d R_e C_c C_g + R_d R_e C_g C_l + R_c R_t C_c C_d + \\
 & R_c R_t C_d C_t + R_d R_t C_c C_g + R_d R_t C_d C_g + R_d R_t C_g C_t + R_e R_t C_c C_d + R_e R_t C_c C_g + R_e R_t C_d C_g + \\
 & R_e R_t C_c C_l + R_e R_t C_d C_l + R_e R_t C_c C_t + R_e R_t C_g C_t + R_e R_t C_l C_t ,
 \end{aligned} , \tag{D.30}$$

$$b_1 = R_c C_d + R_d C_g + R_e C_c + R_e C_g + R_e C_l + R_t C_c + R_t C_d + R_t C_t , \tag{D.31}$$

and

$$b_0 = 1. \tag{D.32}$$

The nodal voltage equation for node V_4 is given by the relationship

$$\frac{V_4 - V_3}{R_c} + \frac{V_4 - \frac{V_{dc}}{s}}{(1/sC_d)} = 0. \quad (D.33)$$

The above expression can be simplified as follows:

$$\frac{-V_3}{R_c} + \frac{V_4}{R_c} + sC_d V_4 - C_d V_{dc} = 0. \quad (D.34)$$

$$\begin{aligned} & - \left(\frac{V_4}{R_c} + \frac{sC_c C_g V_g}{(1 + sC_g R_d) + \left(\frac{1}{R_e} + sC_c + sC_l + \frac{sC_g}{1 + sC_g R_d} \right)} + \right. \\ & \left. \frac{\frac{sC_c C_l V_{i1}}{\frac{1}{R_e} + sC_c + sC_l + \frac{sC_g}{1 + sC_g R_d}} + C_c V_{i2} - \frac{sC_c^2 V_{i2}}{\frac{1}{R_e} + sC_c + sC_l + \frac{sC_g}{1 + sC_g R_d}} + C_l V_{i3}}{\frac{1}{R_e} + sC_c + sC_l + \frac{sC_g}{1 + sC_g R_d}} \right) / \\ & \frac{\left(\frac{s^2 C_c^2}{\frac{1}{R_c} + \frac{1}{R_t} + sC_c + sC_l + \frac{sC_g}{1 + sC_g R_d}} \right)}{R_c} + \end{aligned}$$

$$\frac{V_4}{R_c} + sC_d V_4 - C_d V_{dc} = 0 \quad (D.35)$$

This yields the following expression for V_4 :

$$V_d(s) = \left(\begin{array}{l} C_d V_{dc} + \frac{sC_c C_g V_g}{R_c (1 + sC_g R_d) \left(\frac{1}{R_e} + sC_c + sC_l + \frac{sC_g}{1 + sC_g R_d} \right)} \left(\frac{1}{R_c} + \frac{1}{R_l} + sC_c + sC_l - \frac{s^2 C_c^2}{\frac{1}{R_e} + sC_c + sC_l + \frac{sC_g}{1 + sC_g R_d}} \right) \\ + \frac{sC_c C_l V_{i1}}{R_c \left(\frac{1}{R_e} + sC_c + sC_l + \frac{sC_g}{1 + sC_g R_d} \right)} \left(\frac{1}{R_c} + \frac{1}{R_l} + sC_c + sC_l - \frac{s^2 C_c^2}{\frac{1}{R_e} + sC_c + sC_l + \frac{sC_g}{1 + sC_g R_d}} \right) \\ - \frac{sC_c V_{i2}}{R_c \left(\frac{1}{R_c} + \frac{1}{R_l} + sC_c + sC_l - \frac{s^2 C_c^2}{\frac{1}{R_e} + sC_c + sC_l + \frac{sC_g}{1 + sC_g R_d}} \right)} \\ + \frac{sC_c^2 V_{i2}}{R_c \left(\frac{1}{R_e} + sC_c + sC_l + \frac{sC_g}{1 + sC_g R_d} \right)} \left(\frac{1}{R_c} + \frac{1}{R_l} + sC_c + sC_l - \frac{s^2 C_c^2}{\frac{1}{R_e} + sC_c + sC_l + \frac{sC_g}{1 + sC_g R_d}} \right) \\ + \frac{C_l V_{i3}}{R_c \left(\frac{1}{R_c} + \frac{1}{R_l} + sC_c + sC_l - \frac{s^2 C_c^2}{\frac{1}{R_e} + sC_c + sC_l + \frac{sC_g}{1 + sC_g R_d}} \right)} \\ + \frac{I}{\left(\frac{1}{R_c} + sC_d - R_c \left(\frac{1}{R_c} + \frac{1}{R_l} + sC_c + sC_l - \frac{s^2 C_c^2}{\frac{1}{R_e} + sC_c + sC_l + \frac{sC_g}{1 + sC_g R_d}} \right) \right)} \end{array} \right) \Bigg/ \Bigg/$$

(D.36)

which can be simplified to give

$$\begin{aligned}
 & s^3 R_c R_d R_e R_t C_c C_d C_g C_l V_{dc} + s^3 R_c R_d R_e R_t C_c C_d C_g C_l V_{dc} + s^3 R_c R_d R_e R_t C_d C_g C_l C_t V_{dc} + \\
 & s^2 R_c R_d R_e C_c C_d C_g V_{dc} + s^2 R_c R_d R_e C_d C_g C_l V_{dc} + s^2 R_c R_d R_t C_c C_d C_g V_{dc} + \\
 & s^2 R_c R_d R_t C_d C_g C_l V_{dc} + s^2 R_c R_e R_t C_c C_d C_l V_{dc} + s^2 R_c R_e R_t C_c C_d C_t V_{dc} + \\
 & s^2 R_c R_e R_t C_d C_g C_l V_{dc} + s^2 R_c R_e R_t C_d C_l C_t V_{dc} + s^2 R_d R_e R_t C_c C_d C_g V_{dc} + s^2 R_d R_e R_t C_d C_g C_l V_{dc} + \\
 & s^2 R_d R_e R_t C_c C_g C_l V_{i1} + s^2 R_d R_e R_t C_c C_g C_l V_{i2} + s^2 R_d R_e R_t C_c C_g C_l V_{i3} + s^2 R_d R_e R_t C_g C_l C_t V_{i3} + \\
 & s R_c R_d C_d C_g V_{dc} + s R_c R_e C_c C_d V_{dc} + s R_c R_e C_d C_g V_{dc} + s R_c R_e C_d C_l V_{dc} + s R_c R_t C_c C_d V_{dc} + \\
 & s R_c R_t C_d C_l V_{dc} + s R_d R_t C_d C_g V_{dc} + s R_e R_t C_c C_d V_{dc} + s R_e R_t C_d C_g V_{dc} + s R_e R_t C_d C_l V_{dc} + \\
 & s R_e R_t C_c C_g V_{dc} + s R_e R_t C_c C_l V_{i1} + s R_e R_t C_c C_g V_{i2} + s R_e R_t C_c C_g V_{i2} + s R_e R_t C_c C_l V_{i2} + \\
 & s R_d R_t C_g C_l V_{i3} + s R_e R_t C_c C_l V_{i3} + s R_e R_t C_g C_l V_{i3} + s R_e R_t C_l C_l V_{i3} + R_c C_d V_{dc} + R_t C_d V_{dc} + \\
 & \frac{R_t C_c V_{i2} + R_t C_l V_{i3}}{s^4 R_c R_d R_e R_t C_c C_d C_g C_l + s^4 R_c R_d R_e R_t C_c C_d C_g C_t + s^4 R_c R_d R_e R_t C_d C_g C_l C_t +} \\
 & s^3 R_c R_d R_e C_c C_d C_g + s^3 R_c R_d R_e C_d C_g C_l + s^3 R_c R_d R_t C_c C_d C_g + s^3 R_c R_d R_t C_d C_g C_t + \\
 & s^3 R_c R_e R_t C_c C_d C_g + s^3 R_c R_e R_t C_c C_d C_l + s^3 R_c R_e R_t C_c C_d C_t + s^3 R_c R_e R_t C_d C_g C_t + \\
 & s^3 R_c R_e R_t C_d C_l C_t + s^3 R_d R_e R_t C_c C_d C_g + s^3 R_d R_e R_t C_c C_g C_l + s^3 R_d R_e R_t C_d C_g C_l + \\
 & s^3 R_d R_e R_t C_c C_g C_t + s^3 R_d R_e R_t C_g C_l C_t + s^2 R_c R_d C_d C_g + s^2 R_c R_e C_c C_d + s^2 R_c R_e C_d C_g + \\
 & s^2 R_c R_e C_d C_l + s^2 R_d R_e C_c C_g + s^2 R_d R_e C_g C_l + s^2 R_c R_t C_c C_d + s^2 R_c R_t C_d C_t + s^2 R_d R_t C_c C_g + \\
 & s^2 R_d R_t C_d C_g + s^2 R_d R_t C_g C_t + s^2 R_e R_t C_c C_d + s^2 R_e R_t C_c C_g + s^2 R_e R_t C_d C_g + s^2 R_e R_t C_c C_l + \\
 & s^2 R_e R_t C_d C_l + s^2 R_e R_t C_c C_t + s^2 R_e R_t C_g C_t + s^2 R_e R_t C_l C_t + s R_c C_d + s R_d C_g + s R_e C_c + \\
 & s R_e C_g + s R_e C_l + s R_t C_c + s R_t C_d + s R_t C_l + 1
 \end{aligned}$$

(D.37)

The above equation is reordered and yields the following equation:

$$\begin{aligned}
 & (R_c R_d R_e R_t C_c C_d C_g C_l V_{dc} + R_c R_d R_e R_t C_c C_d C_g C_t V_{dc} + R_c R_d R_e R_t C_d C_g C_l C_t V_{dc}) s^3 + \\
 & + (R_c R_d R_e C_c C_d C_g V_{dc} + R_c R_d R_e C_d C_g C_l V_{dc} + R_c R_d R_t C_c C_d C_g V_{dc} + R_c R_d R_t C_d C_g C_t V_{dc} + \\
 & R_c R_e R_t C_c C_d C_g V_{dc} + R_c R_e R_t C_c C_d C_l V_{dc} + R_c R_e R_t C_c C_d C_t V_{dc} + R_c R_e R_t C_d C_g C_t V_{dc} + \\
 & R_c R_e R_t C_d C_l C_t V_{dc} + R_d R_e R_t C_c C_d C_g V_{dc} + R_d R_e R_t C_d C_g C_l V_{dc} + R_d R_e R_t C_d C_g C_t V_{dc} + R_d R_e R_t C_l C_g C_t V_{dc} + \\
 & R_d R_e R_t C_c C_g C_l V_{i2} + R_d R_e R_t C_c C_g C_l V_{i3} + R_d R_e R_t C_g C_l C_t V_{i3}) s^2 + \\
 & (R_c R_d C_d C_g V_{dc} + R_c R_e C_c C_d V_{dc} + R_c R_e C_d C_g V_{dc} + R_c R_e C_d C_l V_{dc} + R_c R_t C_c C_d V_{dc} + \\
 & R_c R_t C_d C_l V_{dc} + R_d R_t C_d C_g V_{dc} + R_e R_t C_c C_d V_{dc} + R_e R_t C_d C_g V_{dc} + R_e R_t C_d C_l V_{dc} + \\
 & R_e R_t C_c C_g V_{dc} + R_e R_t C_c C_l V_{i1} + R_d R_t C_c C_g V_{i2} + R_e R_t C_c C_g V_{i2} + R_e R_t C_c C_l V_{i2} + \\
 & R_d R_t C_g C_l V_{i3} + R_e R_t C_c C_l V_{i3} + R_e R_t C_g C_l V_{i3} + R_e R_t C_l C_t V_{i3}) s + \\
 & \frac{(R_c C_d V_{dc} + R_t C_d V_{dc} + R_t C_c V_{i2} + R_t C_l V_{i3})}{(R_c R_d R_e R_t C_c C_d C_g C_l + R_c R_d R_e R_t C_c C_d C_g C_t + R_c R_d R_e R_t C_d C_g C_l C_t) s^4 +} \\
 & (R_c R_d R_e C_c C_d C_g + R_c R_d R_e C_d C_g C_l + R_c R_d R_t C_c C_d C_g + R_c R_d R_t C_d C_g C_t + \\
 & R_c R_e R_t C_c C_d C_g + R_c R_e R_t C_c C_d C_l + R_c R_e R_t C_c C_d C_t + R_c R_e R_t C_d C_g C_t + \\
 & R_c R_e R_t C_d C_l C_t + R_d R_e R_t C_c C_d C_g + R_d R_e R_t C_c C_g C_l + R_d R_e R_t C_d C_g C_l + \\
 & R_d R_e R_t C_c C_g C_t + R_d R_e R_t C_g C_l C_t) s^3 + \\
 & (R_c R_d C_d C_g + R_c R_e C_c C_d + R_c R_e C_d C_g + R_c R_e C_d C_l + R_d R_e C_c C_g + R_d R_e C_g C_t + \\
 & R_c R_t C_c C_d + R_c R_t C_d C_t + R_d R_t C_c C_g + R_d R_t C_d C_g + R_d R_t C_g C_t + R_e R_t C_c C_d + \\
 & R_e R_t C_c C_g + R_e R_t C_d C_g + R_e R_t C_c C_l + R_e R_t C_d C_l + R_e R_t C_c C_t + R_e R_t C_g C_t + R_e R_t C_l C_t) s^2 + \\
 & (R_c C_d + R_d C_g + R_e C_c + R_e C_g + R_e C_l + R_t C_c + R_t C_d + R_t C_t) s + 1
 \end{aligned} \tag{D.38}$$

Equation D.38 can be expressed in the format:

$$V_4(s) = \frac{c_3 s^3 + c_2 s^2 + c_1 s^1 + c_0}{d_4 s^4 + d_3 s^3 + d_1 s^2 + d_1 s^1 + d_0} \tag{D.39}$$

where

$$c_3 = R_c R_d R_e R_t C_c C_d C_g C_l V_{dc} + R_c R_d R_e R_t C_c C_d C_g C_t V_{dc} + R_c R_d R_e R_t C_d C_g C_l C_t V_{dc}, \tag{D.40}$$

$$\begin{aligned}
 c_2 = & R_c R_d R_e C_c C_d C_g V_{dc} + R_c R_d R_e C_d C_g C_l V_{dc} + R_c R_d R_t C_c C_d C_g V_{dc} + R_c R_d R_t C_d C_g C_t V_{dc} + \\
 & R_c R_e R_t C_c C_d C_g V_{dc} + R_c R_e R_t C_c C_d C_l V_{dc} + R_c R_e R_t C_c C_d C_t V_{dc} + R_c R_e R_t C_d C_g C_t V_{dc} + \\
 & R_c R_e R_t C_d C_l C_t V_{dc} + R_d R_e R_t C_c C_d C_g V_{dc} + R_d R_e R_t C_d C_g C_l V_{dc} + R_d R_e R_t C_d C_g C_t V_{dc} + \\
 & R_d R_e R_t C_l C_g C_t V_{dc} + R_d R_e R_t C_c C_g C_l V_{i2} + R_d R_e R_t C_c C_g C_l V_{i3} + R_d R_e R_t C_g C_l C_t V_{i3}
 \end{aligned} \tag{D.41}$$

$$\begin{aligned}
 c_1 = & R_c R_d C_d C_g V_{dc} + R_c R_E R_m C_c C_d V_{dc} + R_c R_e C_d C_g V_{dc} + R_c R_e C_d C_l V_{dc} + R_c R_l C_c C_d V_{dc} + \\
 & R_c R_l C_d C_l V_{dc} + R_d R_l C_d C_g V_{dc} + R_e R_l C_c C_d V_{dc} + R_e R_l C_d C_g V_{dc} + R_e R_l C_d C_l V_{dc} + R_e R_l C_c C_g V_g + , \quad (D.42) \\
 & R_e R_l C_c C_l V_{i1} + R_d R_l C_c C_g V_{i2} + R_e R_l C_c C_g V_{i2} + R_e R_l C_c C_l V_{i2} + R_d R_l C_g C_l V_{i3} + R_e R_l C_c C_l V_{i3} + \\
 & R_e R_l C_g C_l V_{i3} + R_e R_l C_l C_l V_{i3}
 \end{aligned}$$

$$c_0 = R_c C_d V_{dc} + R_l C_d V_{dc} + R_l C_c V_{i2} + R_l C_l V_{i3}, \quad (D.43)$$

$$d_4 = R_c R_d R_e R_l C_c C_d C_g C_l + R_c R_d R_e R_l C_c C_d C_g C_l + R_c R_d R_e R_l C_d C_g C_l C_l, \quad (D.44)$$

$$\begin{aligned}
 d_3 = & R_c R_d R_e R_c C_d C_g + R_c R_d R_e R_c C_d C_g C_l + R_c R_d R_l C_c C_d C_g + R_c R_d R_l C_d C_g C_l + R_c R_e R_l C_c C_d C_g + \\
 & R_c R_e R_l C_c C_d C_l + R_c R_e R_l C_c C_d C_l + R_c R_e R_l C_d C_g C_l + R_c R_e R_l C_d C_l C_l + R_d R_e R_l C_c C_d C_g + \\
 & R_d R_e R_l C_c C_g C_l + R_d R_e R_l C_d C_g C_l + R_d R_e R_l C_c C_g C_l + R_d R_e R_l C_g C_l C_l, \quad (D.45)
 \end{aligned}$$

$$\begin{aligned}
 d_2 = & R_c R_d C_d C_g + R_c R_E R_m C_c C_d + R_c R_e C_d C_g + R_c R_e C_d C_l + R_d R_e C_c C_g + R_d R_e C_g C_l + \\
 & R_e R_l C_c C_d + R_e R_l C_d C_l + R_d R_l C_c C_g + R_d R_l C_d C_g + R_d R_l C_g C_l + R_e R_l C_c C_d + R_e R_l C_c C_g + \\
 & R_e R_l C_d C_g + R_e R_l C_c C_l + R_e R_l C_d C_l + R_e R_l C_c C_l + R_e R_l C_g C_l + R_e R_l C_l C_l, \quad (D.46)
 \end{aligned}$$

$$d_1 = R_c C_d + R_d C_g + R_E R_m C_c + R_E R_m C_g + R_e C_l + R_l C_c + R_l C_d + R_l C_l, \quad (D.47)$$

and

$$d_0 = 1. \quad (D.48)$$

Appendix.E The performance of mathematical calculations with Mathematica software

$V_g=800 \cdot 10^3$
 $V_{i1}=0$
 $V_{dc}=300 \cdot 10^3$

 $R_m=20 \cdot 10^3$
 $C_g=15.625 \cdot 10^{-9}$
 $R_d=375$
 $R_E=1780$
 $C_l=2530 \cdot 10^{-12}$
 $C_d=0.02 \cdot 10^{-6}$
 $C_t=20 \cdot 10^{-12}$
 $R_c=1000 \cdot 10^3$
 $R_t=700 \cdot 10^6$
 $V_{i2}=299.572 \cdot 10^3$
 $V_{i3}=299.572 \cdot 10^3$

$C_c=10 \cdot 10^{-9}$

800000
0
300000
20000
 1.5625×10^{-8}
375
1780

253

100000000000
 $2. \times 10^{-8}$
1

50000000000
1000000
700000000
299572.
299572.
1

100000000

APPENDIX E – THE PERFORMANCE OF MATHEMATICAL CALCULATIONS USING MATHEMATICA SOFTWARE

$$V3 == \left(R_t (C_d V_{dc} + C_d C_g R_d S V_{dc} + C_c C_d R E S V_{dc} + C_d C_g R E S V_{dc} + C_d C_l R E S V_{dc} + C_c C_d C_g R_d R E S^2 V_{dc} + C_d C_g C_l R_d R E S^2 V_{dc} + C_c C_g R E S V_g + C_c C_d C_g R_c R E S^2 V_g + C_c C_l R E S V_{i1} + C_c C_d C_l R_c R E S^2 V_{i1} + C_c C_g C_l R_d R E S^2 V_{i1} + C_c C_d C_g C_l R_c R_d R E S^3 V_{i1} + C_c V_{i2} + C_c C_d R_c S V_{i2} + C_c C_g R_d S V_{i2} + C_c C_g R E S V_{i2} + C_c C_l R E S V_{i2} + C_c C_d C_g R_c R_d S^2 V_{i2} + C_c C_d C_g R_c R E S^2 V_{i2} + C_c C_d C_l R_c R E S^2 V_{i2} + C_c C_g C_l R_d R E S^2 V_{i2} + C_c C_d C_g C_l R_c R_d R E S^3 V_{i2} + C_t V_{i3} + C_d C_t R_c S V_{i3} + C_g C_t R_d S V_{i3} + C_c C_t R E S V_{i3} + C_g C_t R E S V_{i3} + C_l C_t R E S V_{i3} + C_d C_g C_t R_c R_d S^2 V_{i3} + C_c C_d C_t R_c R E S^2 V_{i3} + C_d C_g C_t R_c R E S^2 V_{i3} + C_d C_l C_t R_c R E S^2 V_{i3} + C_c C_g C_t R_d R E S^2 V_{i3} + C_g C_l C_t R_d R E S^2 V_{i3} + C_c C_d C_g C_t R_c R_d R E S^3 V_{i3} + C_d C_g C_l C_t R_c R_d R E S^3 V_{i3}) \right) /$$

$$(1 + C_d R_c S + C_g R_d S + C_c R E S + C_g R E S + C_l R E S + C_c R_t S + C_d R_t S + C_t R_t S + C_d C_g R_c R_d S^2 + C_c C_d R_c R E S^2 + C_d C_g R_c R E S^2 + C_d C_l R_c R E S^2 + C_c C_g R_d R E S^2 + C_g C_l R_d R E S^2 + C_c C_d R_c R_t S^2 + C_d C_t R_c R_t S^2 + C_c C_g R_d R_t S^2 + C_d C_g R_d R_t S^2 + C_g C_t R_d R_t S^2 + C_c C_d R E R_t S^2 + C_c C_g R E R_t S^2 + C_d C_g R E R_t S^2 + C_c C_l R E R_t S^2 + C_d C_l R E R_t S^2 + C_c C_t R E R_t S^2 + C_g C_t R E R_t S^2 + C_l C_t R E R_t S^2 + C_c C_d C_g R_c R_d R E S^3 + C_d C_g C_l R_c R_d R E S^3 + C_c C_d C_g R_c R_d R_t S^3 + C_d C_g C_t R_c R_d R_t S^3 + C_c C_d C_g R_c R E R_t S^3 + C_c C_d C_l R_c R E R_t S^3 + C_c C_d C_t R_c R E R_t S^3 + C_d C_g C_t R_c R E R_t S^3 + C_d C_l C_t R_c R E R_t S^3 + C_c C_d C_g R_d R E R_t S^3 + C_c C_g C_l R_d R E R_t S^3 + C_d C_g C_l R_d R E R_t S^3 + C_c C_g C_t R_d R E R_t S^3 + C_g C_l C_t R_d R E R_t S^3 + C_c C_d C_g C_l R_c R_d R E R_t S^4 + C_c C_d C_g C_t R_c R_d R E R_t S^4 + C_d C_g C_l C_t R_c R_d R E R_t S^4)$$

$$V3 == \frac{700000000 (0.00900171 + 0.0000607073 S + 6.74482 \times 10^{-9} S^2 + 1.59663 \times 10^{-15} S^3)}{1 + 21.0341 S + 0.141333 S^2 + 5.36223 \times 10^{-6} S^3 + 3.73079 \times 10^{-12} S^4}$$

$$\text{Simplify}\left[V3 == \frac{700000000 (0.00900171 + 0.0000607073 S + 6.74482 \times 10^{-9} S^2 + 1.59663 \times 10^{-15} S^3)}{1 + 21.0341 S + 0.141333 S^2 + 5.36223 \times 10^{-6} S^3 + 3.73079 \times 10^{-12} S^4} \right]$$

$$V3 == \frac{299572. (150.807 + S) (8868.71 + S) (4.2154 \times 10^6 + S)}{(0.0475571 + S) (149.629 + S) (26706.4 + S) (1.41044 \times 10^6 + S)}$$

$$\text{InverseLaplaceTransform}\left[V3 == \frac{299572. (150.807 + S) (8868.71 + S) (4.2154 \times 10^6 + S)}{(0.0475571 + S) (149.629 + S) (26706.4 + S) (1.41044 \times 10^6 + S)}, S, t \right]$$

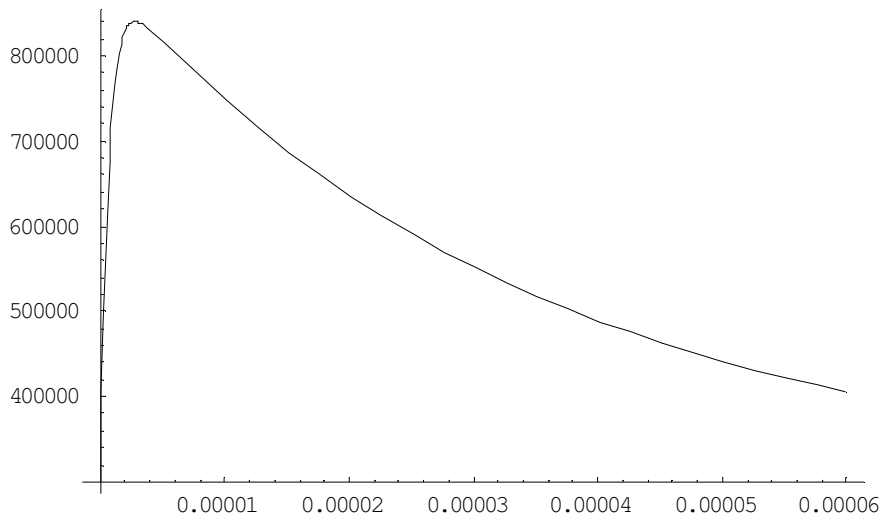
$$V3 \text{DiracDelta}[t] == 299572. \left(-2.01435 e^{-1.41044 \times 10^6 t} + 2.02177 e^{-26706.4 t} - 0.0077336 e^{-149.629 t} + 1.00032 e^{-0.0475571 t} \right)$$

$$\text{FindMaximum}\left[299572. \left(-1.99577 e^{-1.42801 \times 10^6 t} + 1.99576 e^{-28720.8 t} + 7.91247 \times 10^{-6} e^{-49.9183 t} + 0.999998 e^{-1.42857 \times 10^{-9} t} \right), \{t, 0\} \right]$$

$$\{840283., \{t \rightarrow 2.79172 \times 10^{-6}\}\}$$

APPENDIX E – THE PERFORMANCE OF MATHEMATICAL CALCULATIONS USING MATHEMATICA SOFTWARE

```
Plot[299572. (-1.99577 e-1.42801×106 t +  
1.99576 e-28720.8 t + 7.91247×10-6 e-49.9183 t +  
0.999998 e-1.42857×10-9 t), {t, 0, 60*10-6}]
```



-Graphics-

APPENDIX E – THE PERFORMANCE OF MATHEMATICAL CALCULATIONS USING MATHEMATICA SOFTWARE

$$V4 = \frac{6.3072 \times 10^6 + 42555.5 S + 1.60867 S^2 + 1.11924 \times 10^{-6} S^3}{1 + 21.0341 S + 0.141333 S^2 + 5.36223 \times 10^{-6} S^3 + 3.73079 \times 10^{-12} S^4}$$

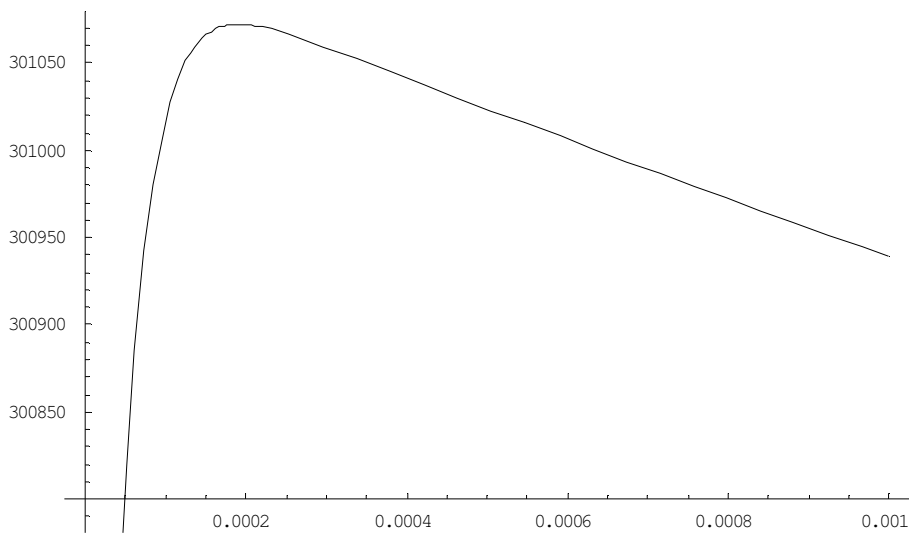
$$\text{InverseLaplaceTransform}\left[V4 = \frac{6.3072 \times 10^6 + 42555.5 S + 1.60867 S^2 + 1.11924 \times 10^{-6} S^3}{1 + 21.0341 S + 0.141333 S^2 + 5.36223 \times 10^{-6} S^3 + 3.73079 \times 10^{-12} S^4}, S, t\right]$$

$$V4 \text{DiracDelta}[t] = 21.3929 e^{-1.41044 \times 10^6 t} - 1136.06 e^{-26706.4 t} + 1162.7 e^{-149.629 t} + 299952. e^{-0.0475571 t}$$

$$\text{FindMaximum}\left[21.3929 e^{-1.41044 \times 10^6 t} - 1136.06 e^{-26706.4 t} + 1162.7 e^{-149.629 t} + 299952. e^{-0.0475571 t}, \{t, 0.00012\}\right]$$

{301072.,{t→0.0001913}}

$$\text{Plot}\left[21.3929 e^{-1.41044 \times 10^6 t} - 1136.06 e^{-26706.4 t} + 1162.7 e^{-149.629 t} + 299952. e^{-0.0475571 t}, \{t, 0, 0.001\}\right]$$



-Graphics-

Appendix.F HSPICE code for the simulation of the composite waveform generator

The code below is for simulation of the composite waveform generator.

```

*component names and values
.options post=2 probe
Cg  0    1    10 e-9
Cl  0    2    1.2e-9
Rd  1    2    375
Re  2    0    6.1e3

*assign initial values
.IC  v(1)=10e3
.IC  v(2)=0

*do transient analysis – use initial conditions
.tran 0.01u 10u UIC

*output transient data to user interface/measure Vt
.probe v(t)=v2
.probe vo=v(1)
.probe vc1=v 1 2
.probe IR1=I(R1)
.probe IR2=I(R2)
.probe IC1=I(C1)
.probe IC2=I(C2)

Print

.end

```

Appendix.G MATLAB code

G.1 Comparison of methods: mathematical model, HSPICE and the practical measured

This code executes the graphical plotting of three different graphs, namely a waveform generated with the mathematical model, a waveform measured from the practical circuit and a HSPICE generated waveform. The last two waveforms are each compared with the mathematical model waveform.

```

ChargingV=dlmread('D:\Lab Tests\Test 10\TEK00000.csv','');

t0=ChargingV(:,1);
V0=ChargingV(:,2);

plot(t0,V0,'m');

hold on
V0Avg=(mean(V0(1:100)));
plot(t0,V0Avg,'b');

m=dlmread('D:\Lab Tests\Test 10\TEK00002.csv','');

t=m(:,1);
V=m(:,2);

time=t;
V1=V;
Voltage=V1*970;
figure;
plot(time,Voltage,'k');

hold on
HF_minus_DC=Voltage-(mean(Voltage(1:100)));

```

APPENDIX G – MATLAB CODE

```

plot(time,HF_minus_DC,'b');

%HV probe at Node 3
n=dlmread('D:\Lab Tests \Test 10\TEK00001.csv',';');
time2=n(:,1);
voltage2=n(:,2);
hold on;
plot(time2,voltage2,'r');

%Low pass filter to get DC component from HV probe measurement
[b,a]=butter(2,0.1/4000000,'low');

filtfilt_LP=filtfilt(b,a,voltage2);

figure;
plot(time2,filtfilt_LP,'b');

finalvalue=(filtfilt_LP+HF_minus_DC);
hold on
plot(time,finalvalue);

% hold on
% plot(time2,voltage2,'r');

% Mathematical approach
e=2.718;
t=0:0.1e-6:8.8e-6;
V3t=5018*(-1.89986*e.^((-2.36159*10^6).*t)+1.9014*e.^((-13799.6).*t)+0.0237373*e.^((-20.3462).*t)+0.974719*e.^((-0.484178).*t));

hold on
plot(t,V3t,'m');

% HSPICE waveform
kondja=tblread('C:\text.txt',' ');

```


APPENDIX G – MATLAB CODE

```
HSPICE_t=kondja(:,1);
HSPICE_V=kondja(:,2);

hold on
plot(HSPICE_t,HSPICE_V,'k');

%compare simulated vs measured
figure
plot(time,finalvalue);
hold on
plot(t,V3t,'m')
title('mathematical model against practical test')
xlabel('time in sec')
ylabel('voltage in V')

%compare simulated vs HSPICE
figure
plot(HSPICE_t,HSPICE_V,'k');
hold on
plot(t,V3t,'m')
title('mathematical model against HSPICE')
xlabel('time in sec')
ylabel('voltage in V')
```

G.2 Illustration of the drying process

This code executes the graphical plotting of the drying process of the insulator. The two graphs are recorded from two separate tests performed under similar conditions.

```

o=dlmread('M:\Leakage\27 08\Purple\TEK00002.csv','');
p=dlmread('M:\Leakage\27 08\Purple\TEK00004.csv','');

t1=o(:,1);
lx=o(:,2);
t2=p(:,1);
ly=p(:,2);

time1=t1+4.6;           %setting time axis to zero
time2=t2+4.72;        %setting time axis to zero
l1=lx;
l2=ly;
Current1=l1*0.5;      %multiplying with current the ratio of the measuring probe
Current2=l2*0.5;      %multiplying with current the ratio of the measuring probe

figure;
subplot(2,1,1)
plot(time1,Current1,'b');
ylabel('Current [A]')
xlabel ('time [sec]')
title('Surface discharge current at a voltage of 5 kV')
subplot(2,1,2)
plot(time2,Current2,'b');
ylabel('Current [A]')
xlabel ('time [sec]')

```

G.3 Plots of flashover impulses

This code executes the plotting of impulses recorded from the performed tests.

```
poluttet_dry=dlmread('C:\2008 Academics\2008\Lab Measurements\18 Mar
08\TEK00003.csv',';');
```

```
t0=poluttet_dry(:,1);
V0=(poluttet_dry(:,2)*8000)+20000;
```

```
plot(t0,V0,'m');
ylabel('Voltage [V]')
xlabel ('time [sec]')
title('Negative impulse flashover at 20kV dc bias')
```

```
pos_poluttet_dry=dlmread('C:\2008 Academics\2008\Lab measurements\20 Mar
08\TEK00002.CSV',';');
```

```
t1=pos_poluttet_dry(:,1);
V1=(pos_poluttet_dry(:,2)*8000)+20000;
```

```
figure;
plot(t1,V1,'m');
ylabel('Voltage [V]')
xlabel ('time [sec]')
title('Positive impulse flashover at 20kV dc bias')
```

```
pos_poluttet_dry=dlmread('C:\2008 Academics\2008\Lab measurements\17 Mar 08\Polluted
dry neg impls.CSV',';');
```

```
t2=pos_poluttet_dry(:,1);
V2=(pos_poluttet_dry(:,2)*8000);
figure;
plot(t2,V2,'m');
ylabel('Voltage [V]')
xlabel ('time [sec]')
title('Negative impulse flashover at no dc bias')
```

APPENDIX G – MATLAB CODE

```
pos_poluttet_dry=dlmread('C:\2008 Academics\2008\Lab measurements\18 Mar
08\TEK00002.CSV',';');

t3=pos_poluttet_dry(:,1);
V3=(pos_poluttet_dry(:,2)*8000);
figure;
plot(t3,V3,'m');
ylabel('Voltage [V]')
xlabel ('time [sec]')
title('Negative impulse flashover at no dc bias')
```